Politecnico di Torino

Master's Degree Thesis

in the Course of Environmental and Land Engineering

Thermal activation of tunnels of different sizes

Supervisor:

Marco Barla

Candidate:

Matin Kabiri Tadi

Co-Supervisors:

Alessandra Insana

Martina Scerbo

July 2025

Table of contents

List of figures

List of tables

Acknowledgements

First and foremost, I am deeply grateful to Professor Marco Barla for his insightful supervision and availability during this research, and for trusting me with the opportunity to assist him during the NUMGE course. I am also immensely thankful to Dr. Alessandra Insana, not only for her supervision throughout my academic journey but also for her support in overcoming the challenges of my first ever didactic work experience. My sincere thanks go to Martina Scerbo for her constant willingness and availability to support me throughout the progression of this research. Finally, my heartfelt appreciation goes to my family, who have always believed in me and supported me unconditionally, even during the challenging moments of their own lives.

Abstract

Today's world is facing two issues regarding its energy demand. First, it needs secure and accessible energy sources for supporting humans lives to allow their progress. Second, fossil fuels as the main sources of energy are threatening the future of life on earth due to their emissions. Shallow geothermal energy as a renewable energy source is a promising subject of study whose real-world implementations can contribute to overcome these issues.

This research focuses on energy tunnels as a main energy geostructure that allow shallow geothermal energy exploitation from the ground. The geothermal performance of energy tunnels is dependent on geometrical and thermophysical parameters of the tunnel and its surroundings, i.e. ground and tunnel air. However, the effect of tunnel size has not been studied on this energy geostructure's thermal output. Therefore, in this research the diameter of tunnels with segmental lining is chosen as a study parameter that represents the size of an energy tunnel. To investigate the role of the diameter on the geothermal output of an energy tunnel, a finite element software (i.e. COMSOL) is used for simulating the thermo-hydraulic behavior of the tunnel. The numerical model was validated using the results of previous real field test campaigns. Subsequently, the validated model was used to capture the geothermal output of the tunnel under an extensive parametric study that investigated the effect of seasonality, tunnel diameter, groundwater flow velocity and direction, intrados thermal boundary condition, and ground temperature and thermal conductivity. The study concluded by implementing the ratio of groundwater flow velocity over inner diameter as a characteristic parameter that allows plotting design charts for preliminary assessment of energy tunnel projects. These charts showed good agreement with some available numerical and real case studies, indicating a higher reliability compared to more generalized design charts that did not consider the role of diameter in geothermal performance of energy tunnels.

1 Introduction

1.1 Background

The global push for renewable energy is fueled by concerns over fossil fuel dependency, environmental harm, and the urgent need to combat climate change. While fossil fuels dominate global energy consumption, their limited availability and susceptibility to geopolitical risks raise significant energy security challenges. Furthermore, the environmental impacts of fossil fuel use, especially greenhouse gas emissions, have played a major role in global warming. The European Union, through initiatives like the Renewable Energy Directive (2018/2001/EU), has set ambitious goals to increase renewable energy use and achieve carbon neutrality by 2050 (European Union, 2018). Shifting to renewable energy sources is crucial to addressing climate challenges while building a resilient and sustainable energy system for the future.

Geothermal energy, a natural heat source originating from the Earth's internal thermal processes, is a promising solution for today’s cooling or heating demands. It can be harnessed in various forms, including shallow geothermal systems. Shallow geothermal energy harnesses the stable temperatures found just below the Earth’s surface, providing a consistent and reliable means of temperature regulation for buildings. Unlike other renewable sources,

such as wind or solar, geothermal energy is available continuously, making it a dependable option unaffected by weather or seasonal variations. Additionally, shallow geothermal systems have a low environmental impact, offering long-term sustainability with minimal land use and no direct emissions. The European Union recognizes the potential of shallow geothermal energy, promoting its use as part of broader decarbonization strategies under the Renewable Energy Directive (2018/2001/EU), which supports increased integration of this technology to meet both current and future energy needs in a more sustainable manner (European Union, 2018).

Among the methods for utilizing shallow geothermal energy, energy geostructures stand out as an innovative approach. These systems integrate the structural roles of geotechnical infrastructure, such as foundations, retaining walls, and tunnel linings, with the capacity to harness geothermal energy (Brandl, 2006). For example, energy piles have been effectively used for the purpose of renewable heating and cooling in building foundations through the integration of geothermal energy without the high costs associated with traditional geothermal systems that entail extensive drilling and the requirement of backfill materials (Aresti et al., 2024; Brandl, 2006). Energy retaining walls have been incorporated into underground structures including basements, car parks and metro stations to provide a geothermal supply for the buildings despite having more complex thermal design than energy piles (Zhong et al., 2023). Expanding on this concept, energy tunnels represent another innovative form of energy geostructures that combines structural functionality with geothermal energy exchange. By tapping into the stable geothermal energy beneath the earth's surface, energy tunnels simultaneously satisfy transportation needs, and a renewable energy source demand for managing indoor temperature (Barla & Di Donna, 2018). Their constant availability and minimal environmental impact make them highly beneficial in urban areas, where space for renewable energy installations is restricted.

Energy tunnels are an emerging area of research with considerable untapped potential. They combine geothermal energy extraction with urban infrastructure, offering a sustainable solution, particularly in space-constrained areas. However, the absence of standardized design guidelines and limited real-scale experimental data emphasize the need for further

study. Investigating the influence of various design factors could drive progress in this field, positioning energy tunnels as a vital technology for sustainable urban heating and cooling systems.

Recent progress in energy tunnels has been largely influenced by the use of numerical modeling, especially for analyzing thermo-hydraulic performance. Techniques like finite element modeling have made it possible to simulate real-world conditions, considering factors such as groundwater flow and tunnel airflow. These models play a crucial role in improving system design, enabling engineers to enhance thermal efficiency, predict long-term performance, and assess the geostructural impact of thermal activation.

1.2 Problem statement

Numerical investigations of energy tunnels remain indispensable due to the intricate thermal and mechanical interactions they entail. While experimental testing is often constrained by cost and environmental considerations, numerical modeling provides a practical and adaptable approach to exploring new ideas and assessing feasibility. These models enable the evaluation of performance under diverse soil conditions and thermal loads, which are difficult to reproduce in real-world experiments. Given the site-specific nature of energy tunnels, numerical analysis not only facilitates design optimization but also supports the development of efficient, reliable, and sustainable solutions for long-term operation.

The parameters influencing energy tunnels, such as thermal conductivity, soil conditions, and heat exchange efficiency, have been investigated. However, the role of tunnel size in their performance remains underexplored. This research gap offers an opportunity to investigate how tunnel size affects the geothermal output of the tunnel. Gaining insights into this relationship is essential for optimizing energy tunnel designs and enhancing their effectiveness in diverse applications.

1.3 Thesis objectives

This thesis examines how tunnel diameter, as an indicator of tunnel size, influences the geothermal performance of energy tunnels with segmental lining. The research explores the mechanisms controlling geothermal output in tunnels of varying diameters, providing deeper insight into how size affects their efficiency. Additionally, the thesis addresses a current research gap by considering the potential of applying thermal activation to smaller structures like microtunnels, opening pathways for future investigation and application.

1.4 Thesis structure

The thesis consists of seven chapters. The present chapter gives an introduction for the scope and objectives of the research.

Chapter two discusses the background for the shallow geothermal energy and energy geostructures in the literature. The main focus is to clarify the concept of energy tunnels by introducing their multiphysical aspects and design procedures.

Chapter three describes the available assumptions for simulating energy tunnels in COMSOL when comparing the previous ones in FEFLOW models.

Chapter four includes the strategies that were used for ensuring the reliability of the energy tunnels themo-hydraulic simulations in COMSOL. Verification attempts against previous numerical results and validation attempts against field tests results are presented along with the base model parameters, boundary conditions and setup.

Chapter five is dedicated to analyzing the effect of tunnel diameter on the geothermal output of energy tunnels by performing sensitivity analyses on parameters and boundary conditions of the model.

Chapter six presents a new method for applying the tunnel diameter effect to energy tunnels' design charts. The validity of this method is shown by comparing the charts' readings with previous numerical and real energy tunnel case studies.

Chapter seven summarizes the findings of the thesis and opens up about the possibility of extending the current research in the future.

2 Harnessing the subsurface: a review of energy geostructures

2.1 Shallow geothermal energy

Geothermal energy is a renewable energy source that is generated and stored in the ground. It is derived from two main sources: the radioactivity of elements within the Earth's core, which contributes to deep geothermal energy, and solar radiation that penetrates the Earth's upper crust, which primarily fuels shallow geothermal energy. Shallow geothermal energy taps into the stable thermal conditions of the upper layers of the Earth, typically within 400 meters of the surface. Unlike deep geothermal systems that rely on high temperatures found at greater depths, shallow systems exploit the relatively constant ground temperatures, usually between 10°C and 16°C at a much lower depth, depending on geographic location. This temperature stability in the shallow subsurface is largely due to the geothermal gradient in the Earth's crust, where ground temperature increases by approximately 3°C for every 100 meters of depth (Laloui & Di Donna, 2013). In Figure 2-1, this phenomenon is demonstrated by ground temperature measurements taken at various depths over the year in the Mezzi Po test site in Turin, Italy (Bucci et al., 2020). The same trend can be seen in Figure 2-2 for the monthly temperature profile along the ground depth in Istanbul, Turkey (Aydin et al., 2015).

These stable temperatures are maintained year-round, so their difference from the above-ground temperatures makes Ground Source Heat Pump (GSHP) systems highly efficient for both heating and cooling applications. The combination of solar energy stored in the ground and the consistent thermal characteristics of the shallow subsurface allows for sustainable and cost-effective energy solutions.

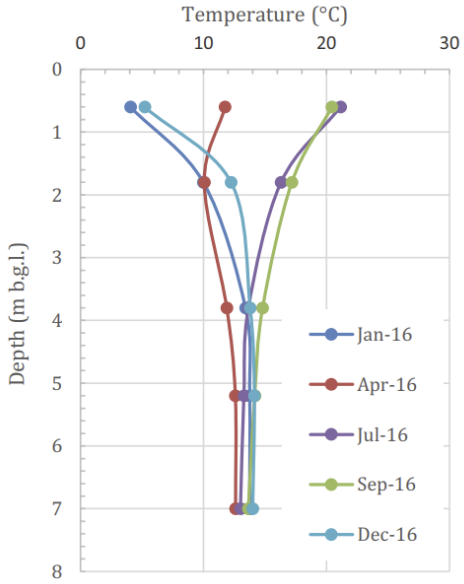

Figure 2-1. Monthly temperature variations along the ground depth at Mezzi Po, Turin, Italy (Bucci et al., 2020)

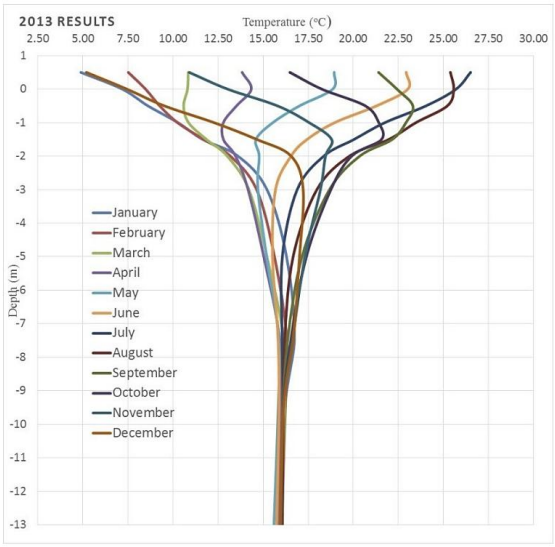

Figure 2-2.Monthly temperature variations along the ground depth at Istanbul, Turkey (Aydin et al., 2015)

2.2 Heat pump system

In nature, heat naturally flows from a body at a higher temperature to those at a lower temperature, and this process occurs spontaneously according to the second law of thermodynamics. However, the reverse process, where heat moves from a colder area to a warmer one, does not happen independently. This is where heat pumps come into play, as they are devices specifically designed to reverse the natural flow of heat. These machines transfer heat from a lower-temperature source to a higher-temperature area by using energy. To accomplish this, heat pumps require an external energy input, which can be electrical, mechanical, or geothermal, to drive the process. The energy supplied is necessary because it compensates for the difference between the heat extracted from the low-temperature source and the heat delivered to the high-temperature area.

The operation of a heat pump relies on a refrigerant, a special fluid that circulates within a closed-loop system. The refrigerant changes its state between liquid and vapor depending on the temperature and pressure conditions. This closed-loop system consists of four main components: a compressor, an expansion valve, a condenser, and an evaporator. The

evaporator and condenser function as heat exchangers, formed by coiled tubes that are in contact with a secondary fluid, which can be water or air, depending on the system design. The refrigerant absorbs heat from the surroundings in the evaporator and releases it in the condenser, heating the target environment. The compressor plays a crucial role by increasing the pressure and temperature of the refrigerant, providing it with the energy required to carry out the heat transfer. The expansion valve, on the other hand, reduces the pressure of the refrigerant before it enters the evaporator, allowing it to absorb heat efficiently from the cooler environment. This process enables the system to continuously extract heat from the colder source and transfer it to the warmer area, effectively providing heating even in cold climates. A scheme of its performance is represented in Figure 2-3.

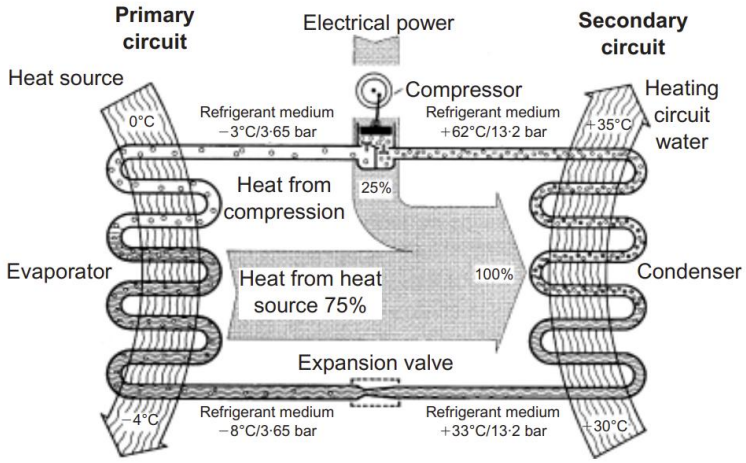

Figure 2-3. Scheme of a heat pump's performance (Brandl, 2006)

2.2.1 Ground-source heat pump (GSHP)

As previously mentioned, the ground temperature below a certain depth remains constant throughout the year. Depending on seasonal air temperatures, this makes the ground an ideal source or sink for heat. In the winter, the ground acts as a heat source for the heat pump, while in the summer, it serves as a heat sink. A Ground-Source Heat Pump (GSHP) takes advantage of this stable ground temperature to provide efficient heating and cooling for buildings. As depicted in Figure 2-4, a GSHP comprises the primary unit (heat exchanger),

the secondary unit (piping to deliver the energy to consumers), and the heat pump unit (Singh et al., 2019).

During the winter (heating mode), the system absorbs heat from the ground using a network of buried pipes known as a ground loop. These pipes contain a fluid that absorbs heat from the earth as it circulates. The absorbed heat is then transferred to the heat pump inside the building, where the compressor increases the temperature and pressure of the refrigerant, making it hot enough to provide heating. This heat is distributed through the building via radiators, air ducts, or underfloor heating systems. After releasing the heat, the circulating fluid cools down and returns to the ground loop, ready to collect more heat, ensuring continuous operation.

In summer (cooling mode), the process reverses. The GSHP extracts heat from the building and transfers it back into the ground, which acts as a heat sink due to its lower temperature. The thermal energy of the air inside the building is absorbed to initiate the evaporation of the heat pump's refrigerant. The refrigerant transfers this energy to the condenser of the heat pump where the heat can be delivered to the ground by the ground loop pipes. This cycle is repeatedly done to lower the indoor temperature of the building.

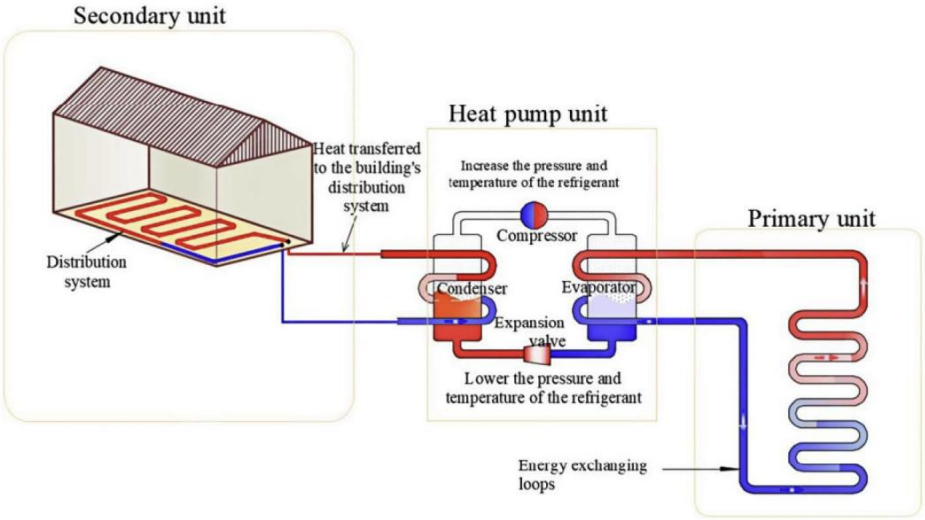

Figure 2-4. A scheme for the operation of a ground-source heat pump in the heating mode (Singh et al., 2019)

2.2.2 Types of piping loop of GSHPs

Closed and open-loop systems are two primary configurations of ground-source heat pump systems, each with distinct advantages and limitations. Open-loop GSHP systems extract heating or cooling energy directly from the ground, using water pumped from aquifers via heat pumps, as shown in Figure 2-5. The water is reinjected into the ground after transferring its thermal energy to the building. Open-loop systems require high ground permeability and good groundwater quality for optimal performance to minimize clogging (Brandl, 2006). Also, the presence of some regulations for the temperature of the discharging water or the possibility of contamination by the piping system for aquifers adds more limits for the prevalence of using such systems in many countries (Abesser, 2010).

On the other hand, closed-loop GSHP systems circulate working fluid within a sealed loop buried underground in trenches or boreholes, as shown in Figure 2-6. These systems do not allow fluid to exit the system, making them less susceptible to clogging issues like those in open systems. However, closed loops typically have higher costs and slightly lower efficiency compared to open-loop systems but provide reliable performance by avoiding mineral precipitation problems (Brandl, 2006).

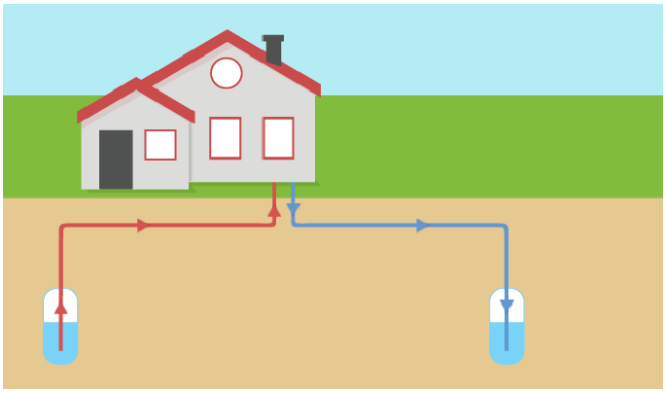

Figure 2-5. Diagram of an open-loop GSHP system (Gopher Heating and Air Conditioning)

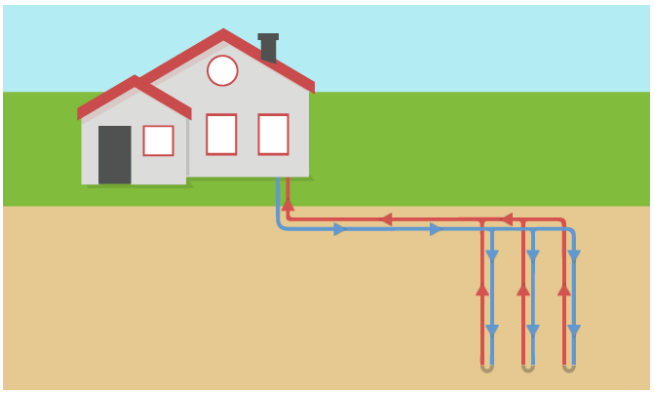

Figure 2-6. Diagram of a closed-loop GSHP system (Gopher Heating and Air Conditioning)

2.2.3 Heat hump performance indicators

Heat pumps are designed to transfer heat from one location to another, either for heating or cooling, and require external energy, typically electricity, to operate key components like compressors, fans, and pumps. This energy input allows the system to move heat against its natural flow, extracting heat from cooler areas and releasing it into warmer spaces (Insana, 2020). To evaluate their performance the coefficient of performance (COP) is defined for the heating mode of a heat pump as:

$$\mathrm{COP} = \frac{\text{heating energy output of the condenser [W]}}{\text{energy input of the compressor [W]}} \quad (1)$$

In the cooling mode of a heat pump, the energy efficiency ratio (EER) is used and defined as:

$$\mathrm{EER} = \frac{\text{cooling energy output of the evaporator [W]}}{\text{energy input of the compressor [W]}} \quad (2)$$

For economic viability, the COP should ideally be at least four, which indicates that 75% of the energy output in the secondary circuit comes from the ground. In comparison, the remaining 25% is supplied by electricity. Consequently, the temperature in the secondary circuit should be limited to 35-45 °C, while the temperature in the absorber pipes of the primary circuit should stay between 0-5 °C. Both the COP and EER are instantaneous indicators of energy performance, providing a snapshot of a heat pump's efficiency at a given

moment. However, they are unsuitable for evaluating long-term operational efficiency (Insana, 2020). Therefore, for long-term heating performance evaluation, the seasonal COP (SCOP) is defined as:

$$\text{SCOP} = \frac{\text{total heating energy output [kWh]}}{\text{total energy input [kWh]}} \tag{3}$$

For cooling purposes, seasonal EER (SEER) is defined as:

$$\text{SEER} = \frac{\text{total cooling energy output [kWh]}}{\text{total energy input [kWh]}} \tag{4}$$

2.3 Energy geostructures

Shallow geothermal energy can be proficiently harnessed through the incorporation of a closed-loop geothermal system within the structural components of civil engineering projects, which gives rise to the innovative concept of energy geostructures. Geotechnical structures, including piles, diaphragm walls, basement slabs or walls, tunnel linings, and anchors utilized in tunnels or retaining structures, can be modified to function as energy geostructures, thereby enabling the utilization of geothermal energy with significant economic and environmental advantages (Barla & Di Donna, 2016). This approach eliminates the necessity for distinct boreholes customarily associated with geothermal systems, thereby markedly diminishing the capital expenditure associated with the extracted geothermal energy (Loveridge et al., 2020). Additionally, their integration into building foundations and infrastructure makes them ideal for urban areas with limited land availability, while their dual-purpose design reduces the environmental footprint of construction projects.

The ground loop pipes in energy geostructures are not in direct contact with the soil, and their selection is influenced by several important factors. Flexibility is a primary characteristic, allowing the pipes to bend and adapt to the structural and thermal demands during installation and operation. Additionally, the materials used for these pipes must be compatible with reinforcing cages and other structural components, ensuring secure

attachment and effective functioning within the energy geostructure. Installation considerations are also crucial, with a focus on planning the layout and ensuring robust and efficient connections within the piping network. These features collectively contribute to the successful implementation and long-term reliability of energy geostructures (Laloui & Rotta Loria, 2019).

The pipes in energy geostructures are commonly constructed from high-density polyethylene, a material known for its durability and resistance to corrosion, high pressures, and extreme temperatures. Given the long lifespan of energy geostructures, it is essential to choose a material that can ensure the geothermal plant's reliability over time (Insana, 2020). The pipes usually have a diameter ranging from 10 to 40 mm and a wall thickness between 2 and 4 mm (Laloui & Rotta Loria, 2019).

The heat transfer fluid circulating within the pipes is typically water, a water-antifreeze mixture, or a saline solution. Water-antifreeze mixtures, often enhanced with corrosion inhibitors, are an effective and durable option. Antifreeze solutions serve to reduce the freezing point of the circulating fluid. Commonly employed additives in such solutions are ethylene glycol and propylene glycol. While ethylene glycol is recognized for its toxicity and demands careful handling and proper disposal to mitigate risks, propylene glycol is comparatively less harmful and is, therefore, a safer choice in certain situations (Laloui & Rotta Loria, 2019).

2.3.1 Energy piles

The utilization of shallow geothermal energy requires ground-loop pipes to extend to sufficient ground depths to access stable subsurface temperatures. Building foundations, particularly piles, provides an ideal solution as they are structural elements capable of reaching significant depths within the ground. Integrating the primary circuit of pipes into these piles facilitates efficient thermal exchange with stable underground temperatures. This approach marked the inception of the concept of energy piles, which are the most prevalent

type of energy geostructures. Their performance modes are similar to a normal vertical GSHP system in winter or summer, as shown in Figure 2-7.

Energy piles can be divided into two main types: cast-in-situ and driven energy piles. Cast-in-situ energy piles are constructed on-site by drilling a borehole, installing reinforcement cages equipped with heat exchanger pipes, and pouring concrete, offering high customization and suitability for various soil conditions with minimal noise and vibration during their construction. In contrast, driven energy piles are prefabricated, typically made of concrete or steel with embedded heat exchanger pipes, and are installed by driving them into the ground, providing rapid and cheaper installation of energy piles with smaller diameters (Sadeghi & Singh, 2023). Depending on the type of energy pile, the pipes must be fixed onto the steel reinforcement cage either at the construction site or during prefabrication in a factory . A close-up view of the attached pipes to the reinforcing steel cage of a cast-in-place pile is shown in Figure 2-8.

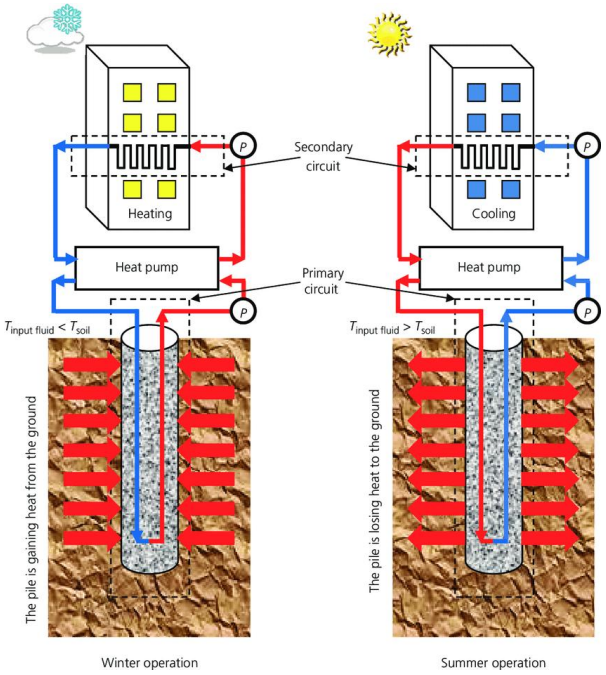

Figure 2-7. Summer and winter modes of operation of a single energy pile (Abuel-Naga et al., 2015)

Figure 2-8. Fixed polyethylene pipes on the reinforcing steel cage of cast-in-place energy piles (Narsilio et al., 2014)

2.3.2 Energy walls

Another prevalent way of harvesting shallow geothermal energy is thermal activation of the underground walls of civil structures, which gives rise to the concept of energy walls. The earliest method of achieving this goal is attaching the geothermal pipes to the reinforcing steel cage of an underground vertical wall before its construction, as shown in Figure 2-9-a. This method of thermal activation can be implemented in the walls of buildings' basements or the diaphragm walls of underground transportation systems (Laloui & Di Donna, 2013). Recently, a very shallow method of thermal activation of basement walls of buildings is introduced by the name of GeothermSkin in Politecnico di Torino. This method enables the utilization of geothermal energy from both existing walls and those under construction. In this approach, a series of pipes will be fixed on the external surface of a finished underground wall using simple clamps (Figure 2-9-b). After the installation process, the excavated space between the intended wall and the ground will be backfilled to allow for the initialization of geothermal energy harvest (Baralis & Barla, 2021).

(a) (b)

Figure 2-9. (a) fitted absorber pipes to the reinforcement steel cage of a diaphragm wall in Vienna (Adam et al., 2023), (b) Attaching GeothermSkin pipes to the basement walls at the Energy Center in Turin (Baralis & Barla, 2021)

2.3.3 Energy tunnels

Tunnels, another type of subterranean structure, offer a promising opportunity to harness the stable thermal conditions of the ground. By transforming these traditionally passive infrastructures into active contributors, tunnels can play a key role in future renewable energy systems. Recent advancements in engineering have highlighted the potential of geothermally activated tunnels, which serve dual purposes: supporting transportation or utility networks while simultaneously providing sustainable heating and cooling solutions. This is achieved through their extensive contact area with the surrounding ground. Following the precedent set by other thermally activated geotechnical structures, tunnels can be equipped with embedded absorber pipes within their elements, effectively transforming them into renewable energy sources, commonly referred to as energy tunnels. A simple scheme of an energy tunnel is depicted in Figure 2-10, where circulating fluid inside the heat absorber pipes of the primary circuit transfers heat between the ground and the GSHP to finally allow for cooling or heating purposes of the secondary circuit inside the buildings.

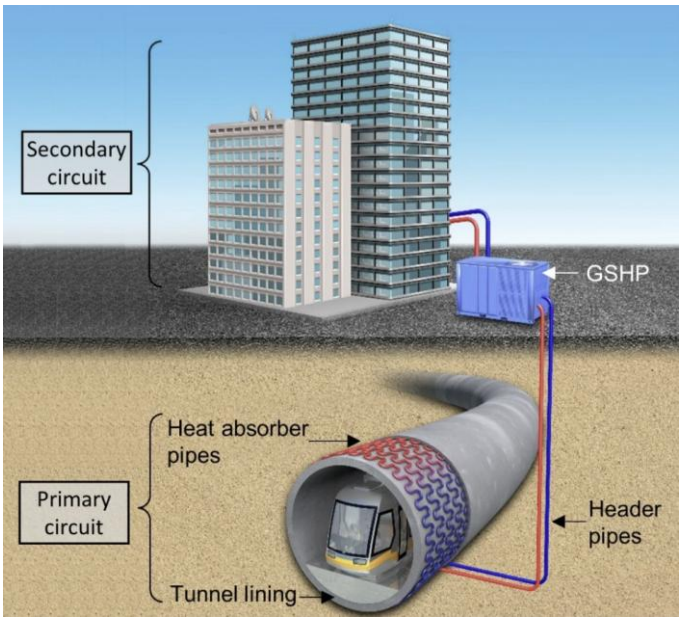

Figure 2-10. A scheme of a typical energy tunnel along with other heat exchanging units (Dai et al., 2023)

Energy tunnels share a characteristic with energy walls, distinct from other energy geostructures: They have a contact surface with the ground on one side and are exposed to air on the other. This boundary with the air inside the tunnel can also affect the thermal efficiency of the tunnel (Nicholson et al., 2013). Therefore, energy tunnels are categorized into hot and cold tunnels (Figure 2-11). Hot tunnels experience a higher inner temperature compared to the surrounding ground due to the movement of trains or vehicles and have a typical inner diameter of 6-7 m (Dai et al., 2023). The cold tunnels, on the other hand, have a lower inner air temperature compared to the surrounding ground and have a shorter length and a larger diameter (10-12 m) compared to the hot tunnels, which make them prone to being affected by the outside ambient temperatures. This aspect of energy tunnels, introduces the potential to also harvest thermal energy from the air inside the tunnels, in case of temperature difference with the ground surface. Additionally, if the space inside the tunnel needs to be cooled (due to passage of vehicles or trains) or heated (freezing temperatures at the tunnel portals), the thermal exchange with a suitable ground-surface temperature is possible.

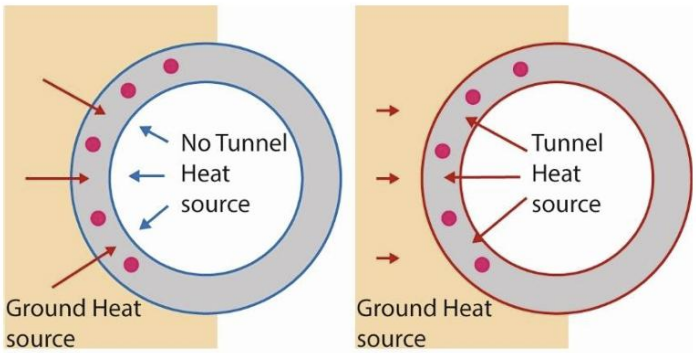

Figure 2-11. A schematic of the cold (left) and hot (right) tunnels (Nicholson et al., 2013)

2.3.3.1 Methods of thermal activation of tunnels

Tunnels differ significantly depending on the ground conditions they traverse, which require tailored construction methods to ensure stability and efficiency. The choice of tunneling approach varies to suit these conditions and optimize performance. Among the most commonly used techniques are cut-and-cover, the New Austrian Tunneling Method (NATM), and Tunnel Boring Machines (TBM). Each of these methods of tunnel construction gives a unique opportunity for thermal activation of the tunnels. Consequently, tunnels will consist of various structural elements in which the absorber pipes can be implemented.

The final geometry of cut-and-cover tunnels results in the presence of vertical (diaphragm walls and pile walls) and horizontal structural elements (concrete slabs) (Kovačević et al., 2013). These elements have been thermally activated similar to previously mentioned energy geostructures. In a cut-and-cover section of the Lainzer tunnel in Vienna, a primary side wall consisting of 59 bored piles was thermally activated to introduce the first energy tunnel in the world. The plant was constructed as a demonstration project as part of a research initiative of the Austrian government, and the first testing of the plant occurred in February 2004, which resulted in the extraction of 40 MWh of heating energy in six weeks to heat an adjacent school (Figure 2-12)(Brandl, 2016).

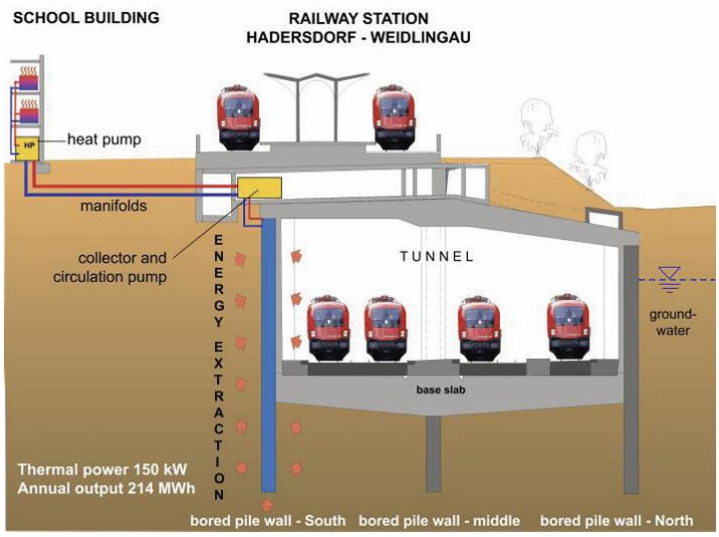

Figure 2-12. Schematic of the cut-and-cover energy tunnel of the Lainzer tunnel(Brandl, 2016)

In most of NATM tunnels, it is necessary to apply shotcrete immediately after tunnel excavation. Therefore, later construction elements for the tunnel support system can be used as geothermal heat exchangers. Energy anchors or nails are one type of geothermal activation of a NATM tunnel as depicted in Figure 2-13 (Brandl, 2016). Absorber pipes are implemented within these anchors and the heat exchange can occur under minimum effect of tunnel air temperatures. Energy anchors can also be of use in cut-and-cover tunnels (Mimouni et al., 2014). Absorber pipes can also be added between the primary and secondary lining of tunnels, where they will be called energy geotextiles (geo composites) (Figure 2-14). Thirdly, the absorber pipes can be placed inside the reinforced concrete of the secondary lining.

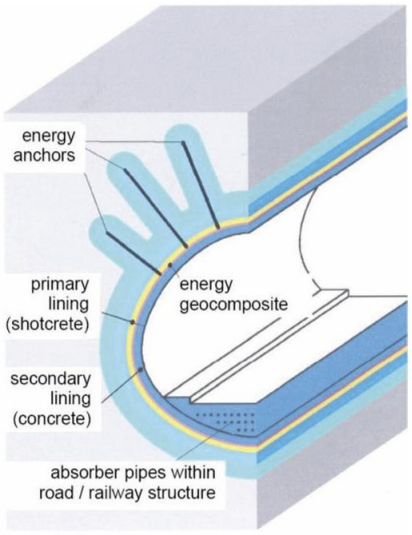

Figure 2-13. Schematic of energy anchors in a NATM tunnel (Brandl, 2016)

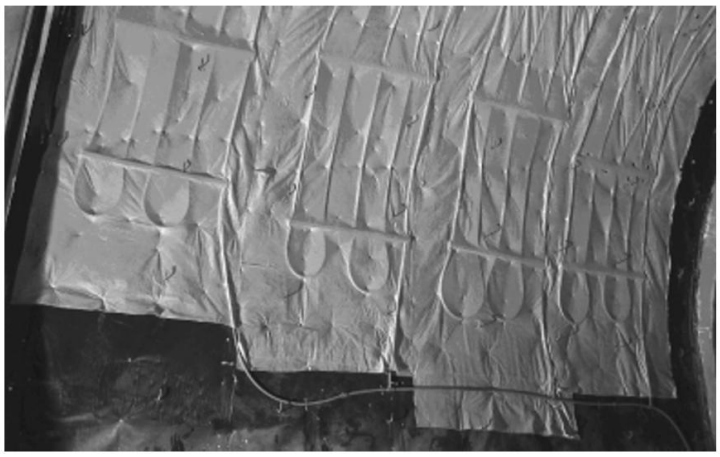

Figure 2-14. Energy geotextile installed on the primary lining at Lot 22 of Lainzer tunnel (Adam & Markiewicz, 2009)

In the tunneling method using the TBMs, the support system consists of precast segmental linings. Due to the fact that these reinforced concrete segments should be built well before the installation period, the implementation of absorber pipes to the reinforcement cage before casting the concrete is not going to slow down the lining installation by TBM. It is also needed to connect the pipe loop of each segment to the adjacent one after the completion of lining installation, which is also a non-interfering action to the timetable of the

TBM. This technology was first implemented as a temporary trial test in the Katzenberg tunnel in Germany (Franzius & Pralle, 2011). After gaining expertise in the Katzenberg tunnel, the technology was used to thermally activate 27 segmental rings (with a total length of 54m) for heating an adjacent municipal building. A picture of the attached absorber pipes to the reinforcement cage and the coupling openings for connecting adjacent segments piping loops is shown in Figure 2-15. The same concept was used in Bengasi Metro Station in Turin Metro Line 1, which will be further elaborated in subsequent sections of this study.

(a) (b)

Figure 2-15. (a). absorber loops attached to the reinforcement cage (b). coupling pockets designed for the connection of pipes among adjacent segments (Frodl et al., 2010)

The absorber pipes inside or between linings of energy tunnels have been used in three different arrangements, as depicted in Figure 2-16. Their effect on the thermal performance of energy geotextiles in Seocheon tunnel showed that the transverse configuration of pipes has the highest energy efficiency while the slinky one outputs the lowest energy rate with respect to its length (Lee et al., 2012).

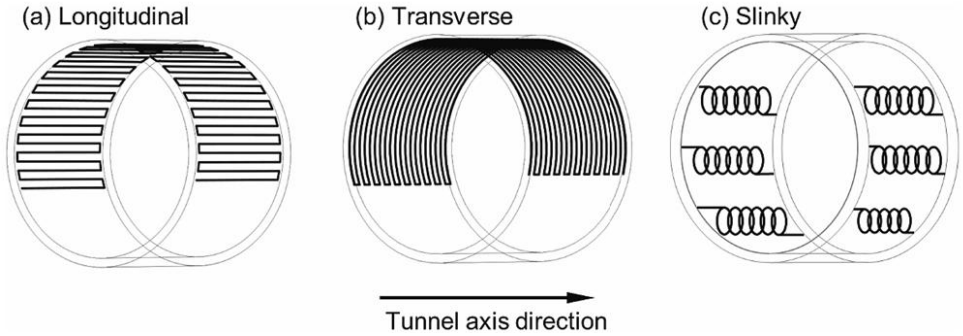

Figure 2-16. Absorber pipe arrangements used in activation of energy tunnels (Dai et al., 2023)

2.3.3.2 Enertun: innovative energy segmental lining

At Politecnico di Torino, a patented design was developed to utilize shallow geothermal energy effectively while addressing key safety concerns using the segmental lining of TBM tunnels. The placement of pipes near the reinforcement cage before casting the concrete and segment installation ensures the structural integrity of the system. This approach eliminates delays for contractors, allowing the tunneling process to proceed without adverse effects on the construction timeline (Barla et al., 2019).

The pipes in the Enertun design are placed transversally, perpendicular to the tunnel axis, to optimize the flow of the heat carrier fluid and reduce bends in the circuit. This configuration significantly decreases hydraulic head losses by 20–30%, ensuring higher energy efficiency (Barla et al., 2019). Compared to previous designs with longitudinal pipe arrangement, this placement method improves performance, particularly in areas with groundwater flow, by achieving up to 10% higher heat exchange efficiency (Figure 2-17).

The Enertun system can incorporate three pipe configurations (Figure 2-18), with one placed near the extrados, the other near the intrados of the tunnel lining segments, or both. The ground configuration, with pipes near the extrados, primarily facilitates heat exchange with the surrounding ground for heating or cooling applications. In contrast, the air configuration, with pipes positioned near the intrados, is designed to interact with the thermal state of the tunnel air. These configurations are specifically designed to address diverse

operational requirements, providing adaptability for applications such as heating adjacent buildings, reducing tunnel air temperature in hot environments, or combining both functions in a single system (ground&air configuration) (Barla et al., 2019).

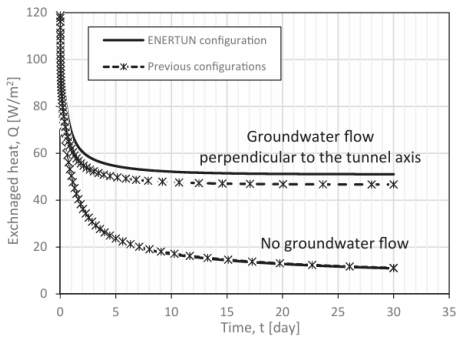

Figure 2-17. Numerical comparison between Enertun thermal output with respect to previous energy segmental lining designs

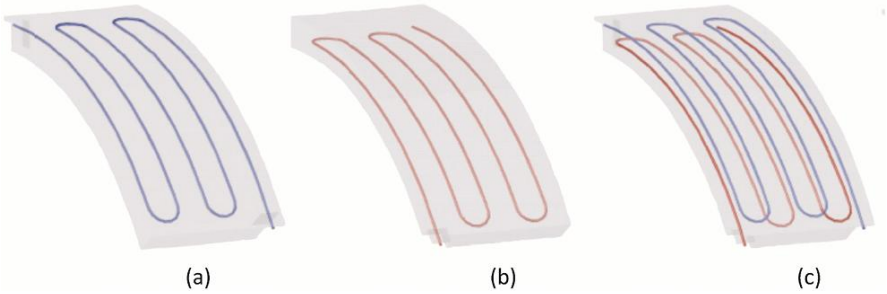

Figure 2-18. Three possible configurations for Enertun: (a) ground (b) air (c) ground&air (Barla et al., 2019)

In order to study the performance of the Enertun design in a real-world environment, a full-scale prototype was installed in the South Extension of Turin Metro Line 1. The energy segments were manufactured by embedding two separate pipe circuits—one near the extrados and one near the intrados—into the reinforced concrete segments during precasting Figure 2-19. Using Tunnel Boring Machines (TBMs), two thermally activated rings were placed in the tunnel approximately 42 meters from Bengasi Station. Hydraulic and fiber optic connections were completed on-site, forming continuous circuits for heat exchange, with header pipes linking the system to a heat pump (Barla et al., 2019).

The testing phase of the Enertun prototype began in September 2017 with the monitoring of undisturbed conditions to establish baseline data, followed by multiple tests conducted during winter 2017/2018 and summer 2018. These tests assessed the system's performance in heating and cooling modes using both ground and air configurations. A comprehensive monitoring system was employed, including vibrating wire strain gauges, fiber optic sensors, and temperature probes to measure stresses, strains, and thermal variations in the tunnel lining, as well as the temperatures of groundwater, tunnel air, and the heat carrier fluid. The thermal power extracted during the tests reached approximately 51.3 W/m², with a total heat output of 1.1 MW per kilometer of tunnel, demonstrating the system's capacity to provide energy for around 480 residential apartments. The results confirmed that the thermal activation of tunnel linings is both effective and reliable, with the stresses and strains induced remaining within safe elastic limits (Barla et al., 2019).

The final experimental scheme for evaluating the Enertun energy tunnel system included a comprehensive set of heating and cooling mode tests performed in both ground and air configurations. A total of 12 tests were carried out during the winter of 2017/2018 and the summer of 2018, with durations ranging from 1.5 to 12 days. The heat flux achieved varied from 40.8 W/m² to 66.4 W/m², with the highest performance recorded during ground cooling tests due to favorable temperature gradients and higher fluid flow rates. The results demonstrated that the system could reliably produce a thermal power of up to 1559 W/m and confirmed the efficiency of the Enertun design, which maintained consistent performance irrespective of seasonal variations and operational durations. These findings validate the system's robustness and scalability for long-term geothermal energy harvesting in tunnel infrastructures (Insana & Barla, 2020).

Figure 2-19. Absorber pipes of Enertun lining attached to the reinforcement cage during molding process (Barla et al., 2019)

2.3.3.3 Multiphysical phenomena in energy tunnels

To effectively analyze and design energy tunnels, it is crucial to understand the multiphysical processes that govern their operation. The construction and utilization of these tunnels—like other energy geostructures—involve heat transfer, mass transfer, and deformation (Laloui & Rotta Loria, 2019). During construction or thermal activation, the ground's energy balance is altered, necessitating a shift toward a new equilibrium to account for these processes. Common triggers for such disturbances include mechanical loads from the structural support function of energy geostructures, as well as thermal loads linked to their energy transfer role (Rotta Loria, 2020). Following these perturbations, heat and mass flows arise, along with expansions and contractions in both the geostructures and the surrounding ground. In conclusion, these effects stem from mechanical and thermal factors, highlighting the need for a reliable thermo-hydro-mechanical (THM) coupling to interpret energy tunnel behavior.

A thorough understanding of heat transfer processes is particularly important for capturing the full scope of the multiphysical interactions in energy geostructures. In the case of tunnel-based ground heat exchangers (GHEs), the surrounding ground, and the tunnel air—collectively referred to as energy tunnel systems—various modes of heat transfer occur (Figure 2-20). Conduction typically prevails in the ground, tunnel lining, and pipe walls, although convective processes may also emerge in the ground if groundwater flow is present.

Within the carrier fluid circulating in the pipes, forced convection is predominant, whereas heat transfer in the tunnel air space involves convection, supplemented by conduction–convection across the tunnel-wall-air interface. Additionally, heat–mass coupling (TH) appears in the absorber pipes and can extend into the groundwater and tunnel air. Thermo-mechanical coupling (TM) arises in the tunnel structure due to temperature-induced changes in the mechanical behavior of the lining, while the surrounding ground experiences thermo-hydro-mechanical (THM) coupling, reflecting the interconnected effects of temperature variations on pore water pressure and soil or rock deformation. To be able to assign the proper coupling, each of these coupled processes must be fully recognized and adequately addressed in both design and analysis.

Figure 2-21 highlights how temperature (T), hydraulic processes (H), and mechanical behavior (M) are interconnected in what is known as thermo-hydro-mechanical (THM) coupling. Temperature changes can alter fluid properties (such as density or viscosity) and cause thermal expansions or contractions in materials, which lead to stresses and strains (the T ↔ M link). Fluid flow can transport heat, affecting temperatures, while shifts in pore water pressure influence effective stress (the H ↔ T and H ↔ M links). Deformation of the soil or rock, in turn, modifies porosity, which affects how fluids move and how the ground responds to stress. In this way, the three domains—temperature, hydraulics, and mechanics—shape one another and must be analyzed together when studying or designing geotechnical systems.

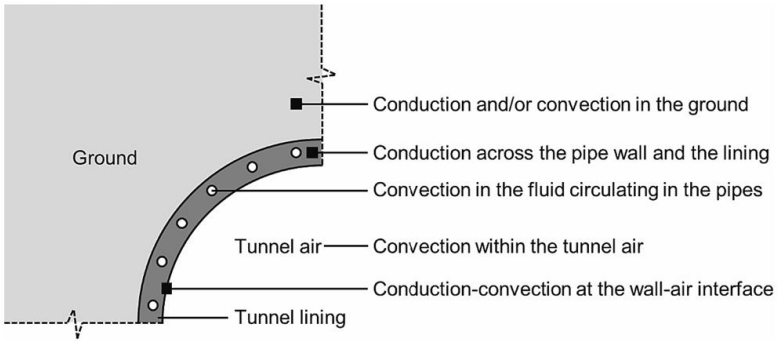

Figure 2-20. Dominant heat transfer mechanism in each component of an energy tunnel (Dai et al., 2023; Rotta Loria, 2020)

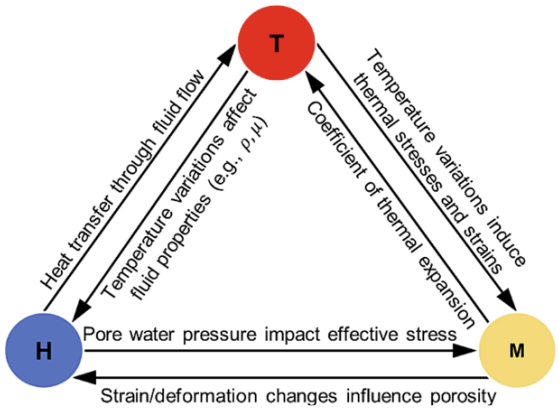

Figure 2-21. A visual depiction of the interplay between thermal, hydraulic, and mechanical factors in energy tunnels (Dai et al., 2023)

2.3.3.4 Design of energy tunnels

Designing an energy tunnel requires more than just standard geotechnical or structural checks. From the earliest planning phases, it must fit into broader urban development and energy distribution strategies. Early coordination ensures that thermal activation is integrated into feasibility studies, helping the tunnel serve sustainable goals. In practice, the design addresses two key technical issues. First, an energy optimization analysis (thermal design) is undertaken to enhance thermal output without raising costs and to assess the ground's thermohydraulic response to temperature changes. Second, a structural design follows, calculating the long-term mechanical effects that arise from those thermal loads. While fully coupled simulations exist, simpler thermo-mechanical and thermo-hydraulic models are often sufficiently accurate. These strategies, along with careful sizing of the hydraulic circuit, lay the groundwork for reliable and efficient energy tunnels (Barla & Insana, 2023). The details of the three main design stages of energy tunnels are described below, following the design flow chart for energy tunnels in Figure 2-22.

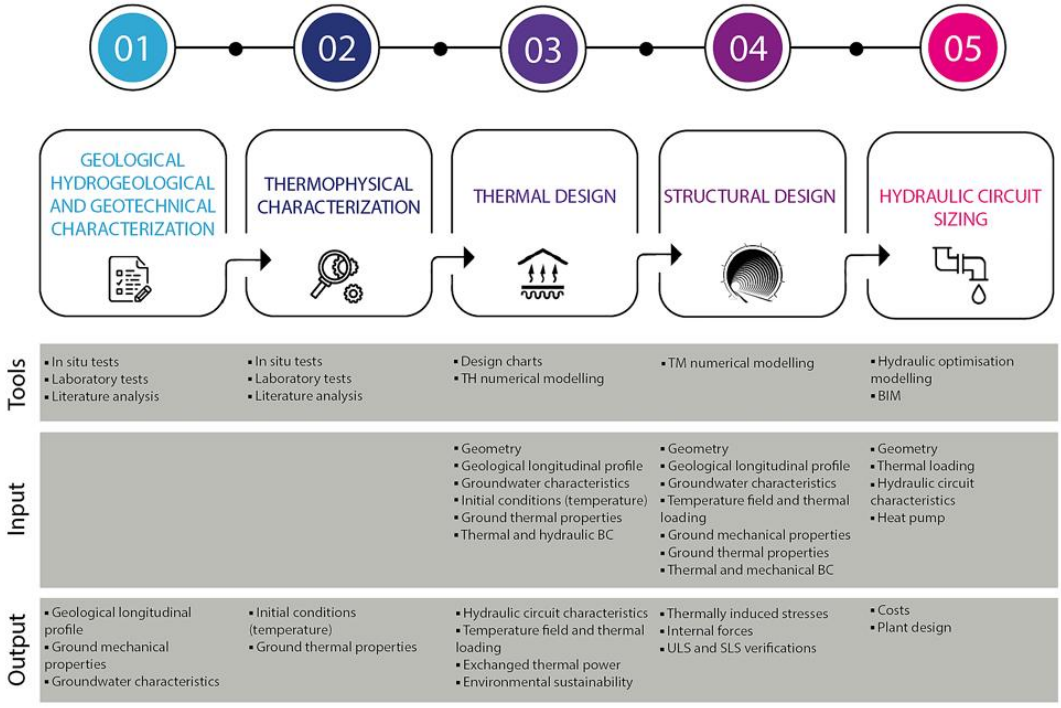

Figure 2-22. Design stages of an energy tunnel (Barla & Insana, 2023)

-Thermal Design

Although structural considerations are undeniably crucial in tunnel projects, the thermal design of an energy tunnel must be tackled at the earliest conceptual stage. This is because understanding how much heat can be exchanged between the lining and the ground lays the foundation for evaluating whether a thermal activation is financially and environmentally viable. In practice, thermal design identifies the maximum amount of heat that can be injected or extracted based on the specific geological and hydrogeological conditions of the site. These conditions include, but are not limited to, the nature of the surrounding soil or rock, and the presence and velocity of groundwater (Barla & Insana, 2023).

Once the relevant in situ parameters have been measured or estimated using the methods of testing in Figure 2-23, the design team can develop a model of the tunnel's interaction with the ground. In many projects, specialized numerical simulations are used to test different operating scenarios. By adjusting inlet temperatures and flow rates in the heat-carrying fluid, these models can mimic both summer and winter operating modes and help designers predict

the short- and long-term consequences of continuous heat exchange. For instance, a thorough approach considers whether cyclical operation—heat transfer in summer balanced by heat extraction in winter—can keep the subterranean temperature stable. This balance is crucial to ensuring that the ground is neither depleted of its geothermal potential nor overheated over time, which could negatively affect both efficiency and surrounding ecosystems.

Properties	Investigations
Thermal conductivity, λ [W/mK]	TRT, needle probe, transient plane source
Thermal specific capacity, S_c [J/kgK]	Transient plane source
Undisturbed temperature, T_0 [°C]	TRT, measures at different depths with level probe with temperature sensor
Effective porosity, n_e	Classification laboratory testing
Horizontal and vertical permeability, k_h, k_v [m/s]	Pumping tests, slug test
Groundwater flow velocity, v [m/s]	Level probe, existing groundwater maps
Groundwater depth, f [m]	Level probe, existing groundwater maps
Groundwater flow direction, df	Level probe, existing groundwater maps

Figure 2-23. Investigations for obtaining hydrogeological and thermal properties of ground for the thermal design of energy tunnels (Barla & Insana, 2023)

A key challenge facing designers of energy tunnels is the relative scarcity of specific regulations or robust, universally recognized guidelines. While broader rules exist for other energy geostructures—such as energy piles or borehole heat exchangers, an exact regulation tailored to tunnels is not yet well established. In many cases, engineers adapt proven methods from these more established systems, using them as a reference point for the scale, geometry, and unique operational conditions of tunnels. For example, thermal response testing, commonly performed on borehole heat exchangers, is also useful for tunnels. Such a test supplies direct insights into the ground's conductivity, the subsurface temperature profile, and how the ground reacts to the injection or extraction of heat over time (Barla & Insana, 2023). Nevertheless, applying these methods in the context of tunnels requires additional care. Tunnels often exhibit complex boundary conditions, especially concerning groundwater flow, which can significantly enhance heat transfer if it replenishes the thermal reservoir. In addition, because of the tunnel's geometry and length, it is essential to consider lateral and

longitudinal variations in the subsurface, as well as the surrounding environment within the tunnel itself. Factors such as air temperature and ventilation speed within the tunnel corridor can affect overall heat transfer rates.

Given the novelty of large-scale energy tunnels, a phased approach is recommended. During preliminary design, designers can rely on numerical methods or design charts of Figure 2-24 that were numerically obtained for Enertun segmental linings by Insana & Barla (2020) to perform a first-round feasibility assessment. These initial findings help decide whether to proceed with a more detailed study. If the results appear geothermally promising, a second phase featuring advanced numerical modeling can capture three-dimensional flow and heat transfer effects, changes in groundwater head, and any anisotropies in soil or rock. Where possible, the thermal design should also include an environmental impact assessment to determine whether local aquifers or ecosystems might be compromised by shifts in temperature over the operational life of the tunnel (Barla & Insana, 2023).

Ultimately, addressing thermal design at the earliest planning phase sets the stage for efficient resource use and minimal environmental disruption. By engaging in thorough site investigations, employing robust numerical tools, and following up-to-date guidelines in the energy geostructure sector, designers can help ensure that energy tunnels fulfill their potential as safe, reliable, and sustainable thermal components of modern cities.

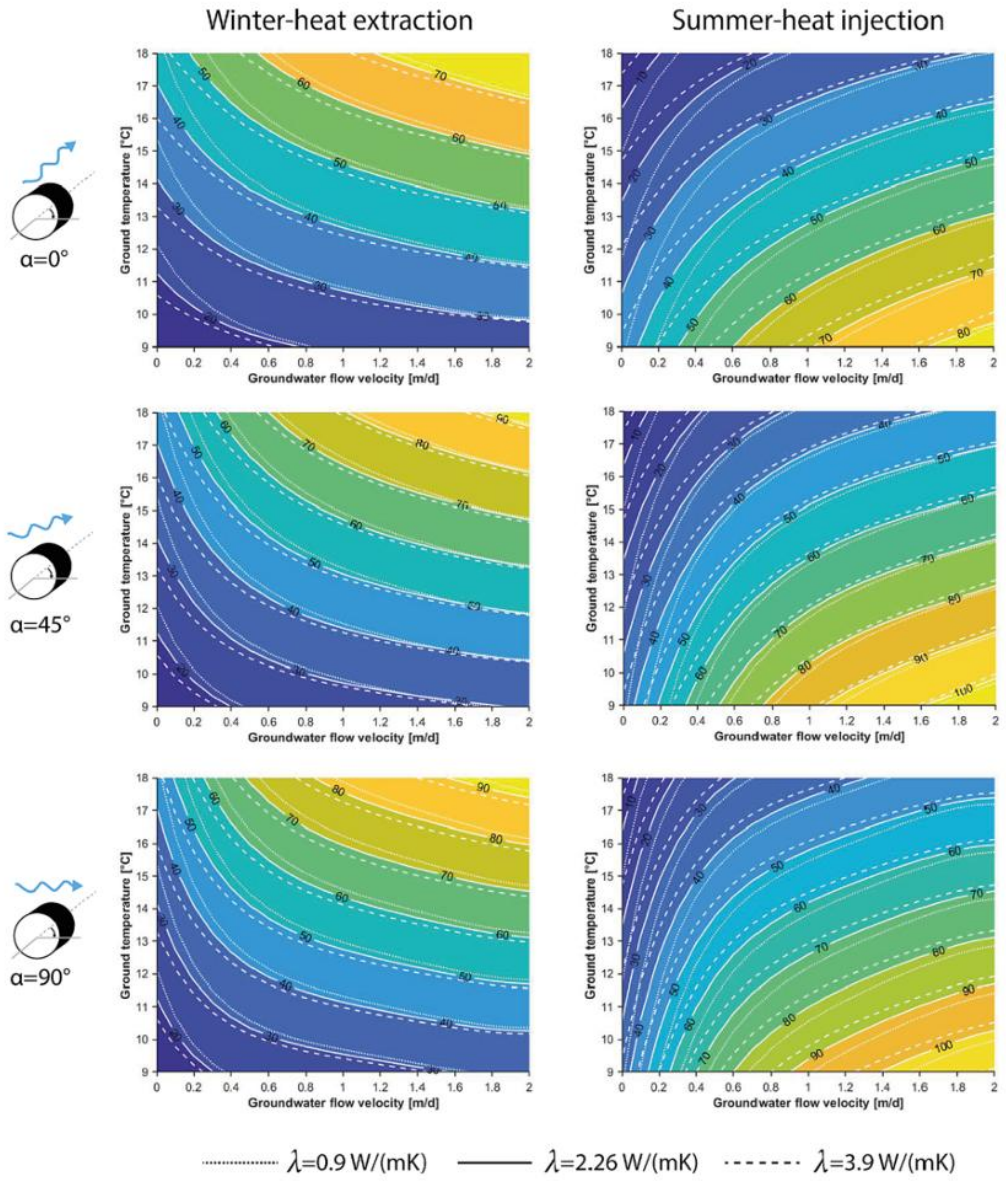

Figure 2-24. Energy tunnel design charts displaying geothermal potential (W/m²) for winter and summer, considering different groundwater flow directions (0°, 45°, and 90°) relative to the tunnel axis (Insana & Barla, 2020)

- *Structural Design*

Structural design in energy tunnels focuses on the additional stresses that arise from thermal activation. Once the tunnel lining is equipped with heat exchanger pipes, circulating fluid can significantly alter temperature distributions within the concrete, thereby influencing

internal forces. Typically, the design must account for seasonal changes, such as heating in winter and cooling in summer, which can create cyclical variations in temperature and stress over the tunnel's service life. In essence, structural engineers must treat thermal activation as another load case, added to the conventional mechanical loads that come from earth pressure, groundwater conditions, and traffic or operational requirements.

Research on energy geostructures, including energy piles, has provided initial guidance on this topic, although no official standards exist specifically for energy tunnels. Still, experimental evidence offers important insights. For instance, studies conducted on Turin Metro Line 1 in alluvial settings showed that the tunnel lining experiences measurable expansions or contractions in the circumferential (hoop) direction as the fluid temperature changes. Under winter operation, the lining cools by 4-6 °C, leading to a small contraction of tens of microstrains and a small drop in compressive stress in the order of several MPa (Insana, 2020). In summer, the lining warms, causing slight expansion and a moderate increase in compressive stress. The magnitude of these fluctuations often remains within a range that does not jeopardize structural integrity. In fact, observed hoop strain changes rarely exceed a few tens of microstrain, suggesting that existing design margins in reinforcing steel and lining geometry are typically adeq(Barla & Insana, 2023).

In projects where more stringent conditions or larger temperature variations are anticipated, designers can perform detailed numerical analyses to capture soil-structure interaction and how heat transfer modifies the stress state. Such thermo-mechanical modeling requires input data on the thermal expansion coefficients of both the concrete and surrounding soil, along with accurate values for the ground's stiffness and strength parameters. The model usually reproduces tunnel construction sequences, then adds the effects of fluid flow and temperature cycles to predict potential stress redistribution. Although this added complexity is justified in high-sensitivity situations, many case studies indicate that, under normal temperature ranges, the lining remains well within safe operating limits. Nonetheless, thorough verification remains crucial because repeated temperature cycles can accumulate and might lead to amplified stresses over time (Barla & Insana, 2023).

Overall, the structural design for energy tunnels must integrate thermal activation into early planning documents so that potential stress variations are accounted for from the outset. This approach not only helps avoid underestimating mechanical demands but also ensures that the chosen lining thickness, reinforcement details, and material properties can handle both conventional loads and periodic thermal shifts without compromising serviceability or long-term durability.

- *Hydraulic network sizing and preliminary cost analysis*

As part of the design process, the hydraulic network that circulates the heat carrier fluid and connects to the heat pump must be tailored for both installation and operational efficiency. Finding the optimal circuit cross-section involves striking a balance between installation costs, which rise with larger diameters, and pumping costs, which tend to drop due to reduced head losses (Rosso et al., 2022). Additional considerations include economic factors (e.g., pipes installation costs and energy prices), thermal comfort targets (e.g., heat exchanger utilization rates), and practical constraints (e.g., pipe length and inlet temperature). Since every site's geometry, energy demand profile, and potential client base vary, these elements must be integrated into a site-specific cost-benefit analysis (Barla & Insana, 2023).

Evaluating costs primarily entails identifying the extra expenses linked to thermal activation beyond standard tunnel construction. These typically involve purchasing and embedding the pipes in precast segments at the manufacturing plant, and the slight increase in workforce required for segment connections and header pipe installations. At the Turin Metro Line 1 test site, for instance, analyses were performed on multiple circuit configurations, calculating installation costs, head losses, and pumping energy requirements. Thermo-hydraulic simulations provided data on the heat power extracted, thereby indicating potential revenues. The findings, shown in Figure 2-25, reveal that an "all-in-parallel" arrangement gives the highest revenue-to-cost ratio for tunnel lengths up to 450 m. Beyond that distance, two rings in series become more advantageous, underscoring the importance of tailoring network design to each project's length and operational demands (Barla & Insana, 2023).

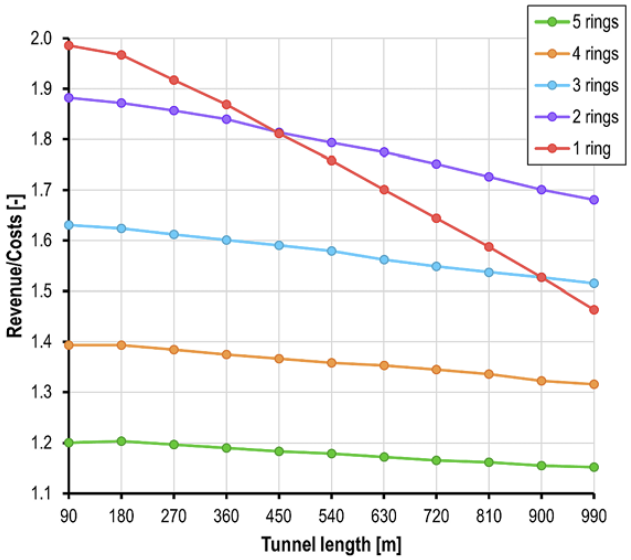

Figure 2-25. Ratio of revenue to costs for various configurations and tunnel lengths, based on operation for 180 days per year at 12 hours per day (Barla & Insana, 2023)

3 Thermo-hydraulic energy tunnel modelling

Engineers have the responsibility of constructing safe structures, an obligation that needs a robust design for ensuring safe performance under various conditions. To accomplish this, the actual behavior of a structure to be designed and constructed must be evaluated in advance, which has resulted in the advancement of several methodologies for performance assessment: analytical solutions, full-scale testing, physical modeling, and numerical modeling. Among these, numerical modeling distinguishes itself for its capability to reproduce complex real-world scenarios with high precision and adaptability. It enables engineers to simulate complex geometries, nonlinear material responses, and multi-physics interactions that are challenging or impossible to tackle using alternative methods. Furthermore, numerical modeling substantially reduces cost and time in comparison to full-scale testing and physical modeling while providing a deep understanding of structural or environmental reactions. This methodology not only enhances the safety and dependability of designs but also promotes innovation by facilitating the investigation of various design alternatives in a virtual setting.

As previously described, the energy tunnels' behavior consists of a simultaneous interplay among thermal, hydraulic and mechanical processes. The most accurate numerical method to simulate this behavior would be a fully coupled THM model. At the same time, it is necessary to find the most efficient, yet feasible, thermal performance for the energy tunnel

based on the available pipe circuit options and characteristics of the tunnel-ground-air system (i.e. thermal design). This design stage allows for the exclusion of mechanical processes from the numerical model when their influence on the thermal performance of the energy tunnel is negligible. This can happen when the effect of mechanical deformations on the pore structure and the resulting changes in thermal and hydraulic conductivities of the domain are neglected.

3.1 Key elements in thermal evaluation of energy tunnels

Numerical models of energy tunnels inevitably have some degree of simplification of real-world conditions. To select an appropriate level of simplification (or to critically assess existing models), it is essential to identify the key influential factors for thermal performance of energy tunnels. If an energy tunnel is placed at a depth where the ground surface air temperature fluctuations do not impact the geothermal output of the system, the key influential factors for the thermal performance would be the ground, tunnel lining, tunnel internal environment, absorber pipes, and the thermal operation mode as shown in Figure 3-1 (Dai et al., 2023; Magdy et al., 2025). The ground effect can vary in terms of the presence of various phases in it. The solid particles, water and air presence can affect the average thermal conductivity of the medium. Additionally, the presence of flowing groundwater can add thermal convection to the heat transfer mechanism of the ground. Tunnel lining can have two main effects on the thermal performance of the tunnel; one is its geometrical and material properties that can influence the conduction that occurs between the pipes and the lining itself. The other is the roughness of the intrados surface that can affect the amount of heat exchange between the tunnel air and the lining itself. Tunnel air flow characteristics also influence the thermal exchange with the lining through its temperature, flow velocity and turbulence. The absorber pipes wall thickness have a role on the conduction from the circulating fluid and the surrounding lining, while the fluid flow velocity, temperature, and turbulence along with pipe diameter impact the geothermal performance of the system through forced convection. Thermal operation mode of the energy tunnel is important since

it is always possible to limit the continuous 24/7 operation to less hours per day (e.g. 8 h ON/16 h OFF) to allow for thermal recharge of the ground when the system's geothermal output has no demand. This offers a higher geothermal output for the following day after the shutoff period.

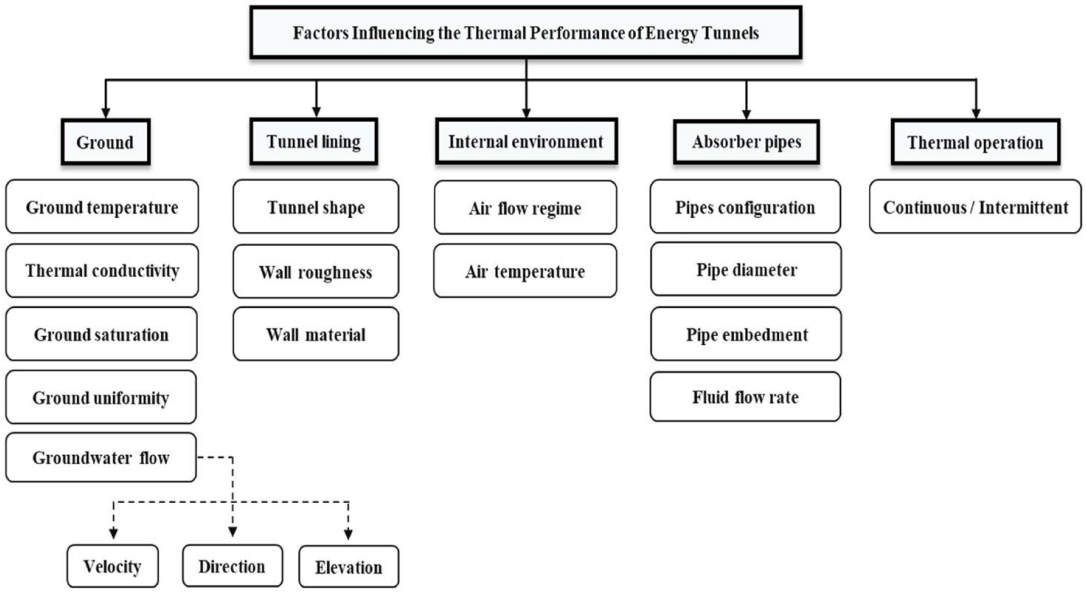

Figure 3-1. Factors influencing the thermal performance of energy tunnels (Dai et al., 2023; Magdy et al., 2025)

3.2 Thermo-hydraulic simulation of energy tunnels in COMSOL

In this study, it is necessary to simulate the thermo-hydraulic behavior of energy tunnels. For doing so the finite element software, COMSOL Multiphysics will be used where it is possible to have a coupled analysis for these energy geostructures. Therefore, the assumptions and laws that allow this simulation in this numerical tool will be introduced in this section. Therefore, three study steps are considered for a coupled thermo-hydraulic

simulation of an energy tunnel under the influence of groundwater flow. Note that the geometry, mesh and specifications of the study are going to be discussed in the next chapter.

It can be assumed that groundwater flow is only inside the soil domain, while the tunnel lining and the grout are solids of non-porous media. Therefore, a first hydraulic steady-state study step can be performed to reproduce the long-term groundwater flow around the already-constructed tunnel. The groundwater flow velocity can be calculated in various ways in COMSOL's subsurface flow module:

- *Darcy's law*

When restrictive hydraulic boundary conditions cause certain zones of the soil to be either fully saturated or completely dry, Darcy's law can be used to calculate the groundwater flow velocity within the fully saturated regions. It is suitable for modelling low-velocity flows in the porous media with very low permeability and porosity, where the pressure gradient is the major driving force and the flow is mainly affected by the frictional resistance inside the pores (COMSOL AB, 2022). The equation for groundwater flow velocity would be:

$$u_{\mathrm{w}} = -\frac{\kappa}{\mu_{\mathrm{w}}}(\nabla p_{\mathrm{w}} - \rho_{\mathrm{w}} g \nabla D) \tag{5}$$

Where u_w represents the Darcy velocity, κ is the permeability of the soil, μ_{w} is the dynamic viscosity of the groundwater, p_w is the groundwater pressure, ρ_{w} is the density of the groundwater, g is the gravitational acceleration vector, and ∇D is a unit vector in the direction over which the gravity acts. In Darcy's law fluid flows by pressure gradients and gravitational forces, with permeability controlling the ease of water movement through the soil.

- *Richard's equation*

If it is intended to calculate the groundwater flow velocity inside a variably saturated soil, Richard's equation can be used in COMSOL. Unlike Darcy's law, which assumes a fully saturated medium, Richard's equation accounts for the effects of capillary pressure, relative permeability, and moisture retention. This enables modelling both saturated and unsaturated

flow regimes inside the ground. As the groundwater moves through the soil, pores will be saturated or drained, leading to variable hydraulic properties inside the domain. Here, the air is assumed to be immobile and at atmospheric pressure. This allows Richards' equation to inherently determine the groundwater table position, as it models the transition between saturated and unsaturated zones based on moisture content and pressure head variations, eliminating the need for an explicit water table definition by geometrical constraints (COMSOL AB, 2022). Eventually, the groundwater flow velocity can be calculated by Richards' equation using the following equation:

$$u_{\mathrm{w}} = -\frac{\kappa_{\mathrm{s}}}{\mu_{\mathrm{w}}} k_{\mathrm{r}} (\nabla p_{\mathrm{w}} - \rho_{\mathrm{w}} g \nabla D) \tag{6}$$

Where κ_{s} is the hydraulic permeability and k_{r} is the relative permeability. As seen in this equation, a retention model is needed to account for relative permeability of each point of the porous medium. In COMSOL, there are van Genuchten, Brooks and Corey, and user defined retention models available to account for this parameter.

- Brinkman equation

The Brinkman equation is used for modelling faster groundwater flows in porous media. It accounts for the effects of pressure, gravity, and fluid velocity (similar to Darcy's law), but also considers kinetic energy losses due to viscous shear (similar to the Navier-Stokes equations). This makes it suitable for cases where the flow transitions from slow movement in porous materials to faster flow in open channels (COMSOL AB, 2022). This can be useful for determining the groundwater flow conditions when an energy geostructure is about to be built close to an existing river, in a highly permeable soil. The groundwater flow velocity by Brinkman equation is calculated by the following equation:

$$\nabla p_{\mathrm{w}} + \frac{\mu_{\mathrm{w}}}{\kappa} u_{\mathrm{w}} - \mu_{\mathrm{e}} \nabla^2 u_{\mathrm{w}} - \rho_{\mathrm{w}} g \nabla D = 0 \tag{7}$$

Where μ_{e} is the effective dynamic viscosity of the groundwater.

More advanced methods of calculating the multiphase movements inside the ground are available in the manual of the software but are not described here.

Now that the groundwater flow is determined inside the soil, a second time-dependent thermo-hydraulic study step can be performed to calculate the in-situ temperatures of the lining, grout and ground before absorber pipe activation. To do this, it is assumed that the groundwater saturation degree, flow velocity and direction of the previous study step does not change for all time steps and is not affected by temperature variations. The heat transfer module of COMSOL is used by assuming thermal conduction inside the grout and lining, while the soil domain can experience both thermal conduction and convection in case of a non-zero groundwater flow velocity.

The thermal conduction in the grout and the lining occurs according to the following equation:

$$\rho_{\mathrm{s}} C_{p,s} \frac{\partial T}{\partial t} - \nabla \cdot (\lambda_{\mathrm{s}} \nabla T) = 0 \tag{8}$$

Where $\rho_{\mathrm{s}} C_{\mathrm{p,s}}$ represents the volumetric heat capacity of the grout or lining at constant pressure, T is temperature, t is time and λ_{s} is the thermal conductivity of the grout or lining.

The heat transfer equation for the soil around the tunnel by assuming the local thermal equilibrium between the solid grains and the groundwater is:

$$\left(\rho C_p\right)_{\mathrm{eff}} \frac{\partial T}{\partial t} + (\rho_w C_{p,\mathrm{w}} u_{\mathrm{w}}) \nabla T - \nabla \cdot (\lambda_{\mathrm{total}} \nabla T) = 0 \tag{9}$$

Where $\left(\rho C_p\right)_{\mathrm{eff}}$ represents the effective volumetric heat capacity of the porous medium at constant pressure, $\rho_w C_{\mathrm{p,w}}$ is the effective volumetric heat capacity of the water at constant pressure, λ_{total} is the total thermal conductivity of the porous medium (accounting for the combined effect of the thermal dispersion and the effective thermal conductivity of all the elements of the porous medium).

In the final study step the coupled thermo-hydraulic analysis is performed by activating the absorber pipes and having the previous step's solution as the initial condition. The heat transfer mechanism inside the pipes is a forced convection that can be simulated using 3D elements which is computationally expensive and increases the needed mesh elements dramatically. However, COMSOL offers the possibility to simulate the heat and fluid transfer in the model by assigning 1D elements to the pipes using the heat transfer in pipes module.

In this way, it is assumed that the velocity profile is fully developed throughout the entire pipe section. While the cross-sectional area is allowed to vary between and within pipe segments, empirical functions such as friction charts are used to describe the viscous pressure drop for both laminar and turbulent flow regimes. The curvature of the pipe is considered to have a negligible effect on pressure loss compared to wall friction. Additionally, shocks are neglected, and all velocity components normal to the pipe axis are assumed to be zero (COMSOL AB, 2022). The heat transfer equation for the fluid within the pipes is:

$$\rho_f A C_{p,\mathrm{f}} \frac{\partial T}{\partial t} + \rho_f A C_{p,\mathrm{f}} u_f \cdot \nabla T = \nabla \cdot \left(A \lambda_f \nabla T \right) + Q_{\mathrm{wall}} \tag{10}$$

Where ρ_f represents the density of the circulating fluid, A is the pipes cross sectional area, $C_{\mathrm{p,f}}$ is the heat capacity of the circulating fluid at constant pressure, u_f is the velocity of the circulating fluid within the pipes, λ_f is the thermal conductivity of the circulating fluid and Q_{wall} is the heat exchanged through the pipe wall that is determined by:

$$Q_{\mathrm{wall}} = U P_{\mathrm{p}} (T_{\mathrm{ext}} - T_{\mathrm{f}}) \tag{11}$$

Where P_{p} is the wetted perimeter of the pipe, T_{ext} is the temperature on the outer side of the pipe, T_{f} is the circulating fluids temperature, and U the effective heat transfer coefficient of the pipes and its equation is going to account for the pipe wall thickness as below:

$$U = \frac{1}{\frac{1}{h_{\mathrm{int}}} + \frac{r_{\mathrm{int}}}{\lambda_{\mathrm{p}}} \ln\left(\frac{r_{\mathrm{ext}}}{r_{\mathrm{int}}}\right)} \tag{12}$$

Where r_{int} and r_{ext} are internal and external pipe radii, respectively, λ_{p} is the pipe wall thermal conductivity, and h_{int} is the film heat transfer coefficients on the inside of the pipe and calculated as below:

$$h_{\mathrm{int}} = \frac{Nu \cdot \lambda_{\mathrm{p}}}{d_{\mathrm{h}}} \tag{13}$$

Where Nu is Nusselt number and d_{h} is the hydraulic diameter of the pipe. It is important to note that one positive factor for increasing the thermal exchange rate of the absorber pipes is having a turbulent flow withing the pipes. This effect is implemented in the model indirectly by the Nusselt number. In COMSOL's heat transfer in pipes module a constant

Nusselt number is assumed for a laminar 1D pipe flow, while this value is going to be higher by increasing the Reynolds number for turbulent pipe flow. Further details about the formulation and exact Nusselt number choices can be found in COMSOL's manual (COMSOL AB, 2022). Having a higher Nusselt number increases the thermal exchange rates of the pipe wall with the lining, leading to a higher geothermal performance for the energy tunnel.

To add the influence of the tunnel internal air on the thermal exchange processes of the model, COMSOL allows a complete thermo-hydraulic 3D simulation of air movements inside the tunnel. However, it is also possible to avoid meshing and simulating the air itself by assigning a simpler thermal boundary condition on the tunnel intrados. Four boundary conditions for this purpose are introduced here:

- *Thermal insulation*

Using this boundary condition the effect of tunnel air on the results are completely ignored. This could be useful in cases where the intention is to avoid influencing the tunnel air during geothermal heat exchange or it would be of interest to see how much the geothermal performance of the energy tunnel would be affected without considering the tunnel air contribution.

- *Dirichlet boundary condition*

In COMSOL this boundary condition is called "Temperature", where a constant temperature is assigned to the tunnel intrados. Here, it is assumed that regardless of the heat fluxes within the lining, grout and ground, the temperature of the tunnel intrados is unchangeable. While this assumption is simple and computationally economic, it ignores the realistic temperature difference between the tunnel's internal air and intrados.

- *Neumann boundary condition*

In COMSOL this boundary condition is called "Heat Flux", where a constant heat flux is assigned to the tunnel intrados. Applying this boundary condition is a challenging due to the need for knowing the exact heat transfer rate between the tunnel intrados and the tunnel's internal air. Also, the exact heat transfer rate is rarely known in advance not to mention its changes with respect to time and space. Another disadvantage of this boundary condition is that the heat transfer rate is irrespective of the temperature difference between the tunnel air and intrados.

- *Cauchy boundary condition*

In COMSOL this boundary condition is called "Convective Heat Flux", where a constant heat flux is assigned to the tunnel intrados. This boundary condition assumes that the heat flux on the intrados is proportional to the temperature difference between the intrados and the tunnel internal air, and is determined by the equation below:

$$q = h_{air}(T_{air} - T_{intrados}) \quad (14)$$

Where q is the heat flux on the tunnel intrados, h_{air} is the heat transfer coefficient, T_{air} is the tunnel air temperature far from the intrados, and $T_{intrados}$ is the temperature on the intrados.

This boundary condition faces two major challenges: one is that the heat transfer coefficient is difficult to estimate due to dependency on the tunnel air velocity and turbulence, and surface roughness. Second, the air temperature is fixed and not influenced by the heat exchange that will happen between the lining and the tunnel air. Overall, this boundary condition is the best choice for simulating the effects of tunnel air on the geothermal performance of energy tunnels when the air's physical presence and movement is not simulated.

The last aspect of energy tunnel modelling is the operation mode. Both continuous and intermittent operation modes can be simulated in COMSOL by assigning proper time steps for activation period of absorber pipe.

3.3 Adaptation of assumptions from FEFLOW to COMSOL

Prior to construction of the south extension of the Turin Metro Line 1 towards Piazza Bengasi, a 3D thermo-hydraulic analysis was performed using FEM code FEFLOW to assess the geothermal potential of thermally activated segments of this tunnel's lining in the future (Barla et al., 2016). This study showed that constructing energy tunnels with longitudinal absorber pipes in this part of the Turin ML1 allows 53 and 74 W/m^2 of geothermal energy to be exploited in winter and summer, respectively. This promising energy outlook was further enhanced up to 10 % in a later, yet similar, study in FEFLOW using ENERTUN pipe configuration by Barla & Di Donna (2018). Therefore, the ENERTUN pipe configuration was used during the construction of the Turin ML1 energy tunnel for its high energy output and lower hydraulic head losses. A field test campaign was undertaken on this energy tunnel by Insana & Barla (2020) whose thermal responses lead to the first FEFLOW-based validation of a TH energy tunnel model against experimental results. This validation paved the way for generating the design charts of Figure 2-24 through a series of parametric studies in the same study using FEFLOW.

In the present study it is intended to reproduce a similar numerical model used by Insana & Barla (2020) in FEFLOW in COMSOL to have a validated base model that allows investigating the effect of diameter changes on the geothermal performance of energy tunnels. For this purpose, it is needed to understand the assumptions or laws that governed the thermo-hydraulic processes of the energy tunnel model in the FEFLOW model. The numerical models of the study for both validation and design chart simulations were almost similar. However, the soil domain was not fully saturated for the model of validation against the field data. Therefore, mesh elements above the water table were assigned to be dry with no thermal convection.

Obtaining a verified or validated model in COMSOL can be done by using two sets of reliable results, one is the design charts readings of Insana & Barla (2020), where the attempt should be to use, as far as possible, the same assumptions and parameters of FEFLOW in COMSOL. In this way, any room for improvement of the model like inputting the pipe wall

thickness to the model to implement its thermal effects into the geothermal performance of the energy tunnel should be avoided. In other words, replicating the inputs and assumptions of the FEFLOW model makes the COMSOL model closer to the reliable results of the design charts. The second method would be to validate the COMSOL model against the field test results of Insana & Barla (2020), in this way minor improvements can be implemented to the model for better representation of the insitu conditions. therefore, it is possible to use Richards' equation instead of Darcy's law for automatic determination of the water table inside the soil and add the pipe thickness to the 1D pipe properties to have its thermal resistance effect in the model. Knowing that the COMSOL model has three study steps, the relevant assumptions of FEFLOW models in both validation and design chart generation phases are mentioned in Table 3-1 along with the approaches to replicate or improve them in COMSOL.

Table 3-1. Adapting the COMSOL model to FEFLOW models' assumptions used by Insana & Barla (2020)

COMSOL study step	**Model of** Insana & Barla (2020)	**Related FEFLOW assumptions**	**COMSOL approach**
Hydraulic (1st)	Validation	- Lining and grout: no groundwater flow by zero porosity assignment - Soil: Darcy's law below water table and no flow above it	- Lining and grout: not selected for hydraulic study - Soil: a) geometrically assigning the water table and imposing Darcy's law below it or b) using Richards' equation with van Genuchten retention model for automated water table and flow calculations
	Design charts	- Lining and grout: no groundwater flow by zero porosity assignment - Soil: fully saturated and Darcy's law in all the domain	- Lining and grout: not selected for hydraulic study - Soil: fully saturated and Darcy's law in all the domain
Thermo-hydraulic (2nd)	Validation	- Lining and grout: conduction - Tunnel air: its effect is indirectly applied by a Cauchy boundary condition - Soil: thermal convection and conduction below water table and above that only conduction occurs	- Lining and grout: conduction - Tunnel air: its effect is indirectly applied by the same Cauchy boundary condition - Soil: a) thermal convection and conduction below water table and above that only conduction occurs or b) both convection and conduction happen where Richard's equation allows a groundwater flow, if not there is only conduction
	Design charts	- Lining and grout: conduction - Tunnel air: its effect is indirectly applied by a Cauchy boundary condition - Soil: both thermal convection and conduction occur in all the saturated domain with non-zero groundwater velocity otherwise only conduction due to a zero darcy velocity	- Lining and grout: conduction - Tunnel air: its effect is indirectly applied by the same Cauchy boundary condition - Soil: both thermal convection and conduction occur in all the saturated domain with non-zero groundwater velocity otherwise only conduction due to a zero darcy velocity
Thermo-hydraulic (3rd)	Validation	- Lining, grout, tunnel air and lining: same as previous step's model - Absorber pipes: forced convection in 1D elements without considering the pipe wall thermal resistance	- Lining, grout, tunnel air and lining: same as previous step's model - Absorber pipes: forced convection in 1D elements with the possibility of having the thermal effects of pipe thickness through heat transfer formulations
	Design charts	- Lining, grout, tunnel air and lining: same as previous step's model - Absorber pipes: forced convection in 1D elements without considering the pipe wall thermal resistance and thickness	- Lining, grout, tunnel air and lining: same as previous step's model - Absorber pipes: forced convection in 1D elements with a negligible input pipe thickness to replicate the FEFLOW analysis

3.4 Summary

This chapter tries to introduce the assumptions and laws that are useful for thermo-hydraulic simulation of energy tunnels based on its structural, geothermal, and surrounding elements. Since COMSOL will be used for numerical modelling in this research the relevant assumptions and laws of the following chapters will be introduced. Achieving the reliability of the numerical model of the present study requires the replication of valid numerical or experimental results of previous energy tunnel studies in the literature. In the COMSOL, the assumptions used in the FEFLOW simulations should be maintained (as far as possible) or can be improved (to better represent the field tests), depending on whether the objective was to reproduce previously obtained numerical results or experimental data.

4 Model setup: from numerical verification to field validation

One of the most widely used numerical techniques for modeling complex engineering problems is the Finite Element Method (FEM). FEM divides a structure or domain into smaller, manageable elements, allowing engineers to solve governing equations for stress, strain, heat transfer, and fluid flow with sufficient precision. Its versatility makes it particularly suitable for solving problems involving coupled processes, such as Thermo-Hydro-Mechanical (THM) interactions, which are crucial in analyzing energy tunnels. To perform a Thermo-Hydro-Mechanical (THM) analysis, software programs like COMSOL Multiphysics provide a suitable platform for integrating various physical phenomena within a single model. As discussed in the previous chapter, COMSOL allows a simpler coupled thermo-hydraulic simulation of energy tunnels, enabling a thermal design of energy tunnels with neglecting the effects of mechanical processes on the geothermal performance of energy tunnels. This is done by simulating the heat transfer between the ground, tunnel lining, and embedded systems, as well as groundwater flow and fluid transport within absorber pipes. Its flexible and powerful solver capabilities allow detailed insights into the thermal efficiency of energy tunnels.

The main goal of this chapter is to make a reliable base model that allows parametric studies on its tunnel diameter. To achieve this goal, the first attempt would be to recreate the same model used for generating design charts by Insana & Barla (2020) in COMSOL and verify it against the charts themselves to have a reliable base model for further analyses. If this fails, the next step would be recreating the same or a bit improved model that was used for validation against field tests by Insana & Barla (2020) in COMSOL to validate the software against the same tests. Now that the validation of the software is complete, it is possible to optimize the input parameters of design chart stage of Insana & Barla (2020) to have a reliable base model. Eventually, this base model can generate similar charts of Figure 2-24 that need validation against previous case studies. The same model can be used in the next chapters for studying the effect of diameter changes in geothermal performance of energy tunnels.

4.1 Thermo-hydraulic verification of the numerical model

Finite element methods (FEM) are widely regarded as a reliable numerical modeling tool in engineering, particularly for simulating complex systems like energy tunnels. However, ensuring the accuracy of such simulations requires validation through reliable field measurements, experimental tests, analytical solutions, or previously validated numerical results from the literature. In a previous study, the 3D FEM software FEFLOW was used to reproduce the measured thermal performance of the energy tunnel of Turin Metro Line 1 by a coupled Thermo-Hydraulic analysis (Insana & Barla, 2020). This validation against the field tests allowed the researchers to confidently use their numerical model for investigation of the effect of ground water velocity and direction, thermal conductivity of ground, and in situ temperature on the geothermal potential of energy tunnels in terms of W/m^2 of outer tunnel lining surface for heating or cooling modes in the design charts of Figure 2-24. It is important to know that in numerical simulations or field tests, the calculation of the geothermal energy output rate for a single absorber pipe loop is done by the following equation:

$$\dot{Q} = \dot{m} c_{\mathrm{f}} (T_{\mathrm{out}} - T_{\mathrm{in}}) \quad (15)$$

Where $\dot{Q}$, $\dot{m}$, c_{f}, T_{out} and T_{in} are the rate of thermal energy (in W), rate of mass flow inside the absorber pipes (in kg/s), heat capacity of the circulating fluid at constant pressure (in $J.kg^{-1}.°C^{-1}$), circulating fluid outlet temperature (in °C) and circulating fluid inlet temperature (in °C), respectively. Finally, the geothermal potential of the design charts is calculated by the following equation:

$$\dot{q} = \frac{\dot{Q}}{\pi D_{\mathrm{out}} L} \quad (16)$$

Where $\dot{q}$, D_{out} and L are geothermal potential (in W/m^2), outer tunnel lining diameter and longitudinal length of the tunnel ring parallel to the tunnel axis, respectively.

To evaluate the numerical reliability of the coupled 3D Thermo-Hydraulic (TH) energy tunnel analyses in COMSOL, the same simulation will be carried out in COMSOL Multiphysics, using, as closely as possible, the same geometry, parameters, initial conditions, and boundary conditions as in the previous FEFLOW model from the design charts. By comparing the results from COMSOL with the design chart values, the consistency of the model can be assessed, and the accuracy of the COMSOL solution can be verified. This ensures that the numerical results align with established data, confirming the reliability of the FEM-based approach of the present study for energy tunnels.

4.1.1 Governing equations

To simulate groundwater movement in fully saturated soil around the tunnel, Darcy's law (eq. 5) is applied as the governing principle. This law describes groundwater flow through the porous media by assuming a linear relationship between the velocity of the groundwater and its pressure gradient. To satisfy the mass conservation for the groundwater flow, the continuity equation must also be considered:

$$\nabla \cdot (\rho_{\mathrm{w}} u_{\mathrm{w}}) = 0 \quad (17)$$

The heat transfer equation for the saturated soil around the tunnel by assuming the local thermal equilibrium between the solid grains and the groundwater was shown in equation 9

of the previous chapter. The heat transfers by conduction in the grout and the lining according to equation 8 of the previous chapter. Also, the heat transfers by forced convection within the 1D elements with a negligible pipe thickness as input, according to equation 10 of the previous chapter.

4.1.2 Geometry and meshing of the domain

The geometry of the model matches the one that was used in obtaining design charts of Figure 2-24 that were generated by Insana & Barla (2020), therefore the soil domain has the dimensions of 149.6 × 74.8 × 21 m (Figure 4-1). The tunnel axis is placed at a depth of 16.6 m below the ground surface with an inner tunnel radius of 3.44 m. The lining and grout thickness values are equal to 30 and 11 cm, respectively (Figure 4-2). The tunnel lining consists of 15 parallel rings of 1.4 m length that are formed by 6 identical segments each (Figure 4-3-a). The geothermal pipes in the ground configuration are modeled as one-dimensional lines positioned 6 cm away from the outer surface of the segmental linings (Figure 4-3-b). Consequently, their placement corresponds to a radius of 3.68 m from the central axis of the tunnel. As for the design charts model, the piping for a single segmental lining includes four bends, resulting in a pipe spacing of 27.5 cm. Additionally, the first and last rows of pipes have a 15 cm distance from the segments' starting and ending surfaces, respectively.

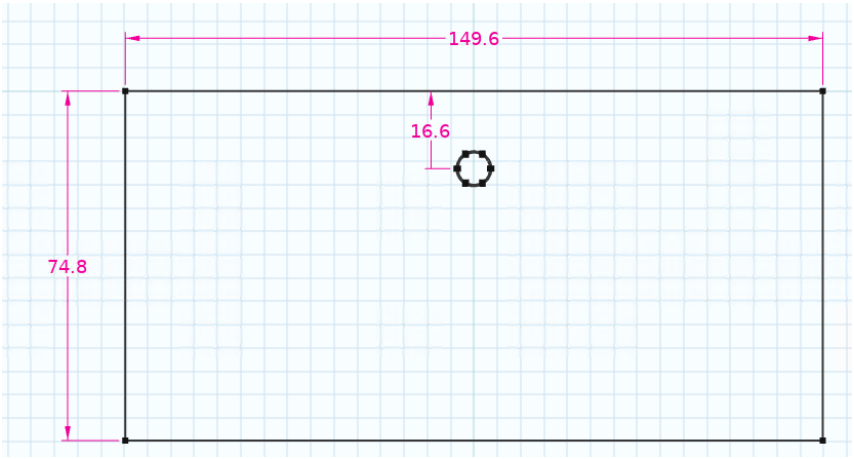

Figure 4-1. Cross-sectional view of the model geometry (dimensions are in meters)

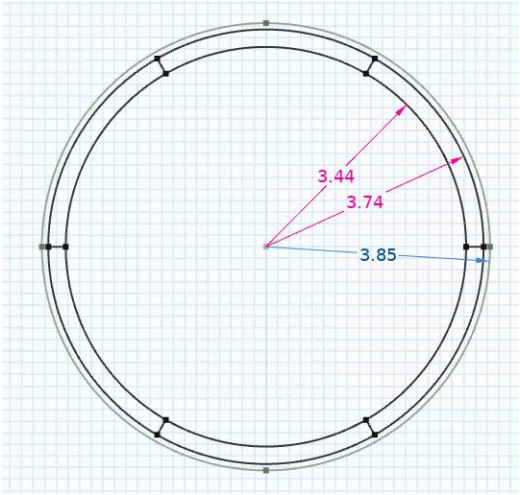

Figure 4-2. Cross-sectional view of the tunnel lining and grout (dimensions are in meters)

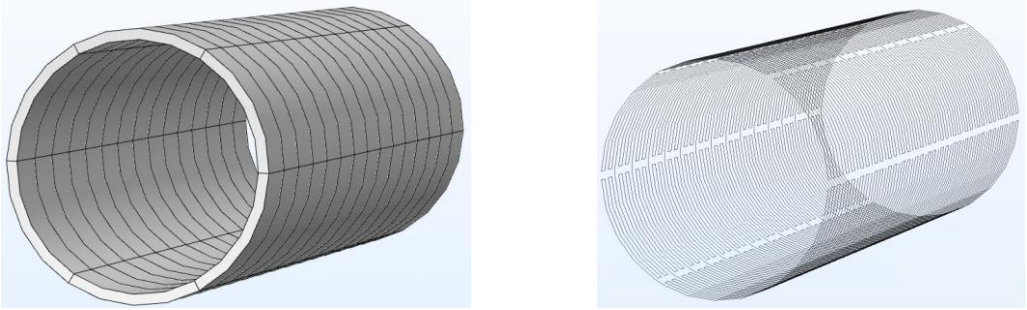

(a) (b)

Figure 4-3. 3D view of (a) the segmental linings and (b) the ground configuration pipes

As illustrated in Figure 4-4, the tunnel's grout and segmental linings were discretized using linear structured prismatic elements, whereas the surrounding soil was meshed with linear tetrahedral and pyramidal elements. Furthermore, the 1D pipe loop was meshed using linear edge elements, resulting in a total of 2,318,790 elements for the entire domain.

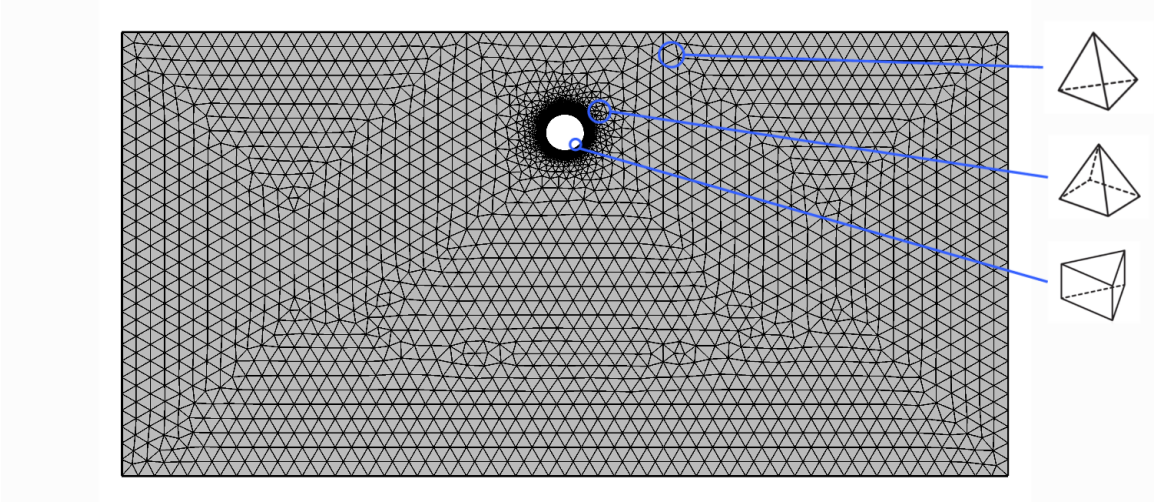

Figure 4-4. Mesh and element types of the model for the verification attempt

4.1.3 Simulation setup and study steps

To simulate the lifetime thermo-hydraulic behavior of the energy tunnel, an initial stationary hydraulic study is conducted exclusively inside the soil domain, assuming the tunnel lining was installed long ago. The ground is fully saturated, and all the boundaries are impermeable except for the two boundaries on the left and right side of the model. The constant hydraulic head of the left and right boundaries is chosen in a way to impose the desired groundwater velocity based on the Darcy's law and perpendicular to the tunnel axis.

In the second step, the thermal boundaries and initial states are introduced to the model and a 30-day time-dependent thermo-hydraulic analysis is performed, while the hydraulic boundaries are kept the same as before and the groundwater velocity is imported from the previous step of the simulation. A constant temperature boundary condition (equal to the initial temperature inside the domain) is applied on the ground surface and the bottom of the model, a convective heat transfer boundary condition is applied to the intrados of the tunnel

lining to account for the heat exchange with the air inside the tunnel while the remaining boundaries are thermally insulated. A visual representation of the above-mentioned boundary conditions is shown in Figure 4-5. The goal of this step of simulation is to achieve the thermo-hydraulic state of the already constructed tunnel, prior to activation of its absorber pipes.

Finally, all 15 energy rings are activated in parallel through their constant inlet points' temperature for another 30 days, while introducing the thermo-hydraulic state of the end of the second step as the initial status of the third. The fluid moves along the 1D pipes (with the constant velocity of 0.9 m/s) and performs the heat exchange with the surrounding lining material. The temperature of the fluid changes as it goes along the whole length of a single set of absorber pipes and the outlet temperature of the fluid of the middle ring determines the final geothermally harvested energy for a single ring.

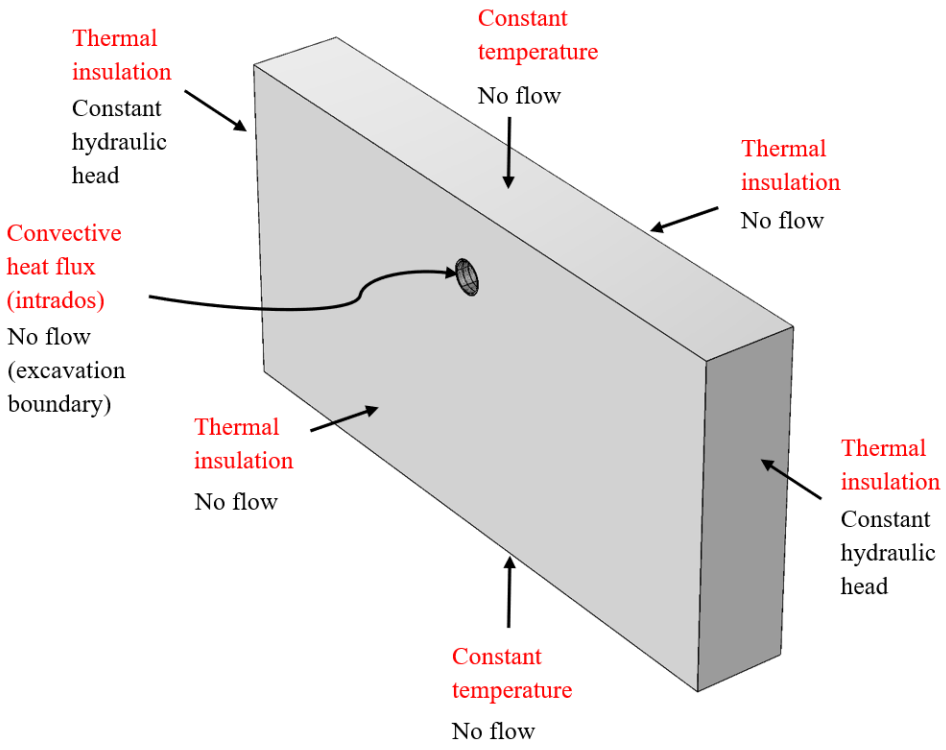

Figure 4-5. Specified thermohydraulic boundary conditions on the computational domain of the verification attempt

4.1.4 Material properties and study parameters

The material properties of the model are presented in Table 4-1 and were chosen equal to the design charts model for any possible parameter (Insana, 2020). It should be noted that the pipe wall thickness and thermal conductivity are neglected in this simulation.

Table 4-1. Material properties of the verification attempt

	Property	**Symbol**	**Unit**	**Value**
GROUND	Horizontal hydraulic conductivity	K_{xx}, K_{zz}	m/s	4.150E-03
	Vertical hydraulic conductivity	K_{yy}	m/s	2.075E-04
	Effective compressibility	C_{eff}	1/Pa	1E-8
	Porosity	n	-	0.25
	Ground thermal conductivity	λ_{gr}	W/mK	0.9 - 2.26 - 3.9
	Fluid-phase volumetric thermal capacity	$\rho_w C_{p,w}$	MJ/m^{3}K	4.2
	Solid-phase volumetric thermal capacity	$\rho_s C_{p,s}$	MJ/m^{3}K	2
	Transverse aquifer thermal dispersivity	α_T	m	0.31
	Longitudinal aquifer thermal dispersivity	α_L	m	3.1
TUNNEL	Lining thermal conductivity	λ_c	W/mK	1.5
	Lining volumetric thermal capacity	$\rho_c C_{p,c}$	MJ/m^{3}K	2.19
	Grout thermal conductivity	λ_g	W/mK	2
	Grout volumetric thermal capacity	$\rho_g C_{p,g}$	MJ/m^{3}K	2.19
PIPES	Fluid's thermal conductivity	λ_f	W/mK	0.542
	Fluid's volumetric thermal capacity	$\rho_f C_{p,f}$	MJ/m^{3}K	4.11
	Fluid's viscosity	μ_f	Pa.s	1.3E-3
	Inner pipe's diameter	d_{in}	m	0.016
	Darcy friction factor	f_D	-	1E-5
AIR	Heat transfer coefficient	h_{air}	W/m^{2}K	5.3

The conditions of the simulations follow the order of the previous study to obtain the design charts for the case of perpendicular groundwater flow (with respect to tunnel axis) as presented in Table 4-2 (Insana, 2020). In this way, the inlet temperature varies based on the seasonal mode of the study, and the air temperature inside the tunnel changes according to the in-situ temperature of the ground.

Table 4-2. Variable study conditions for obtaining design charts (Insana, 2020)

Characteristic	**Symbol**	**Unit**	**Value**
Inlet temperature (winter)	T_{in}	°C	4
Inlet temperature (summer)	T_{in}	°C	28
Ground temperature	T_g	°C	9-12-15-18
Tunnel temperature (winter)	T_{tun}	°C	Variable with ground temperature 7.1-10.1-13.1-16.1
Tunnel temperature (summer)	T_{tun}	°C	Variable with ground temperature 20.7-23.7-26.7-29.7

4.1.5 Results of the verification process

To include the effects of seasonality, in-situ temperature, groundwater velocity, and ground thermal conductivity in the simulations, 9 points on the design charts of Figure 2-24 for the case of perpendicular groundwater flow with respect to the tunnel axis were chosen for simulation by COMSOL. The initial and boundary conditions of each study were set according to Table 4-2. The results of all simulations along with their corresponding design chart readings are presented in Table 4-3. It can be noticed that the numerical results of the present study are, on average, 16.4 % lower than the corresponding design charts reading. Given that both results are obtained using numerical finite element method, the final accuracy is considered unacceptable.

Table 4-3. Results of the verification attempt

Season	v_{gw} [m/d]	λ_{gr} [W/mK]	T_g [°C]	q [W/m²]		Difference [%]
				Design charts	Present Study	
Winter	1.5	2.26	9	29	24.5	-15.5
Winter	1.5	2.26	12	49	41.3	-15.7
Winter	0.5	2.26	15	56	47	-16.1
Winter	2	2.26	15	74	60.9	-17.7
Winter	1.5	2.26	18	89	74.8	-16
Summer	1.5	2.26	9	102	85.1	-16.6
Summer	1.5	0.9	12	80	66.8	-16.5
Summer	1.5	3.9	12	84	69.8	-16.9
Summer	1.5	2.26	15	62	51.6	-16.8

4.1.6 Finding the issue

To resolve the issue, it is first necessary to find the cause of this discrepancy between the two numerical models. One of the key differences between the model used in the present study and the one simulated by FEFLOW for generating design charts is the mesh size. The design charts mesh setup consisted of structured mesh for the whole domain with 6 layers per ring (90 layers for 15 rings), while the mesh used in the present study has tighter structured mesh (20 layers per ring) in the lining and grout and tetrahedral elements for most of soil domain. Thus, a similar fully structured mesh (used for generating design charts) is constructed in COMSOL to compare its results to the model with partially tetrahedral mesh (used for obtaining results of Table 4-3). The tighter mesh elements near the tunnel and higher quality tetrahedral mesh on the outermost corners of the partially tetrahedral mesh are visually represented in Figure 4-6.

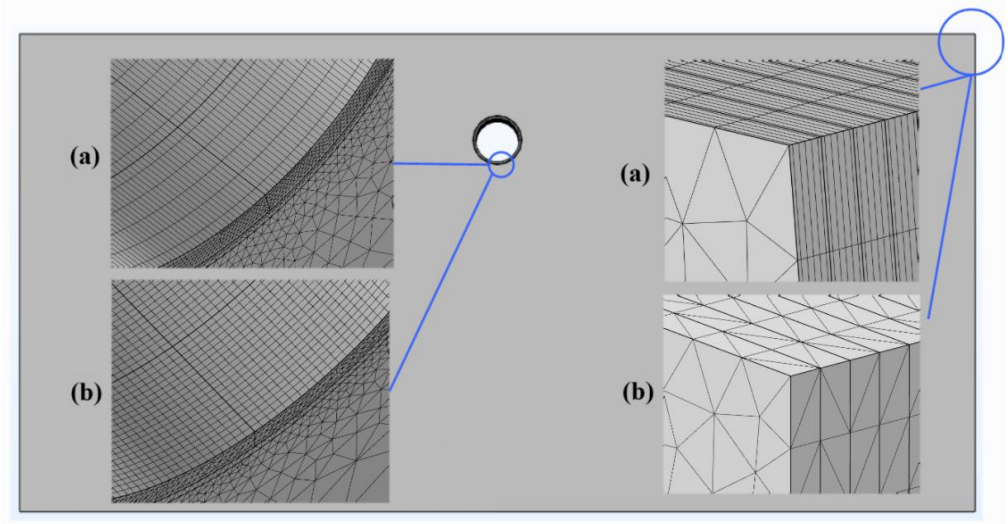

Figure 4-6. Quality of mesh near and far away from the tunnel in the model with (a) fully structured mesh and (b) partially tetrahedral mesh

By repeating the previous studies with both mesh setups, it is noticed that the geothermal potential of the model, when using the fully structured mesh, is quite similar to the design charts readings (Table 4-4). Therefore, the mesh dependency of the model used in generating design charts is the cause of discrepancy between the geothermal output of the two simulation setups. This issue can be caused by long or thin elements in the linings or distant boundaries (Figure 4-6). By examining the changes in total Darcy velocity on a plane perpendicular to the tunnel axis, positioned at a longitudinal depth of 10.5 meters (half of the 21-meter domain thickness), under an imposed average groundwater velocity of 1.5 m/d, the results indicate that the total Darcy velocity variation is nearly identical for both mesh configurations (Figure 4-7). Therefore, the mesh dependency is caused by long mesh elements in the linings of the design charts model.

Table 4-4. Effect of mesh setups on the geothermal potential of the ground

Season	v_{gw} [m/d]	λ_{gr} [W/mK]	T_g [°C]	q [W/m^2]			Difference [%]	
				Design charts	PTM[a]	FSM[b]	PTM	FSM
Winter	1.5	2.26	9	29	24.5	30.1	-15.5	+3.8
Winter	1.5	2.26	12	49	41.3	50.7	-15.7	+3.5
Winter	0.5	2.26	15	56	47	55.6	-16.1	-0.7
Winter	2	2.26	15	74	60.9	75.5	-17.7	+2
Winter	1.5	2.26	18	89	74.8	91.9	-16	+3.3
Summer	1.5	2.26	9	102	85.1	104.7	-16.6	+2.6
Summer	1.5	0.9	12	80	66.8	82.2	-16.5	+2.8
Summer	1.5	3.9	12	84	69.8	86.1	-16.9	+2.5
Summer	1.5	2.26	15	62	51.6	63.6	-16.8	+2.6

[a] Partially Tetrahedral Mesh

[b] Fully Structured Mesh

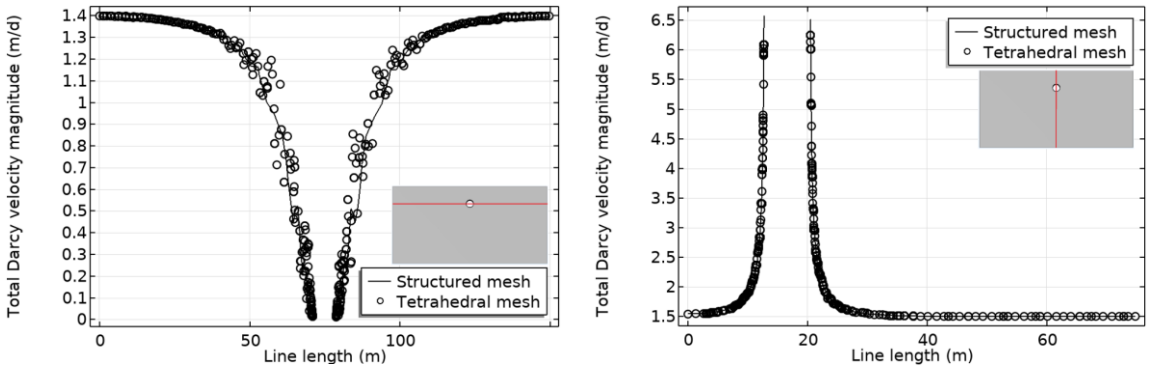

(a) (b)

Figure 4-7. Effect of mesh setups on the total Darcy velocity inside the soil domain and perpendicular to the tunnel axis in (a) x-axis direction (b) y-axis direction

Since the mesh independent results in Table 4-4 have the same percentage of difference with design charts readings, and the design charts values are validated against real and numerical results of previous studies (Insana & Barla, 2020), the mesh dependency did not

affect the accuracy of geothermal potential prediction of the charts. This is possible only by choosing the model parameters that can offset the overestimation of the models. Consequently, it is necessary to validate the model with new mesh by available field test of Turin ML1 energy tunnel to obtain reliable simulation parameters.

4.2 Validation by field data

Now that the previous verification was unsuccessful the validation will be done using the field experiments of Turin ML1. The recorded temperature data of four field tests of Turin ML1 energy tunnel in 2018 are used for validation of the COMSOL and find optimal parameters to be further used in this study (Insana & Barla, 2020). As discussed in the previous chapter, the model that was used in FEFLOW for validation can be slightly improved and recreated in COMSOL for validation against the field test results. In FEFLOW the soil was either fully saturated or completely dry, therefore doing the same in COMSOL requires adding a boundary inside the soil domain to impose this condition for the mesh elements. To avoid this geometrical constraint, the soil is assumed to have a partially unsaturated zone above the groundwater table. Also, in FEFLOW the thermal resistance of the pipe wall thickness was neglected, but here COMSOL allows inputting the pipe wall thickness and thermal conductivity into thermal equations without meshing. Therefore, the validation occurs while having them in the thermal performance calculations of the model.

To simulate groundwater movement in partially saturated and fully saturated soil around the tunnel, Richards' equation is applied as the governing principle along with van Genuchten retention model. Unlike Darcy’s law, which assumes a fully saturated medium, Richards' equation accounts for variably saturated conditions, incorporating the effects of capillary pressure, relative permeability, and moisture retention. This makes it suitable for describing both saturated and unsaturated flow regimes. Additionally, Richards' equation inherently determines the groundwater table position dynamically, as it models the transition between saturated and unsaturated zones based on moisture content and pressure head variations, eliminating the need for an explicit water table definition by geometrical constraints. The

mass conservation expression using Richards' equation is obtained as follows (COMSOL AB, 2022):

$$\rho_{\mathrm{w}}\left(\frac{C_{\mathrm{m}}}{\rho_{\mathrm{w}}g}+\mathrm{S_e}S_p\right)\frac{\partial p_{\mathrm{w}}}{\partial t}+\nabla\cdot\rho_{\mathrm{w}}\left(-\frac{\kappa_{\mathrm{s}}}{\mu_w}k_{\mathrm{r}}(\nabla p_{\mathrm{w}}-\rho_{\mathrm{w}}g\nabla D)\right)=0 \qquad (18)$$

Where C_{m} represents the specific moisture capacity, $\mathrm{S_e}$ is the effective saturation, S_p is the storage coefficient, κ_{s} is the hydraulic permeability and k_{r} is the relative permeability.

Other governing equations of this simulation are the same as the ones described in section 4.1.1.

4.2.1 Geometry and meshing of the domain

All the geometrical dimensions of this validation model are the same as Figure 4-1 and Figure 4-2. However, in the longitudinal direction, parallel to the tunnel axis, there would be 6 tunnel rings with the thickness of 1.4 m each, which results in the total thickness of 8.4 m for the whole domain. The two rings in the middle will be geothermally activated by the ground configuration pipes (Figure 4-8-a) that are constructed using one-dimensional lines inside the linings (Figure 4-8-b). It can be seen that no distinct geometric surfaces are assumed to divide a ring into its individual segments.

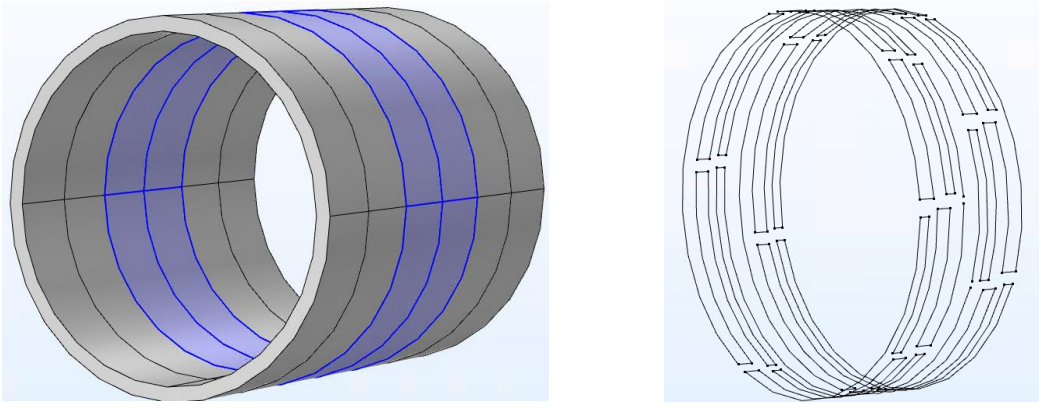

(a) (b)

Figure 4-8. Representation of the geometry of (a) the six tunnel rings along with the two activated ones (b) the two circuits of ground-configuration pipes

The meshing of the domain is as of the previous validation attempt, which means that the tunnel's grout and segmental linings are discretized using linear structured prismatic elements, whereas the surrounding soil is meshed with linear tetrahedral and pyramidal elements (Figure 4-9). Furthermore, the 1D pipe loops are meshed using linear edge elements, resulting in a total of 1,633,714 elements for the entire domain.

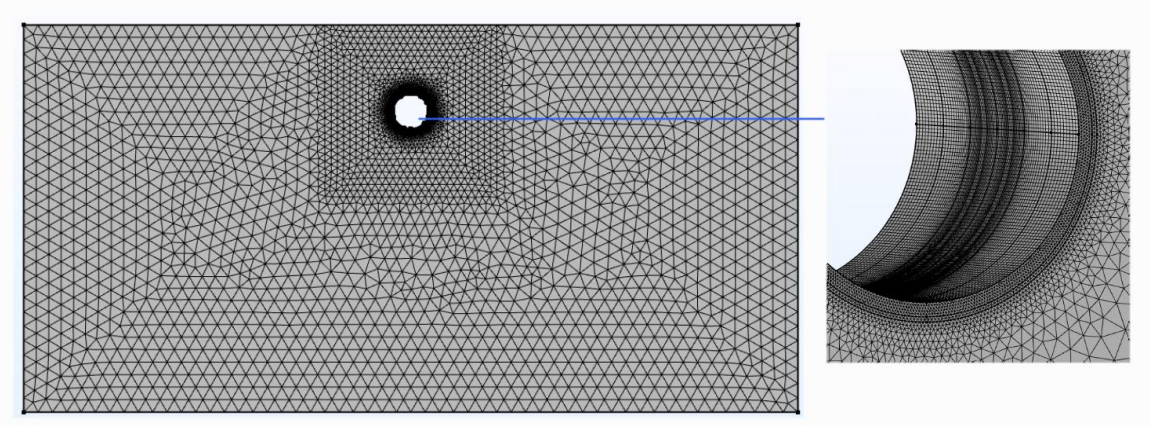

Figure 4-9. Mesh of the model for validation against field data

4.2.2 Simulation setup and study steps

The first step in simulating the transient thermo-hydraulic (TH) behavior of the energy tunnel is to establish a stable long-term groundwater flow of 1.5 m/d within the soil. To achieve this, hydraulic heads of 12.1 m and 12.7 m below the ground surface are applied to the left and right boundaries of the domain, respectively. This setup replicates the groundwater conditions around the Turin ML1 tunnel following a hydraulic steady-state study conducted in COMSOL. To all other boundaries of the domain a no-flow condition is assigned.

The second step is a 30-day transient thermo-hydraulic (TH) study, in which an initial temperature of 17.3 °C is applied to the entire domain. Additionally, the recorded time series of ground surface and tunnel air temperatures (before the starting time of the intended field test) are imposed on the top boundary and the tunnel intrados boundary, respectively. The hydraulic boundaries remain unchanged from the previous step, and the groundwater velocity

is imported from the steady-state hydraulic simulation. The bottom horizontal boundary has a fixed 17.3 °C temperature restriction, while other boundaries are thermally insulated. At this step, the geothermal pipes are not activated, but the final solution serves as the initial condition for the field tests.

Finally, the recorded time series of inlet temperature for each test is applied to the inlet points of the two geothermal loops, while the thermo-hydraulic (TH) solution from the second step serves as the initial condition. All boundary conditions remain unchanged; however, the ground surface and tunnel air temperature boundaries continuously update over time based on the recorded time series after the start of the tests. The fluid flows through the 1D pipes at a constant velocity, exchanging heat with the surrounding pipe wall and tunnel lining (the effect of pipe wall thickness and thermal conductivity is seen in the governing equations). As it travels along the full length of a single set of absorber pipes, its temperature changes, and the outlet temperature of the fluid from each ring determines the total geothermally harvested energy for that ring.

4.2.3 Material properties and study parameters

The new material properties of the simulation are presented in Table 4-5 and most of them are chosen as reported by Insana (2020).Compared to the previous validation attempt, properties for pore air and the pipe wall, and Richards' equation parameters have been added. Additionally, two different values are assigned for grout thermal conductivity and the tunnel air heat transfer coefficient, resulting in four distinct study cases. Other material properties of the model are equal to the values of Table 4-1.

Table 4-5. Material properties for the validation against field data (Insana, 2020)

	Property	Symbol	Unit	Value
GROUND	Fluid-phase volumetric thermal conductivity	λ_w	W/mK	0.65
	Solid-phase volumetric thermal conductivity	λ_s	W/mK	2.8
	Air volumetric thermal conductivity	λ_{air}	W/mK	0.026
	Air volumetric thermal capacity	$\rho_{air} C_{p,air}$	MJ/m^{3}K	0.001
	Residual water volume fraction	θ_r	-	0.02
	van Genuchten parameter	α_{vG}	1/m	5
	van Genuchten parameter	n_{vG}	-	2.5
	van Genuchten parameter	l_{vG}	-	0.5
TUNNEL	Lining thermal conductivity	λ_c	W/mK	1.12
	Grout thermal conductivity	λ_g	W/mK	**0.655 - 1.12**
PIPES	Pipe wall thickness	t_p	m	0.002
	Pipe wall thermal conductivity	λ_p	W/mK	0.35
AIR	Heat transfer coefficient	h_{air}	W/m^{2}K	**1.77 - 5.3**

The simulations replicate four field tests of the Turin ML1 energy tunnel with the specifications of Table 4-6 to validate the model. Three tests were conducted in heating (winter) mode and one in cooling (summer) mode, all of which were performed using ground configuration pipes. The longest field test conducted, 180320_G_H_T45_179180, is later utilized for the parameter optimization of the model (Insana & Barla, 2020).

Table 4-6. Specifications of the Turin ML1 energy tunnel field tests used for validation (Insana & Barla, 2020)

Test code	Circuit	Mode	Fluid velocity [m/s]	Duration [d]
180305_G_H_T45_179180	Ground	Heating	0.55	2.01
180309_G_H_T45_179180	Ground	Heating	0.69	3.07
180320_G_H_T45_179180	Ground	Heating	0.90	7.82
180727_G_C_T10_179180	Ground	Cooling	0.97	3.00

4.2.4 Validation results

The longest test, 180320_G_H_T45_179180 (7.82 days), was used to determine the optimal combination of grout thermal conductivity and tunnel air heat transfer coefficient that best replicates the recorded outlet temperature from the field test. The numerically obtained outlet temperature during the testing period closely matches the measured values when the tunnel air heat transfer coefficient and grout thermal conductivity are set to 5.3 W/m²K and 0.655 W/mK, respectively (Figure 4-10).

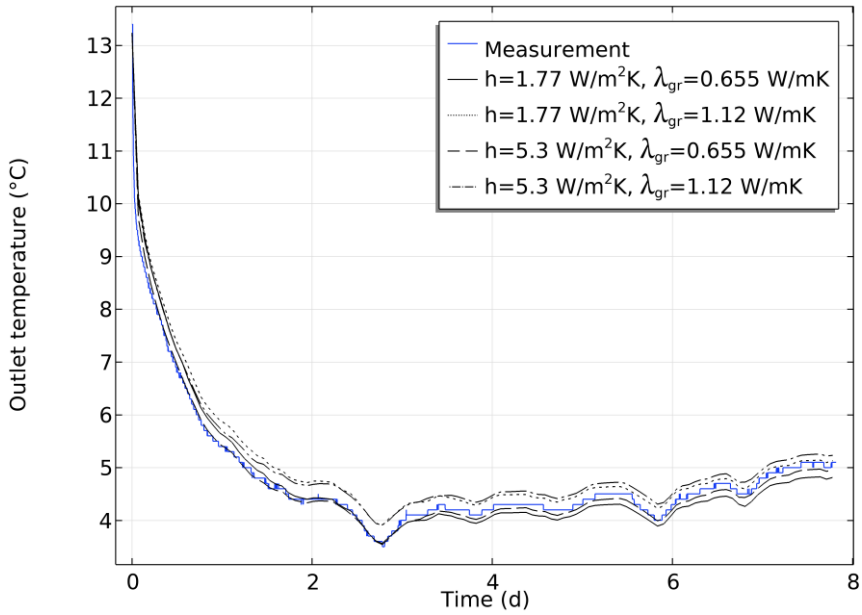

Figure 4-10. Numerical and measured (Insana & Barla, 2020) outlet temperature during test 180320_G_H_T45_179180

Strain gauges of Sl2i, Sl2e, St4i and St4e were placed inside the linings of the Turin ML1 energy tunnel during the period of the test (Insana & Barla, 2020). The numerically obtained temperatures at the locations of the sensors show good correspondence with the recorded ones in Figure 4-11.

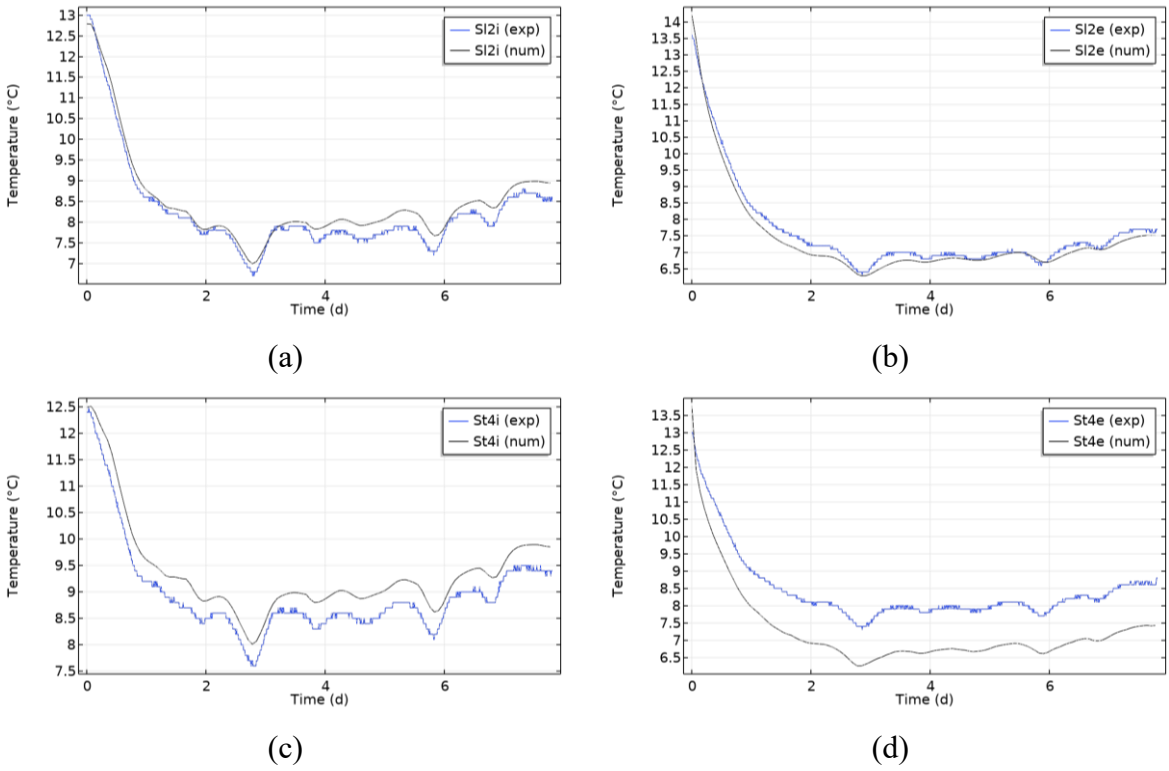

Figure 4-11. Comparison of recorded lining temperature of test 180320_G_H_T45_179180 with the ones calculated by the numerical model for sensor (a) Sl2i (b) Sl2e (c) St4i (d) St4e

By simulating the other three field tests under the conditions specified in Table 4-6, the outlet temperature of the piping circuit in the model is recorded. Comparing these values with the measured outlet temperatures from the 180305_G_H_T45_179180, 180309_G_H_T45_179180, and 180727_G_C_T10_179180 field tests (Figure 4-12), validates the chosen parameters and numerical model setup.

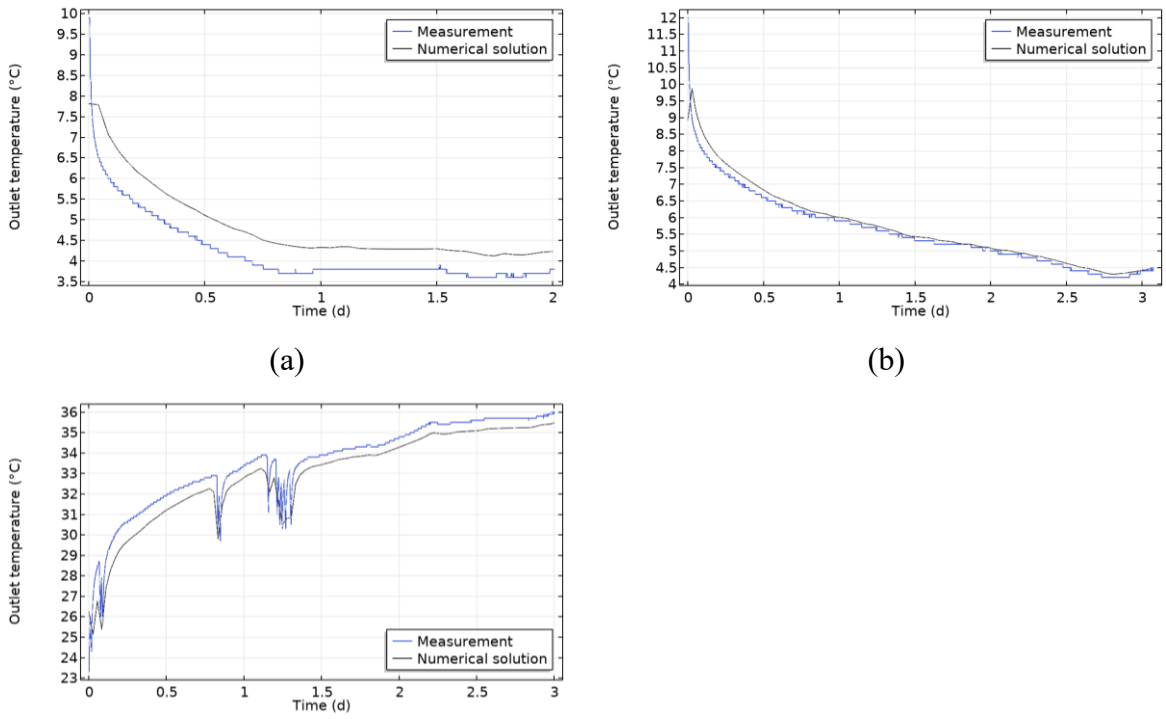

Figure 4-12. Measured and calculated outlet temperature vs time of the test (a) 180305_G_H_T45_179180 (b) 180309_G_H_T45_179180 (c) 180727_G_C_T10_179180

Eventually, it can be noticed that all the parameter values that were used by Insana & Barla (2020) for validation phase of their numerical model were once again stood corrected. This means that there was no mesh dependency inside their validation model and the issue was only present during the design chart generation phase of the numerical simulation. This phenomenon is possible due to tighter mesh spacing in the thermally-activated rings of the validation model compared to the design charts model.

At this stage it is needed to choose or create a base model to do further parametric studies for assessing the effects of the energy tunnel diameter on geothermal performance. The intention is to follow the path of the Insana & Barla (2020) study that resulted in design charts for energy tunnels through regeneration of similar charts without the presence of mesh dependency, while accounting for thermal resistance of pipe wall thickness. To do so, the

model and parameters that were used for the verification attempt (i.e. section 4.1) is reused here with three differences:

First: the design charts in Figure 2-24 have been validated against both real and numerical studies in the literature (Insana & Barla, 2020), therefore generating a base model for the design charts requires the compensation for the underestimation of the geothermal potential of the model of section 4.1. This adjustment is achieved by modifying the fixed inlet temperature from 4 °C to 2.5 °C in winter mode and from 28 °C to 32 °C in summer mode.

Second: the base model has the possibility of accounting for pipe wall thickness and thermal conductivity in heat transfer equations for better representation of a real-case energy tunnel. Therefore, the pipe wall thickness of 4 mm and its thermal conductivity of 0.35 W/mK is inputted to the model.

Third: To simulate the condition in which there are unlimited number of parallel energy rings in the domain, 15 parallel thermally activated rings were created for the verification model where only the outlet temperature of the middle ring (i.e. 8th) was recorded for energy tunnel's geothermal potential assessment. COMSOL can accommodate this infinite number of parallel rings through applying a periodic boundary condition on the two parallel faces perpendicular to the tunnel direction (with zero temperature difference between the two boundaries). Therefore, the simulation domain thickness reduces from 21 m to 1.4 m (containing a single ring), significantly improving computational efficiency and speed. This boundary condition assumes that the domain thickness for a single ring repeats every 1.4 m, with zero temperature difference between the two vertical boundaries. It also ensures that heat flux passing through these boundaries is the same.

Eventually, the thermohydraulic boundary conditions of the model are presented in Figure 4-13. In cases where groundwater flow is perpendicular or parallel to the tunnel axis, constant hydraulic head is applied to the corresponding vertical boundaries, while a no-flow condition is assigned to the remaining boundaries.

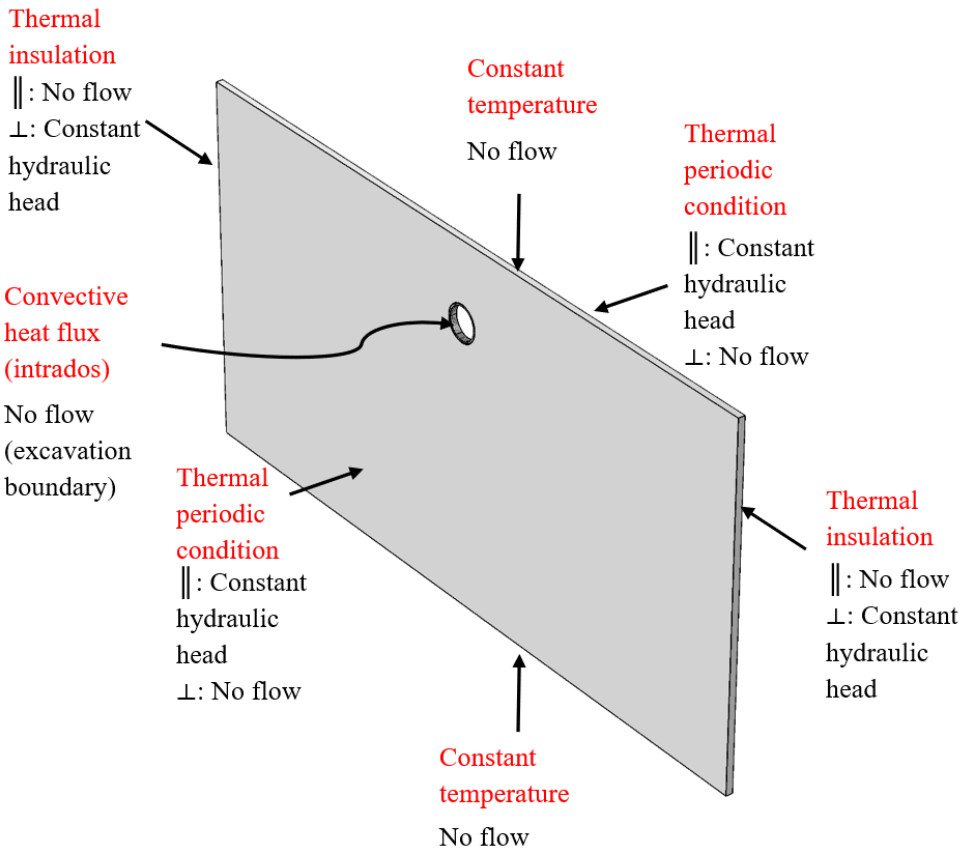

Figure 4-13. Specified thermohydraulic boundary conditions on the computational domain for the design charts model of the present study

Eventually, the design charts developed in this study are presented in Figure 4-14 for estimating the geothermal potential of the ground. The graphs on the left and right correspond to winter and summer mode operations of the energy tunnel, respectively. The top graphs represent the case where groundwater flow is parallel to the tunnel axis, while the bottom graphs correspond to groundwater flow perpendicular to the tunnel axis. In the latter case, the geothermal potential of the ground increases by 10–20%. Each graph illustrates the effect of ground thermal conductivities of 3.9, 0.9, and 2.26 W/mK using lines of different colors: black, white, and the border indicating the color transition, respectively.

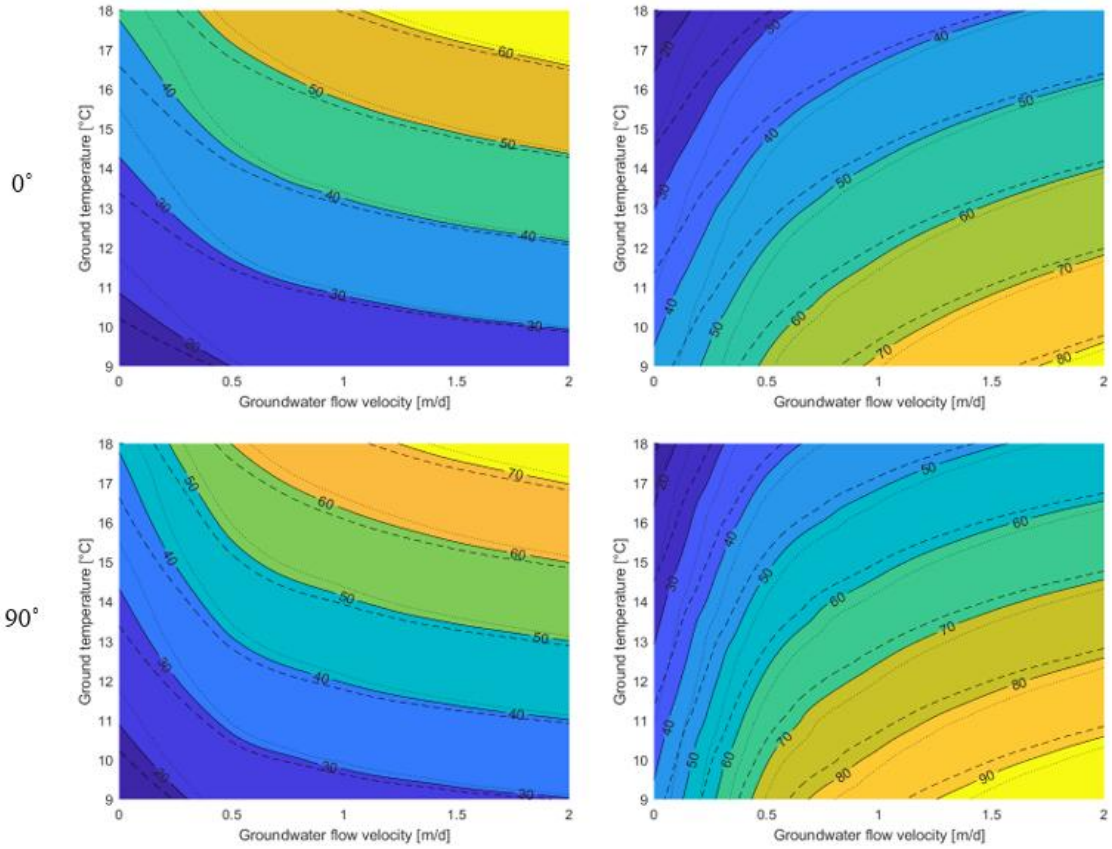

Figure 4-14. Design charts of the present study for geothermal potential in W/m^2

Contour plots of temperature variation for energy tunnels under perpendicular and parallel groundwater flow (2 m/d) relative to the tunnel axis are shown in Figure 4-15 and Figure 4-16, respectively. In all cases, ground thermal conductivity and initial temperature are 2.26 W/mK and 12 °C. Perpendicular groundwater flow affects only horizontal heat transfer, causing asymmetric temperature changes toward the right side of the energy tunnels (in the direction of groundwater flow) in both summer and winter. Parallel groundwater flow, on the other hand, causes a uniform radial heat transfer which produces circular temperature contours around the tunnel.

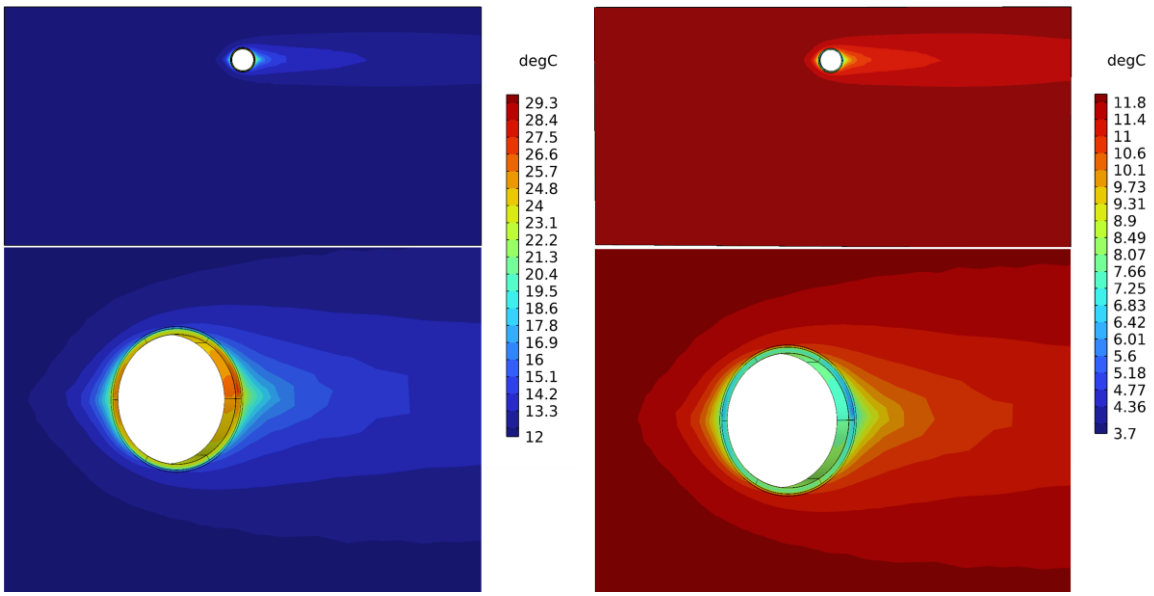

(a) (b)

Figure 4-15. Temperature contours after 30 days of thermal activation with 2 m/d perpendicular groundwater flow, λ_{gr} = 2.26 W/mK and T_g = 12 °C in (a) summer (b) winter

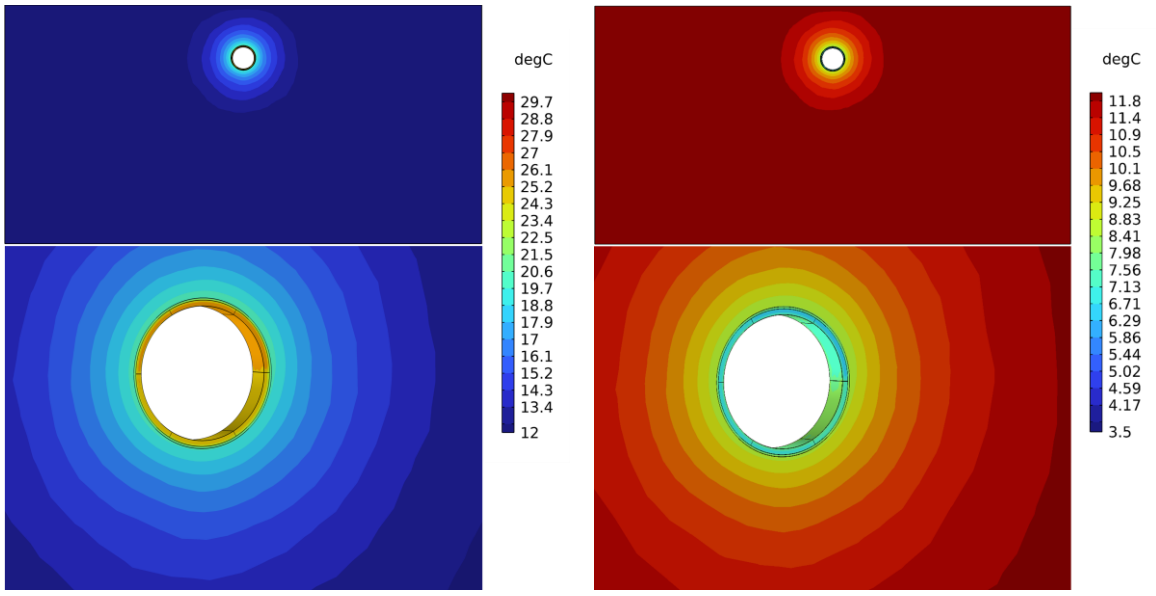

(a) (b)

Figure 4-16. Temperature contours after 30 days of thermal activation with 2 m/d parallel groundwater flow, λ_{gr} = 2.26 W/mK and T_g = 12 °C in (a) summer (b) winter

The final step in validating the geothermal potential readings from the design charts is to predict the performance of real case studies involving energy tunnels with segmental lining. This is done in Table 4-7 along with comparison with the readings of the design charts of Figure 2-24 that were reported by (Insana & Barla, 2020). It can be seen that both design charts' readings match the geothermal performances of Jenbach and Katzenberg energy tunnels with a 10 W/m^2 tolerance. In the case of the Turin ML1, on the other hand, both sets of design charts overestimate the winter mode's performance while underestimating the summer mode's. The first reason for this phenomenon is that the grout and segments' thermal conductivity of the Turin ML1 energy tunnel (i.e., 0.655 and 1.12 W/mK, respectively) differ from the values that were used in the design charts (i.e., 2 and 1.5 W/mK, respectively). Moreover, the inlet temperatures of the field tests were different from the ones that were used in the numerical simulation.

Table 4-7. Validating the present study's design charts against real cases in literature

Case Study	**v_{gw} [m/d] (direction)**	**T_g [°C]**	**λ_{gr} [W/mK]**	**Geothermal potential [W/m^2]**					
				Study result		**Design charts of Figure 2-24 (+/- 10 W/m^2)**		**Present study's design charts of Figure 4-14 (+/- 10 W/m^2)**	
				Winter	**Summer**	**Winter**	**Summer**	**Winter**	**Summer**
Jenbach (Franzius & Pralle, 2011; Moormann et al., 2016)	1 (0°)	10	3.3	18-40	-	28	-	28	-
Katzenberg (Franzius & Pralle, 2011)	0	13	3	17-25	-	29	-	28	-
Turin ML1 (Insana & Barla, 2020)	1.5 (90°)	17.3	2.26	46-53	60-66	85	48	68	54

4.3 Summary

This chapter intends to demonstrate the validity of the current study's thermo-hydraulic analyses for energy tunnels' geothermal performance assessment. First, it was attempted to reproduce a previous study's numerically obtained results, however this objective was not achieved. The reason behind the failed attempt was found to be an underlying mesh dependency in the reference study's numerical model. Consequently, the numerical model was used to reproduce the field test results of an existing energy tunnel. Eventually, the agreement of the results of the model with the field test approved the validity of the TH model of the current study. Then, it was necessary to create a reliable base model to be used for further parametric studies on the changes of energy tunnel diameter on its geothermal performance. This was achieved by introducing a thermo-hydraulic model that generated energy tunnel design charts through parametric studies for the effects of groundwater velocity and orientation, ground thermal conductivity and temperature, and seasonality on the geothermal potential of an energy tunnel with a constant diameter. The validity of this base model was ensured through comparing its design charts readings with previous field test results on energy tunnels.

5 Assessing the role of tunnel diameter in energy tunnel thermal performance

Tunnels come in a variety of sizes, each tailored to meet specific engineering goals. Among their geometric features, the diameter stands out as a key factor that may influence geothermal performance—particularly in energy tunnels with segmental linings. This chapter tries to investigate how tunnel diameter, as an indicator of overall tunnel size, might affect thermal behavior and efficiency. Through thermohydraulic simulations in COMSOL, it explores the mechanisms that could govern geothermal output across different diameters. In doing so, it attempts to better understand the potential role of size in geothermal performance of energy tunnels. Also, it provides a foundation for expectations regarding the geothermal performance of smaller tunnels (such as microtunnels) during thermal activation in future studies.

5.1 Geometry, mesh and simulation setup

To investigate the performance of energy tunnels with varying sizes, five different tunnel diameters were selected to define the geometry of the simulation models. The domain lengths, labeled as L1 and L2 in Figure 5-1, change according to the selected tunnel diameter,

while the third dimension of the domain remains fixed at 1.4 m, equal to a single ring's length. The tunnel depth (D1) also varies according to the selected diameter. L_1, L_2, D_1 are scaled proportionally to the tunnel's inner diameter, such that their values are scaled linearly to the ratio between the considered diameter and that of the validation model. Each tunnel consists of a single ring composed of six segments with varying thicknesses. The ground-configuration pipes are positioned 6 cm from the extrados of each segment, and the spacing between pipes in each row remains constant at 27.5 cm along the tunnel axis. The grout thickness is consistent at 11 cm for all tunnel diameters. These dimensional values are presented in Table 5-1.

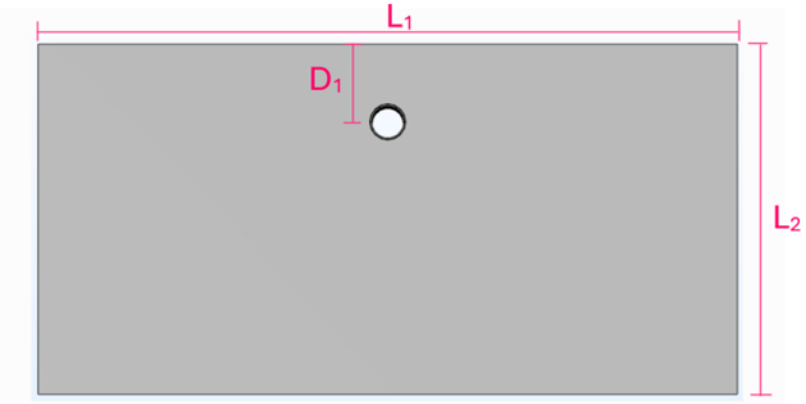

Figure 5-1. Schematic of variable dimensional lengths of the models

Table 5-1. Geometric dimensions of the energy tunnels with varying diameters

Tunnel inner diameter [m]	**Lengths of Figure 5-1**			**Segmental lining thickness [m]**	**Grout thickness [m]**	**Pipe circuit length [m]**
	L_1 [m]	**L_2 [m]**	**D_1 [m]**			
5	108.7	54.4	12.1	0.3	0.11	86.1
7	152.2	76.1	16.9	0.3	0.11	117.7
9	195.7	97.8	21.7	0.45	0.11	153.7
11	239.2	119.6	26.5	0.45	0.11	185.2
13	282.7	141.3	31.4	0.55	0.11	219.7

The tunnels' grout and segmental linings were meshed using linear structured prismatic elements, whereas the surrounding soil was meshed with linear tetrahedral and pyramidal

elements. These elements can be seen in the mesh of the energy tunnel with an internal diameter of 13 m, in Figure 5-2. Moreover, the 1D pipe loop was meshed using linear edge elements, while the effect of pipe wall thickness and thermal conductivity is seen in the governing equations.

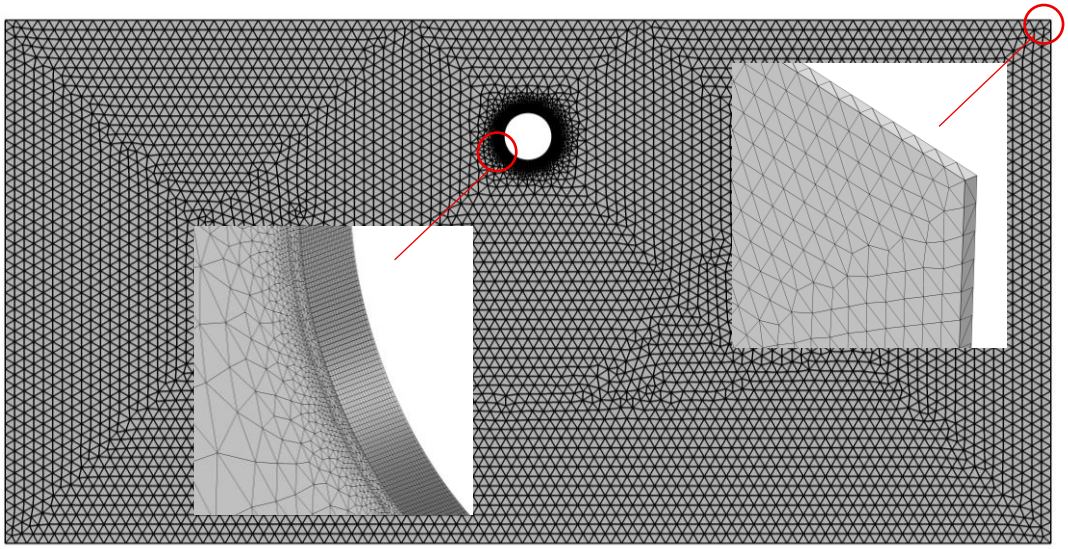

Figure 5-2. Mesh of the energy tunnel with an inner diameter of 13 m

To exclude and analyze the effects of the tunnel air on the geothermal output of the energy tunnels, all the simulations are performed two times, once with a thermal insulation and once with convective heat flux boundary condition for the tunnel inner wall (as shown in Figure 5-3). The reason behind this decision is that the thickness of the reinforced concrete placed between the ground configuration pipes and the air inside the tunnel changes with respect to the tunnel diameter (since the segmental lining thickness itself depends on the diameter and the pipes are always 6 cm apart from the segments' outer walls).

The simulation consists of three study steps that use the governing equations described in the previous chapter. First, a stationary hydraulic-only study is conducted only inside the ground, assuming the tunnel lining was installed long ago. The ground is fully saturated, and to simulate a perpendicular (shown with $\perp$ sign) or parallel (shown with $\parallel$ sign) groundwater flow velocity, two parallel vertical boundaries will be assigned with constant hydraulic heads. Simultaneously, the rest of the boundaries are assigned to have no flow condition. The visual

representation of the hydraulic boundary conditions of the models is shown in Figure 5-3 with black font.

In the second study step, the thermal boundaries and initial states are introduced to the model and a 30-day time-dependent thermo-hydraulic analysis is performed, while the hydraulic boundaries are kept the same as before and the groundwater velocity profile is imported from the previous step of the simulation. A constant temperature boundary condition (equal to the initial ground temperature) is applied on the ground surface and the bottom of the model, a thermal insulation or convective heat transfer boundary condition is applied to the intrados of the tunnel lining to eliminate or account for the heat exchange with tunnel air, respectively. Also, two vertical boundaries that are perpendicular to the tunnel axis are assigned with thermal periodic condition with zero temperature difference between them and the remaining two vertical boundaries are thermally insulated. A visual representation of the above-mentioned boundary conditions is shown in Figure 5-3. The goal of this step of simulation is to achieve the thermo-hydraulic state of the already constructed tunnel, prior to activation of its absorber pipes. It is noteworthy that after 30 days, the ground, grout and lining temperatures are the same and equal to the initial ground temperature for the cases with insulated intrados.

Finally, absorber pipes are activated through their constant inlet temperature for another 30 days, while introducing the thermo-hydraulic state of the end of the second step as the initial state of the third. The fluid moves along the 1D pipes and performs the heat exchange with the surrounding lining material. The temperature of the fluid changes as it travels through the pipe circuit and eventually, the outlet temperature of the fluid determines the final geothermal performance of the tunnel.

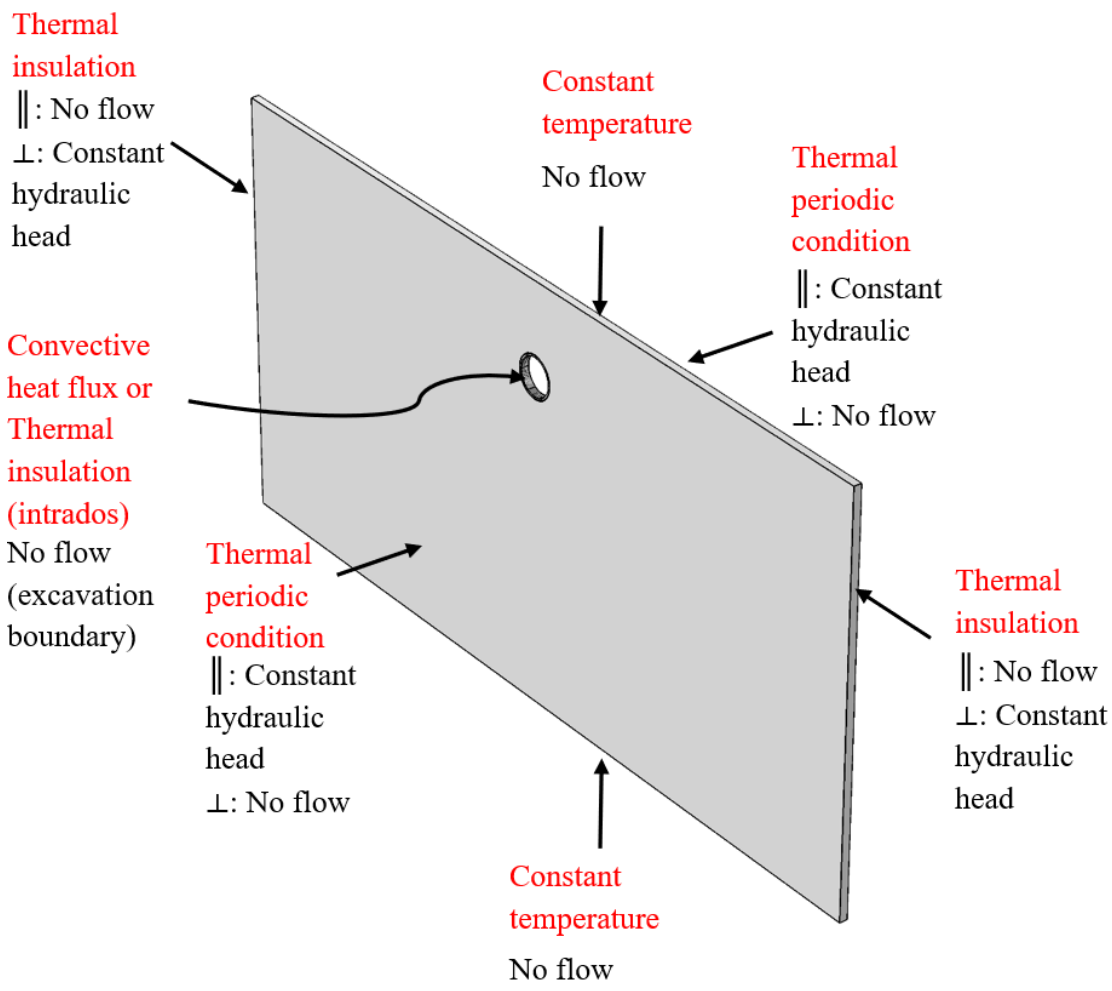

Figure 5-3. Specified thermal (in red font) and hydraulic (in black font) boundary conditions on the computational domain for energy tunnels of various diameters

5.2 Material properties and study parameters

The material properties for the energy tunnels of various diameters are the ones presented in Table 4-1. To clarify the parametric studies that were done in this research, a list of notable parameters, along with two thermal boundary conditions for the tunnel intrados and groundwater flow directions, is presented in Table 5-1. Eventually, it is possible to calculate the number of unique thermo-hydraulic simulations that were done with respect to a single characteristic in Table 5-3. In this table, the second column shows the number of study conditions for a specific characterisitic (e.g. two boundary conditions for intrados). The third

column shows the number of analyses done for a constant diameter and condition when the other characteristics vary (e.g. 240 analyses on a tunnel with a diameter of 11 m and insulated boundaries). The fourth column shows the number of analyses for a single characteristic condition (e.g. 1200 analyses for all tunnels with insulated intrados). The last column shows the total number of numerical analyses (considering all characteristics) which is equal to 2400.

Table 5-2. Model conditions for numerical simulation of energy tunnels with varying diameters

Characteristic	**Unit**	**Value or assigned condition**
Pipe diameter and thickness	mm	20 × 2
Circulating fluid velocity	m/s	0.9
Inlet temperature (winter)	°C	2.5
Inlet temperature (summer)	°C	32
Intrados thermal boundary condition	—	Insulated or convective heat flux
Groundwater flow velocity	m/d	0 - 0.5 - 1 - 1.5 - 2
Groundwater flow direction	—	Parallel or perpendicular to tunnel axis
Ground thermal conductivity	W/mK	0.9 - 2.26 - 3.9
Tunnel inner diameter	m	5 - 7 - 9 - 11 - 13
Lining thickness	cm	Variable with tunnel diameter 30 - 30 - 45 - 45 - 50
Ground temperature	°C	9 - 12 - 15 - 18
Tunnel temperature (winter)	°C	Variable with ground temperature 7.1-10.1-13.1-16.1
Tunnel temperature (summer)	°C	Variable with ground temperature 20.7-23.7-26.7-29.7

Table 5-3. Information about the number of numerical analyses

Characteristic	Number of conditions	Number of simulations per diameter and condition	Number of simulations per condition	Total simulations
Intrados thermal boundary condition	2	240	1200	2400
Groundwater flow velocity	5	96	480	
Groundwater flow direction	2	240	1200	
Ground thermal conductivity	3	160	800	
Ground temperature	4	120	600	
Seasonality	2	240	1200	
Tunnel inner diameter	5	480	480	

5.3 Results in the absence of groundwater flow

The first step in finding the mechanisms influencing the geothermal performance of energy tunnels with different diameters is to compare their results when minimal environmental factors are in play. Therefore, the analysis begins in the absence of groundwater flow for different ground temperatures (corresponding to different tunnel internal air temperatures in the cases of uninsulated tunnel internal walls). Due to variations in pipe circuit length across tunnels with different diameters (Table 5-1), the geothermal output of the energy tunnels is expressed in terms of Watts per meter of pipe circuit length, rather than per square meter of the tunnel segment's outer surface. This approach excludes any geothermal output misjudgments due to inefficient geothermal exploitation (yet high in terms of W/m^2) of the tunnel's outer surface by overly close pipes, while demanding the pipes spacing to be sufficiently large to avoid underperformance of a meter of absorber pipe.

By analyzing the geothermal output of the energy tunnels of different inner diameters in summer mode in Figure 5-4, it is noticed that in all cases, the geothermal output is the highest

for ground thermal conductivity equal to 3.9 W/mK. Also, in cases with insulated tunnel intrados (i.e. Figure 5-4-a2 and b2) a gradual increase in geothermal output with decreasing tunnel diameter is observed, while in Figure 5-4-a1 for the ground temperature of 9 °C, this gradual increase is interfered by steep steps between the diameter decreases from 13 to 11 and 9 to 7 m. The reason behind this irregularity is the fact that the segmental lining thickness at these two points decreases, which allows a better heat transfer with the tunnel internal air that has a temperature of 20.7 °C, which is much less than the inlet temperature of 32 °C. This phenomenon makes the overall geothermal output of the energy tunnel with a distinct diameter (Figure 5-4-a1) higher than the geothermal output of the exact tunnel with the insulated intrados (Figure 5-4-a2) when the ground temperature is equal to T_{ground} = 9 °C (where T_{tunnel} = 20.7 °C). This higher geothermal output for the uninsulated tunnels is not observed for all simulation cases when comparing Figure 5-4-b1 with Figure 5-4-b2, which have T_{ground} = 18 °C. The first reason might lie in the thermal effect that the tunnel internal air can have on the thermal condition of the ground near the tunnels. Since there is an initial thermo-hydraulic step involved in uninsulated cases to simulate the ground thermal condition, the tunnel internal air can change the temperature profiles of the segmental lining, grout and ground for 30 days before thermal activation of the pipes. Therefore, in these cases tunnel internal air temperature of 29.7 °C affects the ground to the degree that the inlet temperature of 32 °C is sometimes unable to harness a higher geothermal output from the system compared to the insulated energy tunnels. The second reason might be that, at the final 30-day TH simulation step (where the absorber pipes are activated), the temperature profile of the lining itself is going to be influenced by the tunnel air temperature (which is close to the inlet temperature). Therefore, the low temperature difference between the lining and the circulating fluid leads to lower thermal energy exchange. This phenomenon is highly noticeable in the case of a tunnel with a distinct diameter and ground thermal conductivity of 3.9 W/mK in Figure 5-4-b1 and b2, where the geothermal output is higher when the tunnel intrados is insulated.

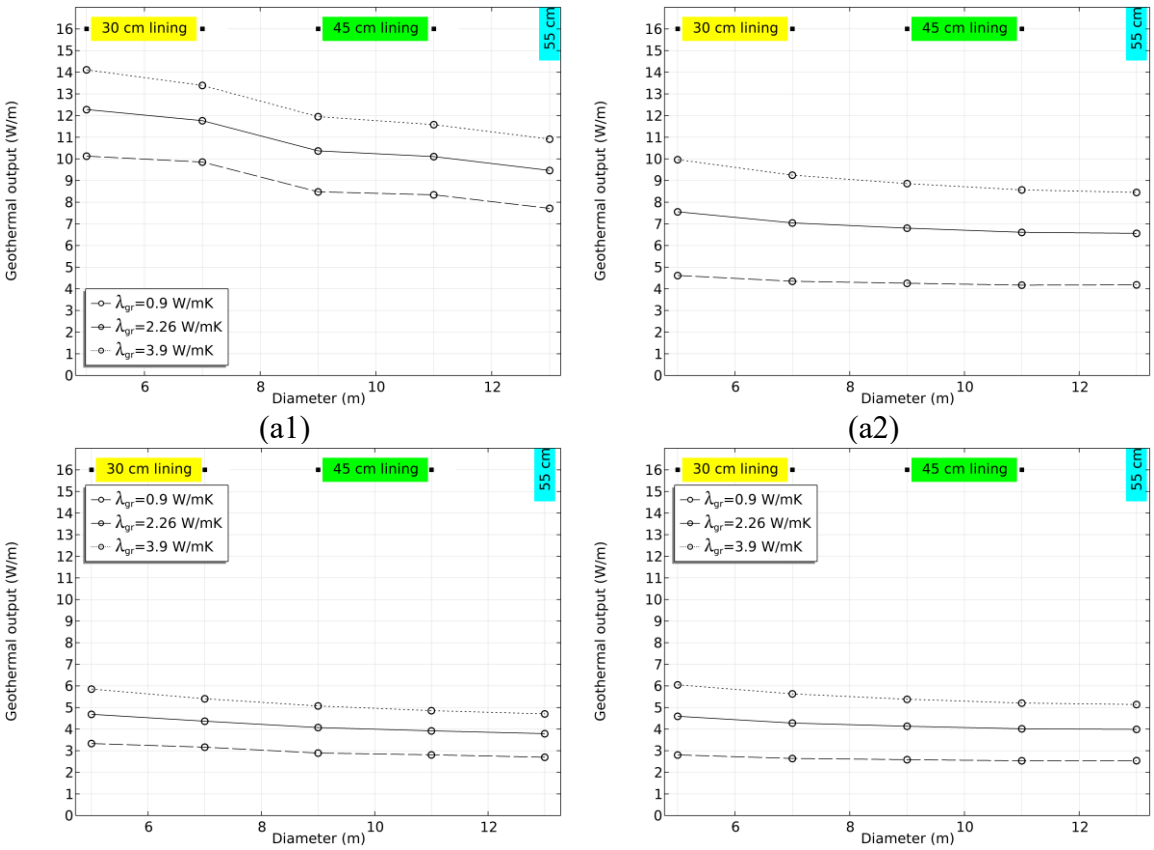

Figure 5-4. Geothermal output for different tunnel inner diameters in summer mode and in the absence of groundwater flow: (a1) uninsulated intrados, T_{ground} = 9 °C and T_{tunnel} = 20.7 °C (a2) insulated intrados, T_{ground} = 9 ° C and T_{tunnel} = 20.7 °C (b1) uninsulated intrados, T_{ground} = 18 °C and T_{tunnel} = 29.7 °C (b2) insulated intrados, T_{ground} = 18 °C and T_{tunnel} = 29.7 °C

The previous analysis of the geothermal performance of the energy tunnels is done for the winter operation mode, where T_{inlet} = 2.5 °C, and its results are shown in Figure 5-5. Unlike the summer mode, the geothermal output of the pipes is higher when ground temperature is 18 °C compared to 9 °C (Figure 5-5-b1&2 versus Figure 5-5-a1&2). Therefore, with a more favorable ground temperature (i.e. 18 °C), the effect of the changes in the ground thermal conductivity is more prominent on the geothermal output. Similar to the summer mode graphs (Figure 5-4), the increase in the geothermal output in terms of Watts per meter of pipe length is recorded when the tunnel inner diameter decreases. Also, for both ground temperatures of 9 and 18 °C, the stepwise irregular geothermal output increase for

the tunnels with uninsulated intrados when the diameter decreases from 13 to 11 m and from 9 to 7 m, is visible due to a decrease in segmental lining thickness in Figure 5-5-a1 and b1. This is similar to the summer mode with uninsulated intrados at T_{ground} = 9 °C and T_{tunnel} = 20.7 °C (Figure 5-4-a), since the tunnel internal air temperatures in the winter mode are 7.1 and 16.1 °C, which are different enough from the inlet temperature of 2.5 °C (unlike Figure 5-4-b1).

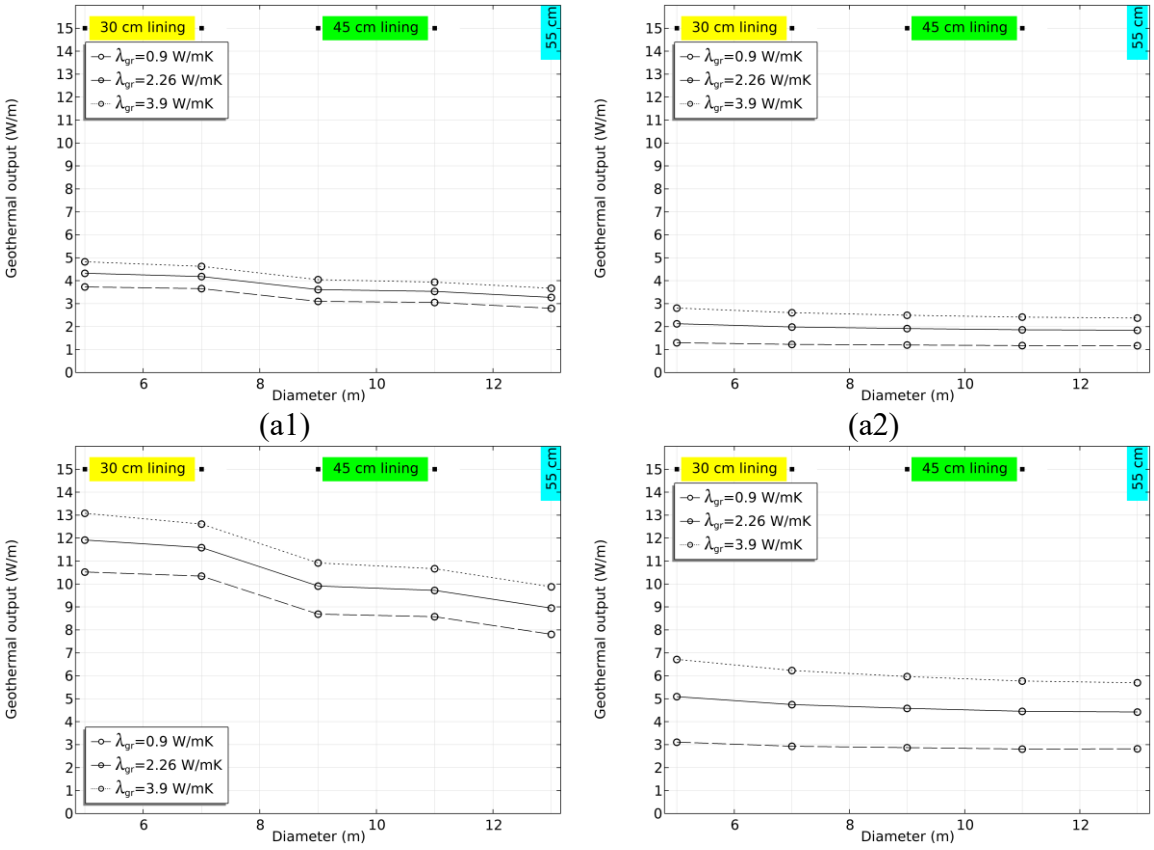

Figure 5-5. Geothermal output for different tunnel inner diameters in winter mode and in the absence of groundwater flow: (a1) uninsulated intrados, T_{ground} = 9 °C and T_{tunnel} = 7.1 °C (a2) insulated intrados, T_{ground} = 9 °C and T_{tunnel} = 7.1 °C (b1) uninsulated intrados, T_{ground} = 18 °C and T_{tunnel} = 16.1 °C (b2) insulated intrados, T_{ground} = 18 °C and T_{tunnel} = 16.1 °C

In analysis of the geothermal output of the energy tunnels with insulated intrados in both summer and winter modes in Figure 5-4 and Figure 5-5, it can be assumed that there might

be an effect of curvature of a constant perimeter length of the tunnel walls on the radial heat flux between the tunnel walls boundary and the ground. To test this idea, a simple 2D planar heat transfer simulation is performed in COMSOL in a domain with dimensions of 300 by 300 m. In this domain, a cavity with diameters of 5, 7, 9, 11, and 13 m is placed where the temperature on its boundary is kept constant and equal to 2.5 °C. The porous domain around the cavity has an initial temperature of 9 °C, while the outer boundaries of the domain are thermally insulated. It is assigned to the ground a thermal conductivity of 2.26 W/mK, and volumetric thermal capacities of solid and water of 2 and 4.2 MJ/m^3K, respectively. These parameters were equal to the values used for energy tunnels' soil domain. The initial thermal condition, boundary conditions and the dimensions of the domain are visually depicted in Figure 5-6. Quadratic Lagrange triangular elements were used to mesh the domain, as shown in the mesh for the 13 m diameter case in Figure 5-7.

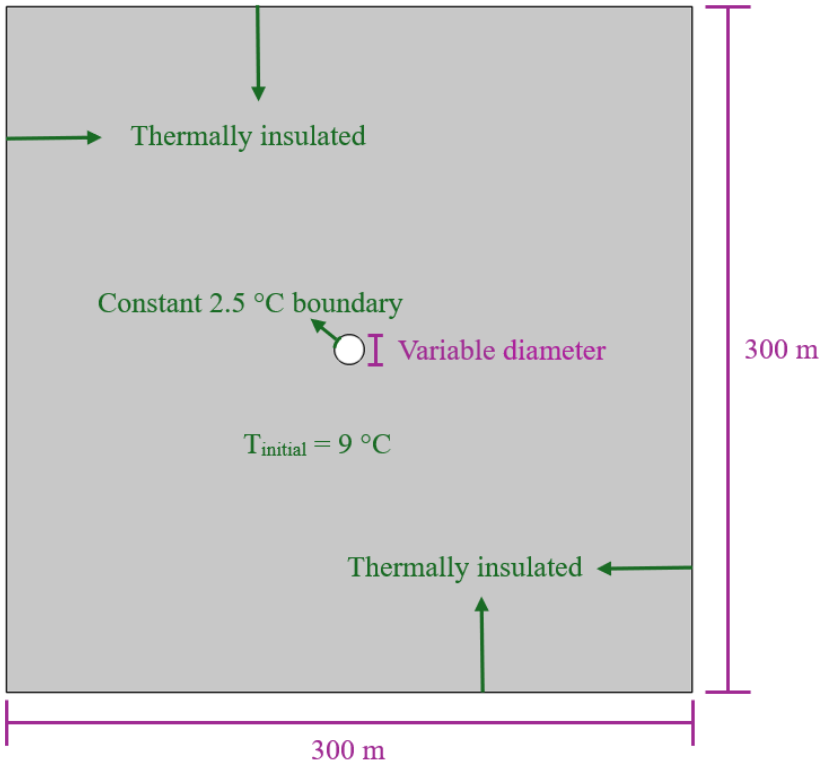

Figure 5-6. Initial, boundary conditions and domain dimensions of the 2D model for planar heat conduction

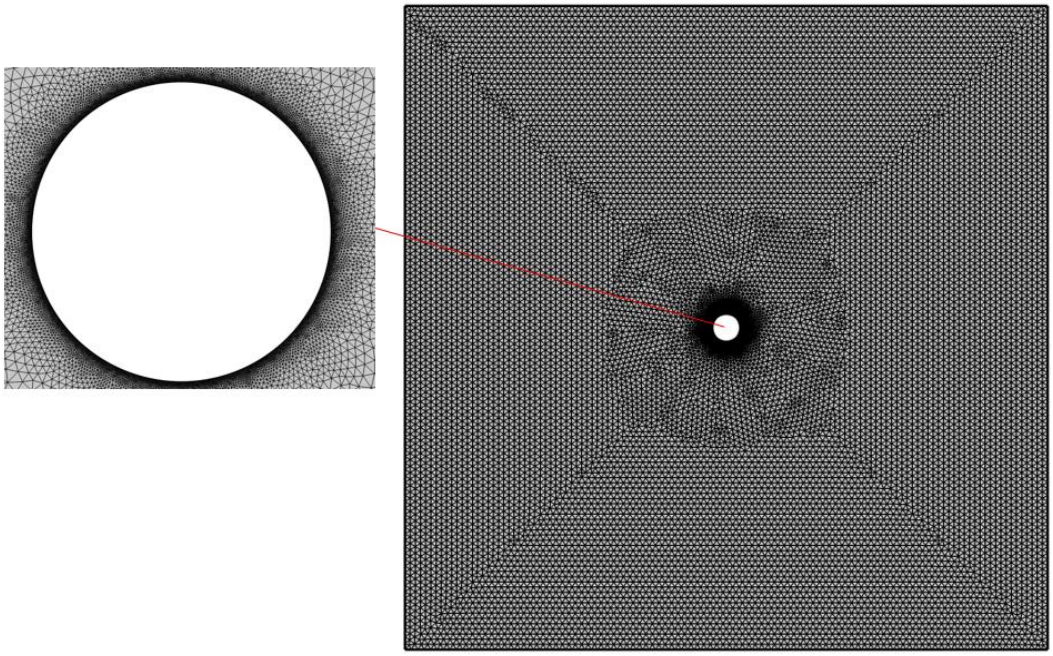

Figure 5-7. Mesh of the 2D model (13 m diameter) for planar heat conduction

The radial heat transfer on the curved boundary is recorded after simulating a 30-day thermal analysis where the heat is exchanged between the curved boundary of the cavity and the soil with the prescribed initial temperature. This radial heat flux at the boundaries of cavities with different diameters is plotted against the time in Figure 5-8. It can be seen that the radial heat flux is the highest for the cavity with a diameter of 5 m (equal to 8.15 W/m^2) and the lowest with a diameter of 13 m (equal to 6.62 W/m^2) which indicates a 19 % difference. This result can justify the assumption that in energy tunnels constructed in the ground without any groundwater flow, where radial conduction is the main heat transfer mechanism, the regions close to the inlet point of a smaller energy tunnel will have a higher heat transfer rate per tunnel perimeter length (or transversal pipe length) with the surroundings (ground or grout). This phenomenon can be repeated for every pipe circuit's row along the direction of the tunnel's axis and eventually decrease the temperature difference between the outlet and the inlet per meter of the pipe length to a lower amount compared to bigger energy tunnels.

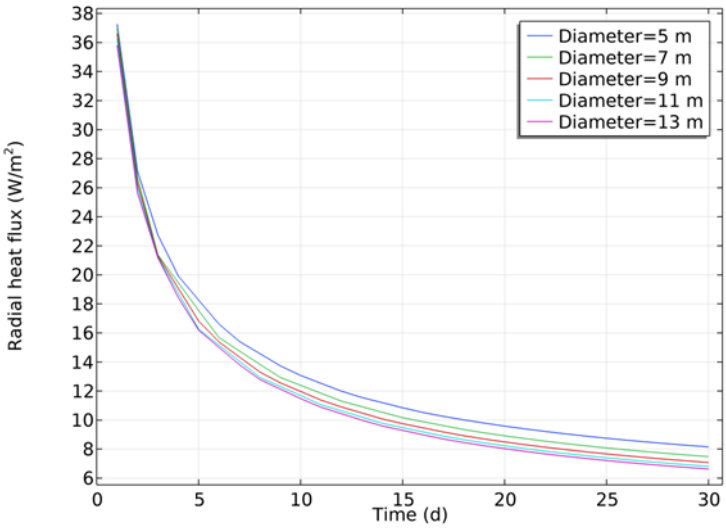

Figure 5-8. Radial heat flux versus time on the cavity's boundary for different diameters in the 2D model for planar heat conduction

5.4 Results for perpendicular groundwater flow

In cases where the energy tunnel is subjected to a groundwater flow perpendicular to its axis, the geothermal output in terms of Watts per meter length of pipe circuit is analyzed in this section. As in previous analyses, when the tunnel intrados is uninsulated, the temperature of the air inside the tunnel changes with respect to seasonality and the ground temperature. The analysis of the geothermal output variation for the energy tunnels with different inner diameters in summer mode (Figure 5-9) shows that whenever the ground thermal conductivity increases (while keeping other parameters constant) the geothermal output of the tunnel will increase, as well. Also, decreasing the tunnel inner diameter (while keeping other parameters constant), results in an increase in geothermal performance of the energy tunnel. This phenomenon is recorded for each of the cases with a certain groundwater flow velocity. This was previously observed for cases without groundwater flow presence. It is also noticeable that this difference in geothermal output of tunnels with different diameters is amplified in the presence of perpendicular groundwater flow. For example, in Figure 5-9-a2 when λ_{gr} = 2.26 W/mK, with a diameter change from 13 to 5 m and no groundwater flow the geothermal output approximately increases 1 W/m, while in the presence of a

groundwater flow velocity of 2 m/d, the output increases more than 6 W/m. This also happened (but is less pronounced) when the groundwater flow velocity increases from a non-zero value. As previously seen, in the summer mode with ground temperature of 18 °C, the tunnel air (with the temperature of 29.7 °C) can have a negative effect on the geothermal output of energy tunnels with identical parameters but insulated intrados. Therefore, by comparing corresponding points of Figure 5-9-b1 and b2, it can be seen that for the cases with non-zero groundwater flow velocity, there is an increase in geothermal output when the tunnel inner walls are insulated. This increase never exceeds 2 W/m but in cases with no groundwater flow, it reaches zero and even reverses to a slight decrease in geothermal performance for the cases with thermally insulated intrados. By comparing the same points of Figure 5-9-a1 and a2 (with ground temperature of 9 °C), a higher geothermal output for energy tunnels with uninsulated inner walls is observed. This means that the 20.7 °C tunnel air indirectly exchanges thermal energy with the circulating fluid due to a large temperature difference with the inlet temperature of 32 °C. It is also noted that although higher ground thermal conductivity improves the geothermal performance of an energy tunnel, its effect is less pronounced in higher groundwater flow velocities. This means that at high groundwater flow velocity values, the thermal exchange is convection dominated.

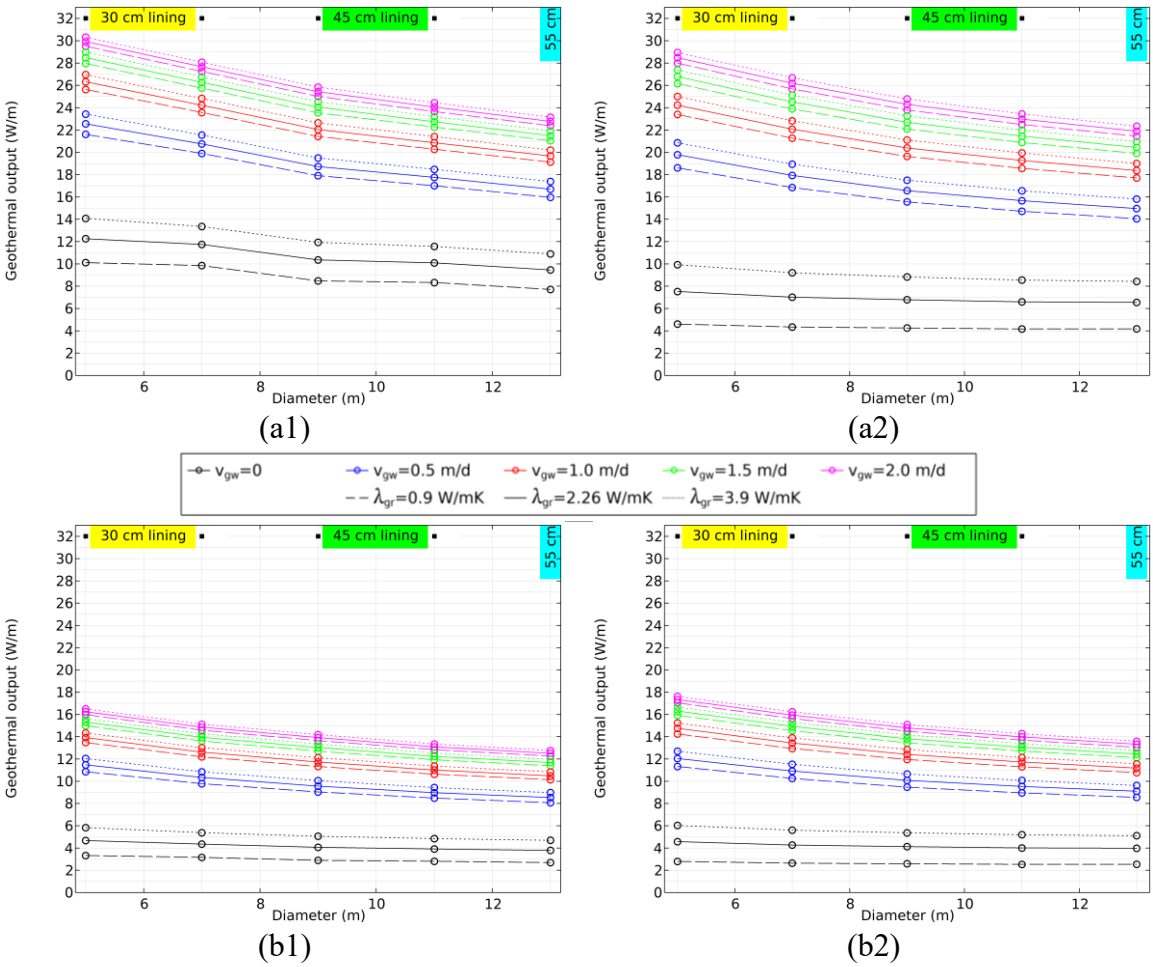

Figure 5-9. Geothermal output for different tunnel inner diameters in summer mode with perpendicular groundwater flow: (a1) uninsulated intrados, T_{ground} = 9 °C and T_{tunnel} = 20.7 °C (a2) insulated intrados, T_{ground} = 9 ° C and T_{tunnel} = 20.7 °C (b1) uninsulated intrados, T_{ground} = 18 °C and T_{tunnel} = 29.7 °C (b2) insulated intrados, T_{ground} = 18 °C and T_{tunnel} = 29.7 °C

When the energy tunnel is performing in the winter mode and a perpendicular groundwater flow, the geothermal output is plotted against the tunnel inner diameter for ground temperatures of 9 and 18 °C in Figure 5-10-a1&2 and Figure 5-10-b1&2, respectively. The ground temperature of 18 °C is more favorable than 9 °C in this operation mode, leading to a higher geothermal output. Also, the geothermal output increases in an energy tunnel with a smaller inner diameter or higher groundwater velocity, like previous simulations. Unlike the summer mode in both ground temperatures of 9 and 18 °C, energy

tunnels show a higher geothermal performance when the tunnel intrados is not insulated, indicating a thermal energy exchange with the air inside the tunnel. The reason is that the tunnel air temperatures (7.1 and 16.1 °C) at both ground temperature conditions are different enough from the inlet temperature of 2.5 °C. In Figure 5-10-a1 and b1, the increase in geothermal output by decreasing the tunnel diameter from 13 to 11 m and from 9 to 7 m experiences a steeper transition due to a reduction in the segmental lining thickness at these points that boosts the thermal exchange with the tunnel air. Moreover, the convection-dominated heat transfer in higher groundwater flow velocities reduces the influence of ground thermal conductivity on the geothermal output of energy tunnels.

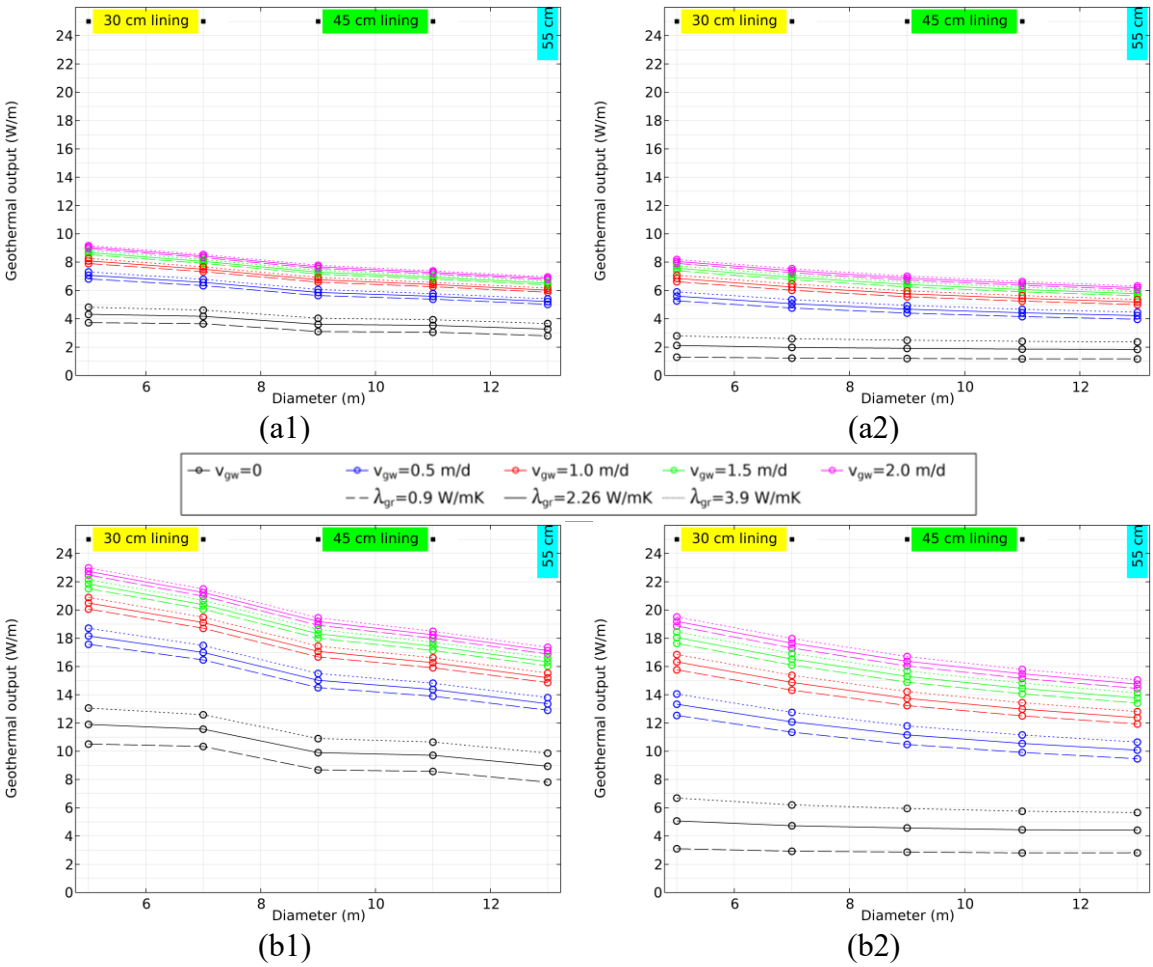

Figure 5-10. Geothermal output for different tunnel inner diameters in winter mode with perpendicular groundwater flow: (a1) uninsulated intrados, T_{ground} = 9 °C and T_{tunnel} = 7.1 °C (a2) insulated intrados, T_{ground} = 9 ° C and T_{tunnel} = 7.1 °C (b1) uninsulated intrados, T_{ground} = 18 °C and T_{tunnel} = 16.1 °C (b2) insulated intrados, T_{ground} = 18 °C and T_{tunnel} = 16.1 °C

5.5 Results for parallel groundwater flow

In cases where the energy tunnel is subjected to a groundwater flow parallel to its axis, the geothermal output in terms of Watts per meter length of pipe circuit are analyzed in this section. As always, the temperature of the tunnel air changes according to the season and ground temperature. The changes in the geothermal output of the energy tunnels with different inner diameters in summer mode and ground temperatures of 9 and 18 °C are shown

in Figure 5-11. As expected, the amount of increase in geothermal output of a specific tunnel by parallel groundwater flow is less than its performance when it is subjected to perpendicular flow (compared to Figure 5-9). The previously observed trend of increase in the geothermal performance of tunnels with smaller diameters prevails here. Moreover, the convection-dominated heat transfer at high groundwater flow velocites reduces the influence of ground thermal conductivity on the geothermal output of energy tunnels, as before. Once again, the geothermal output of the uninsulated tunnel with ground temperature of 18 °C in summer mode (Figure 5-11-b1) becomes less than the performance of the similar tunnel when the intrados are insulated in non-zero groundwater flow. This observation is reversed for the ground temperature of 9 °C in Figure 5-11-a1 and a2 (similar to the cases with perpendicular groundwater flow).

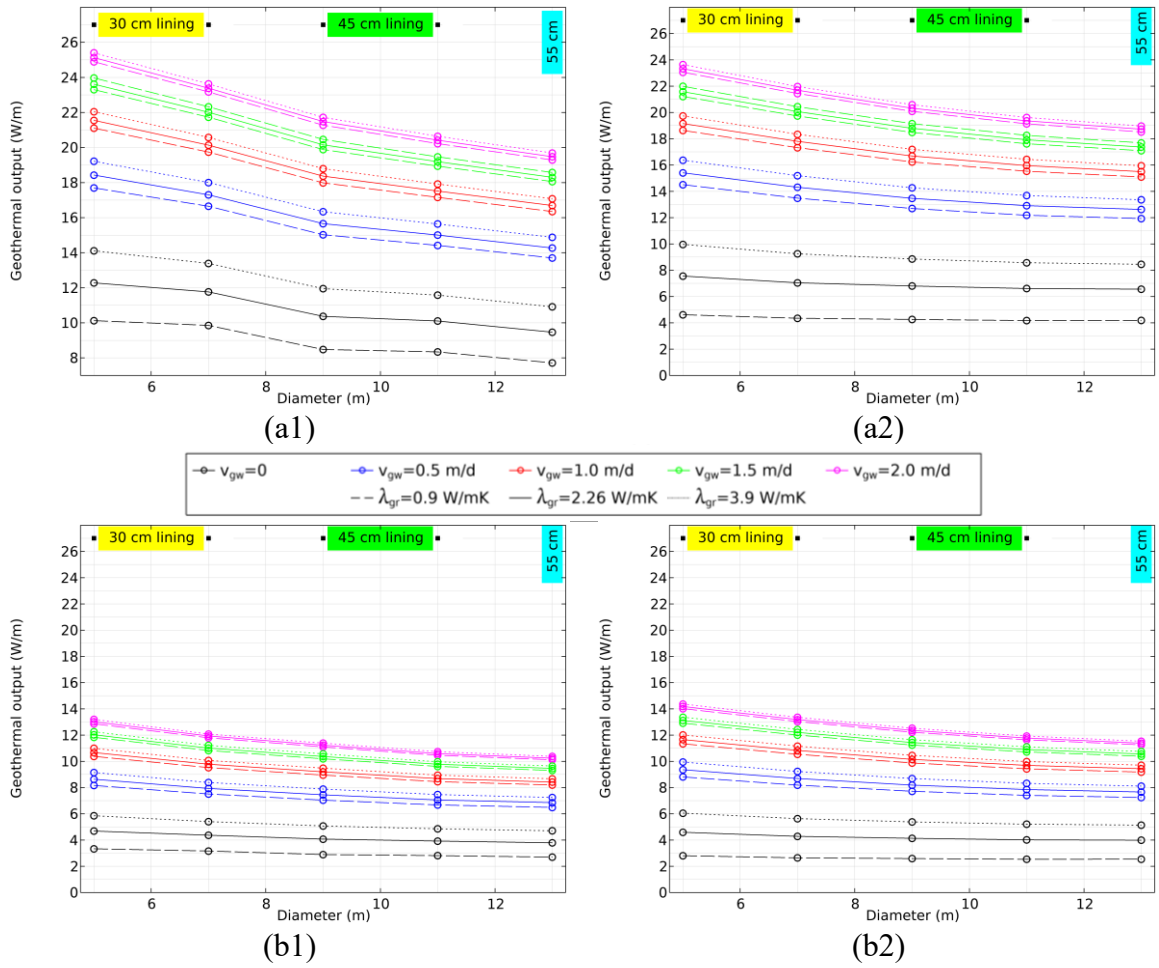

Figure 5-11. Geothermal output for different tunnel inner diameters in summer mode with parallel groundwater flow: (a1) uninsulated intrados, T_{ground} = 9 °C and T_{tunnel} = 20.7 °C (a2) insulated intrados, T_{ground} = 9 ° C and T_{tunnel} = 20.7 °C (b1) uninsulated intrados, T_{ground} = 18 °C and T_{tunnel} = 29.7 °C (b2) insulated intrados, T_{ground} = 18 °C and T_{tunnel} = 29.7 °C

In winter mode, the parallel groundwater flow's effect on the geothermal output of the energy tunnels of various diameters is presented in Figure 5-12. As expected, the geothermal output of a specific tunnel by parallel groundwater flow in winter mode is less than its performance when it is subjected to perpendicular flow (compared to Figure 5-10). Similar to the cases with perpendicular groundwater flow (Figure 5-10), the uninsulated energy tunnels' thermal exchange with the tunnel air improves the geothermal output of the system compared to the insulated ones in both ground temperatures of 9 and 18 °C. However, the

other trends in geothermal output of the tunnels remain the same as the cases in summer mode and parallel groundwater flow.

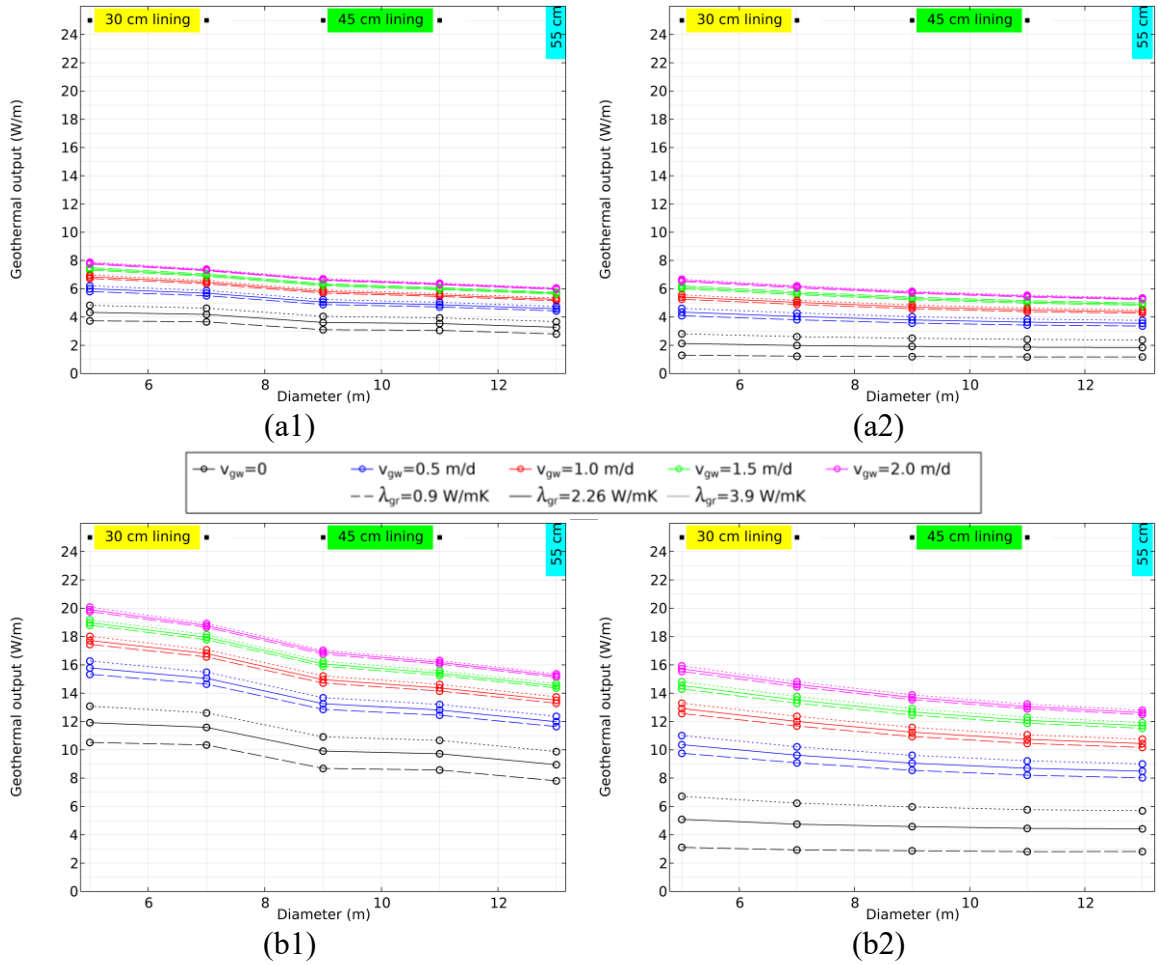

Figure 5-12. Geothermal output for different tunnel inner diameters in winter mode with parallel groundwater flow: (a1) uninsulated intrados, T_{ground} = 9 °C and T_{tunnel} = 7.1 °C (a2) insulated intrados, T_{ground} = 9 ° C and T_{tunnel} = 7.1 °C (b1) uninsulated intrados, T_{ground} = 18 °C and T_{tunnel} = 16.1 °C (b2) insulated intrados, T_{ground} = 18 °C and T_{tunnel} = 16.1 °C

5.6 Summary

In this chapter the influence of diameter variation on the geothermal output (in Watts per meter of pipe length) of energy tunnels was investigated using the validated TH model of previous chapter. To do so, parametric studies that consisted of five diameters for the tunnels

were chosen along with changes in seasonality, tunnel intrados boundary condition, ground temperature and thermal conductivity, and groundwater flow velocity and direction. A total number of 2400 numerical parametric studies were performed, and the results were discussed in three conditions.

In the first condition where the saturated soil does not experience any groundwater flow, a smaller energy tunnel demonstrated a higher geothermal output for two reasons. One was a higher curvature of a certain tunnel perimeter length of an energy tunnel, which increases the radial heat exchange between the smaller tunnel and the ground. The other reason is valid for the case of uninsulated intrados tunnels, where a smaller tunnel has a thinner lining thickness and therefore its geothermal output is enhanced by thermal exchange with the tunnel air which was simulated using convective heat transfer boundary condition with a constant temperature.

The second and third condition were the energy tunnels with parallel and perpendicular groundwater flow directions with respect to their axes. In these conditions also, the increase in geothermal output by decreasing the energy tunnel diameter was observed. It was noted that at higher groundwater flow velocities the heat transfer phenomenon becomes convection-dominated that leads to a lower impact of ground thermal conductivity variations on the geothermal performance of the tunnel.

In all of the conditions, the geothermal output of the tunnel increases when there is no insulation of tunnel intrados except for when the ground temperature is 18 °C in summer mode. At this ground temperature, the tunnel air is assumed to be 29.7 °C, which is relatively close to the inlet temperature of 32 °C and sometimes inhibits a higher thermal exchange with the ground when compared to the insulated cases. Lastly, in identical tunnels an increase in groundwater flow velocity or ground thermal conductivity increases the geothermal output of the energy geostructure.

6 Energy tunnel design tool: quantifying diameter impact on thermal output

In the thermal design stage of an energy tunnel, it is always useful to have a quick preliminary assessment of the geothermal performance prior to any time-consuming numerical simulations using some design charts. In order to have a reliable assessment, the ground hydrothermal parameters in case of a perpendicular groundwater flow were used to generate preliminary design charts by Di Donna & Barla (2016) in terms of Watts per m^2 surface of the tunnel extrados. These charts were further enhanced by adding the various groundwater flow orientations and tunnel air temperatures with respect to the tunnel axis by Insana & Barla (2020). In this chapter, the analyses of the previous chapter that involved the parameters of Table 5-2 will be used to implement the role of diameter on predicting the geothermal output of energy tunnels into new preliminary design charts in terms of Watts per meter length of the absorber pipes.

6.1 Design charts in absence of groundwater flow

When there is no groundwater flow inside the saturated soil domain the geothermal output of the energy tunnel (in W/m) can be predicted in a contour plot that has inner tunnel

diameter and ground temperature as its horizontal and vertical axes, respectively. Drawing the contour lines for three different ground thermal conductivities of 0.9, 2.26, and 3.9 W/mK, using dotted, solid and dashed lines respectively, under two intrados thermal boundary conditions, based on the results illustrated in the previous chapter, leads to the design charts of Figure 6-1. In the case of uninsulated intrados, the steep geothermal output contour lines when diameter changes from 7 to 9 m and from 11 to 13 m is due to lining thickness increases from 30 to 45 cm and from 45 to 55 cm. These increases in the lining thickness cause a lower thermal exchange between the absorber pipes and the heat flux boundary condition of the tunnel intrados that simulates the tunnel air presence with a constant temperature.

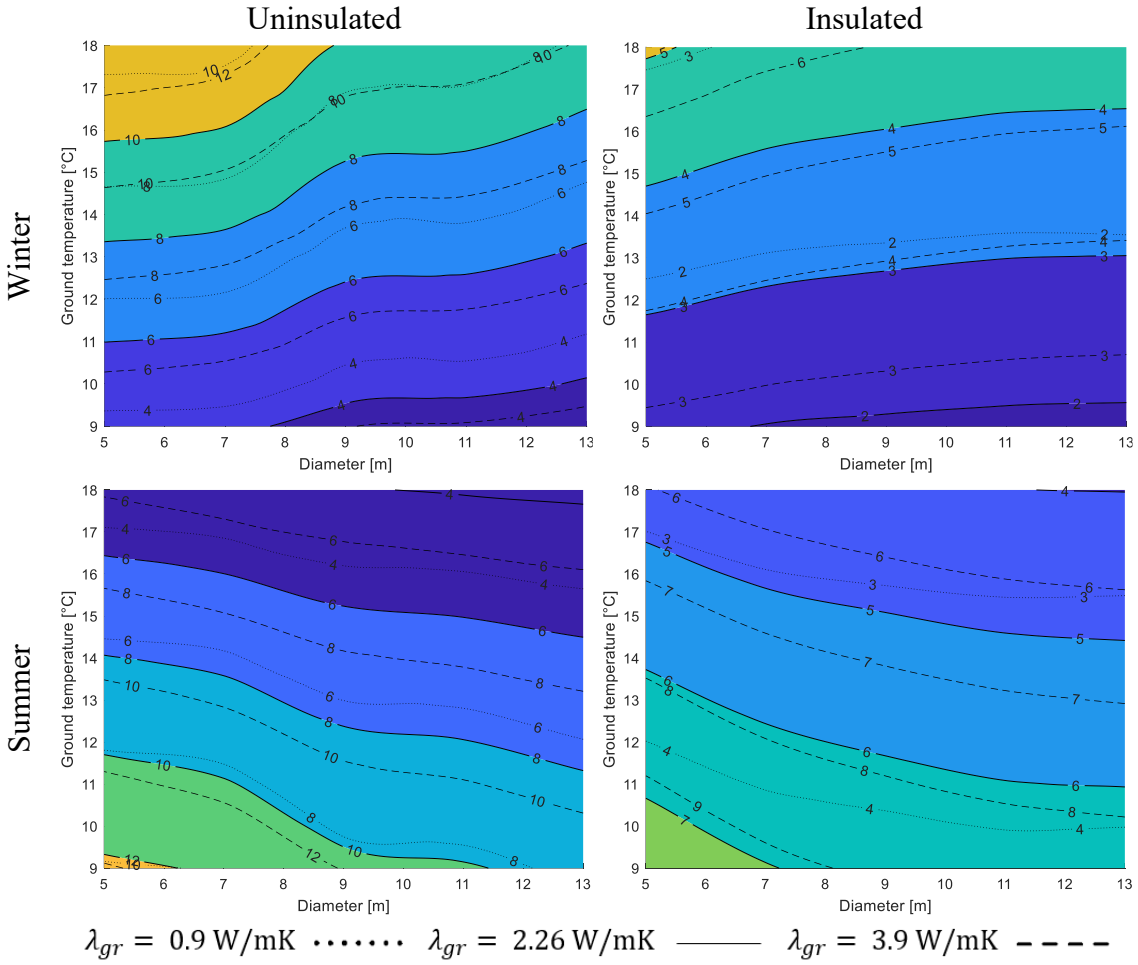

Figure 6-1. Design charts for the geothermal output (in W/m) of energy tunnels for various diameters and ground temperatures

6.2 Design charts for perpendicular groundwater flow

It was noticeable in all graphs of Figure 5-9 and Figure 5-10 that an increase in the perpendicular groundwater flow velocity and a decrease in tunnel inner diameter improved the geothermal output of energy tunnels (when measured per unit length of the pipes). Therefore, the geothermal output of each graph is replotted versus the ratio between groundwater flow velocity and the tunnel's inner diameter (v_{gw}/D_{in}) in Figure 6-2 and Figure 6-3 in summer and winter mode, respectively. It is observed that for the energy tunnels with

insulated intrados, the geothermal potential is a function of v_{gw}/D_{in} at a constant ground thermal conductivity and forms an approximately continuous line in the graphs. This means that when the diameter of the energy tunnel becomes *n* times bigger, its performance can be kept the same if the perpendicular groundwater velocity is also multiplied by *n*. This phenomenon is visible but less precise when the tunnel intrados is uninsulated (Figure 6-2-a1&b1 and Figure 6-3-a1&b1) due to the thermal exchange with the internal tunnel air. However, when the difference between the inlet temperature of summer (i.e. 2.5 °C) is less (Figure 6-2-b1 with tunnel air temperature of 29.7 °C) this continuous function reappears.

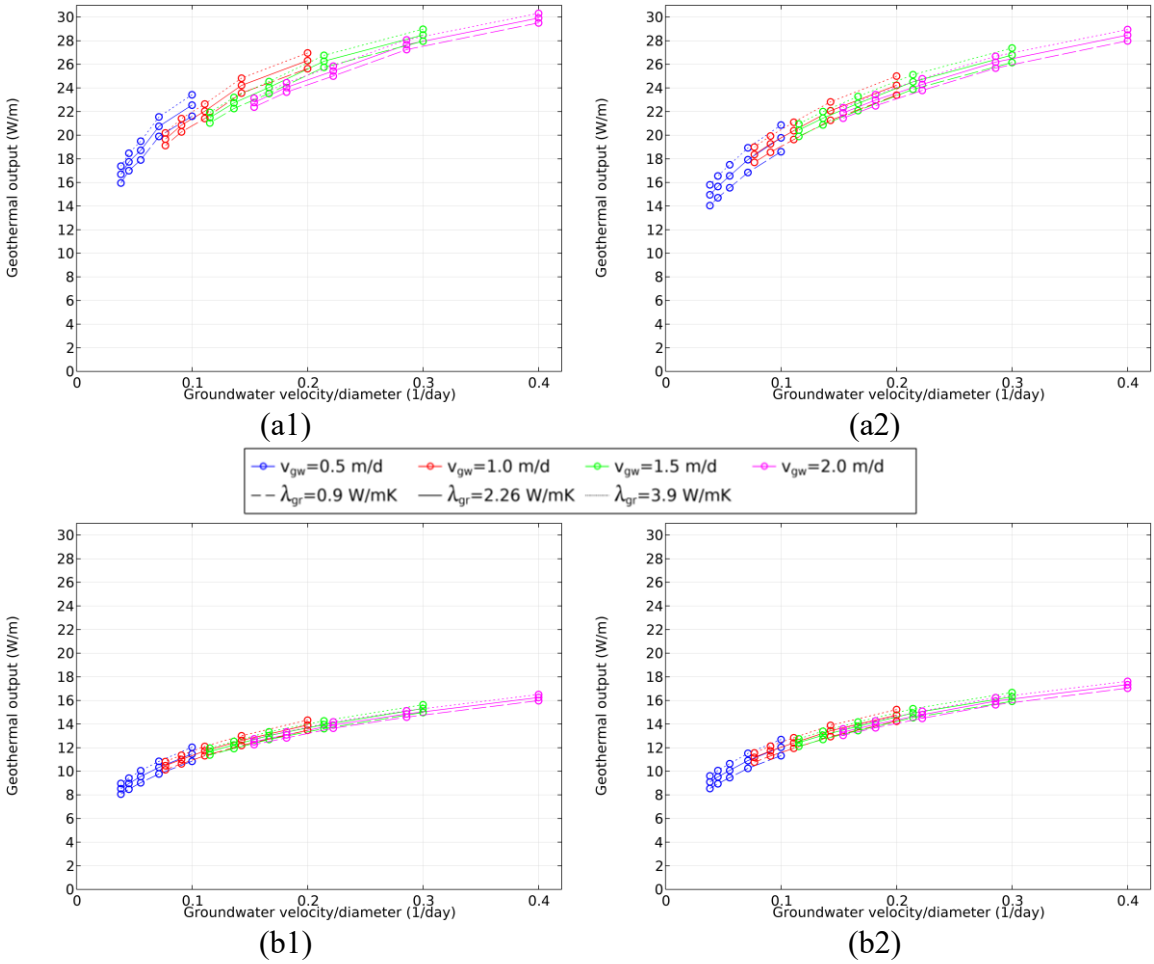

Figure 6-2. Geothermal output versus the ratio between groundwater flow velocity and the tunnel's inner diameter in summer mode with perpendicular groundwater flow: (a1) uninsulated intrados, T_{ground} = 9 °C and T_{tunnel} = 20.7 °C (a2) insulated intrados, T_{ground} = 9 ° C and T_{tunnel} = 20.7 °C (b1) uninsulated intrados, T_{ground} = 18 °C and T_{tunnel} = 29.7 °C (b2) insulated intrados, T_{ground} = 18 °C and T_{tunnel} = 29.7 °C

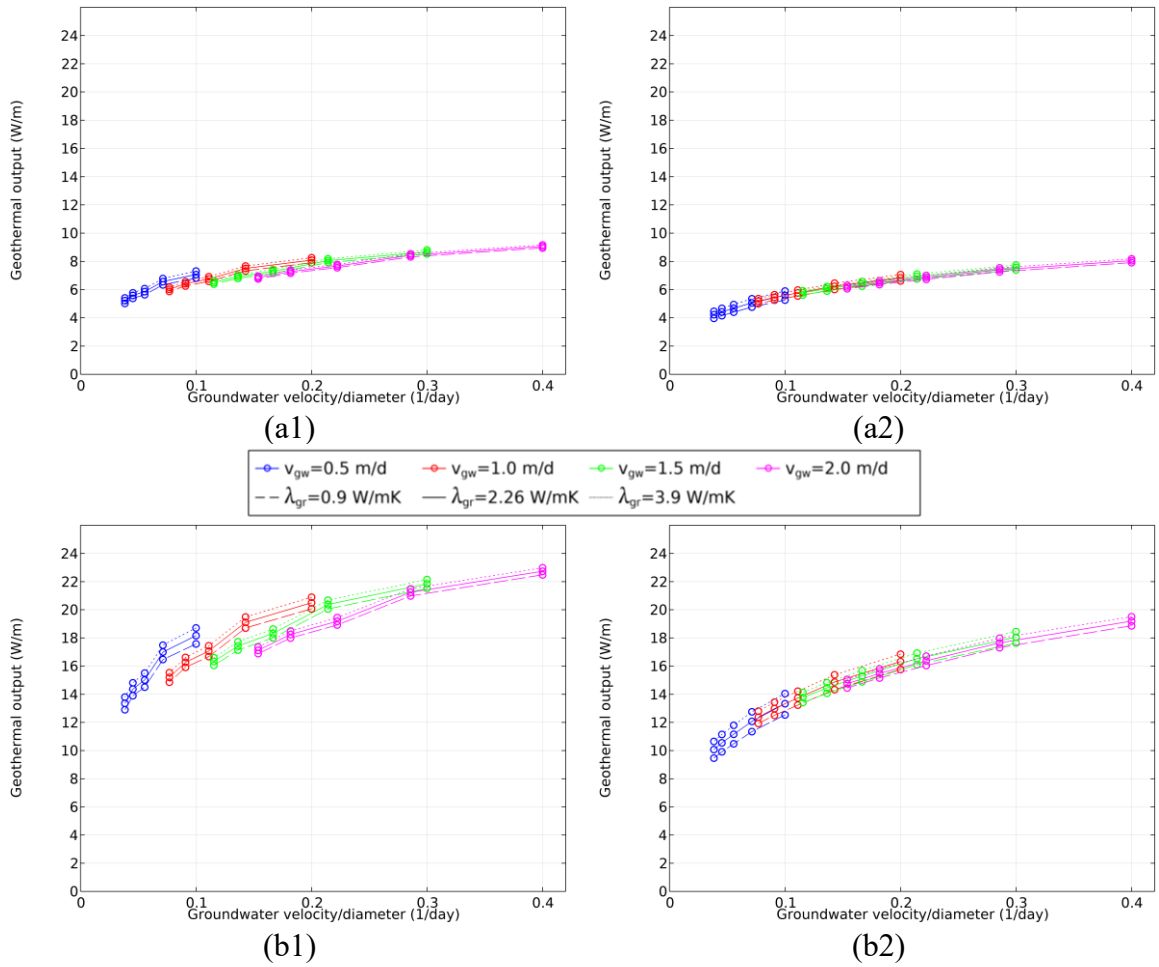

Figure 6-3. Geothermal output versus the ratio between groundwater flow velocity and the tunnel's inner diameter in winter mode with perpendicular groundwater flow: (a1) uninsulated intrados, T_{ground} = 9 °C and T_{tunnel} = 7.1 °C (a2) insulated intrados, T_{ground} = 9 ° C and T_{tunnel} = 7.1 °C (b1) uninsulated intrados, T_{ground} = 18 °C and T_{tunnel} = 16.1 °C (b2) insulated intrados, T_{ground} = 18 °C and T_{tunnel} = 16.1 °C

At this point it is possible to assume that v_{gw}/D_{in} can be used as a key parameter in determining the geothermal performance of an energy tunnel. Therefore, it will be used as the horizontal axis of the design charts for geothermal output of energy tunnels (W/m) when the vertical axis is the ground temperature in Figure 6-4. The only problem with this method is that the v_{gw}/D_{in} in the absence of groundwater flow becomes zero and the intercept of a certain contour line is an average of the geothermal output for all energy tunnel diameters for a certain ground temperature. Therefore, it is advisable to use the charts of Figure 6-1 in cases

with no groundwater flow. Also, the zigzag contour lines in Figure 6-4, are due to a high concentration of simulated results in some regions. This irregularity is more pronounced in the uninsulated design charts due to changes in lining thickness which can directly influence the amount of thermal exchange between the absorber pipes and the convective heat flux boundary condition of the intrados. For instance, at a constant ground temperature, two energy tunnels with groundwater velocity and inner diameter pairs of (1.5 m/d, 13 m) and (0.5 m/d, 5 m) yield v_{gw}/D_{in} ratios of 0.115 and 0.1, respectively. However, the lining thickness of the first tunnel (30 cm) is nearly half the thickness of the second (55 cm). Eventually, by neglecting these variations in the geothermal output prediction of the plots, a fourth-order polynomial interpolation was applied to the contour lines to have smoother version of the charts in Figure 6-5.

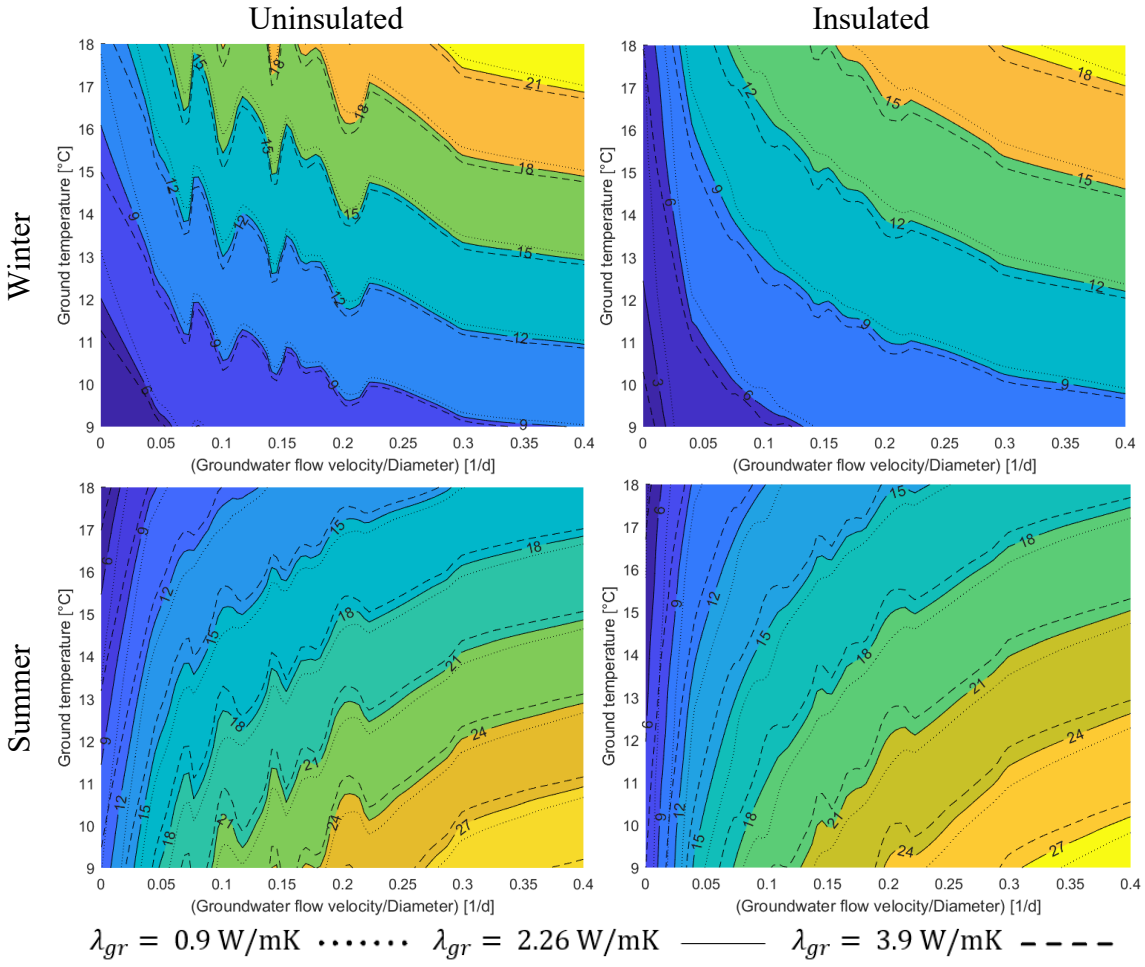

Figure 6-4. Design charts for the geothermal output (in W/m) of energy tunnels with perpendicular groundwater flow for various v_{gw}/D_{in} and ground temperatures

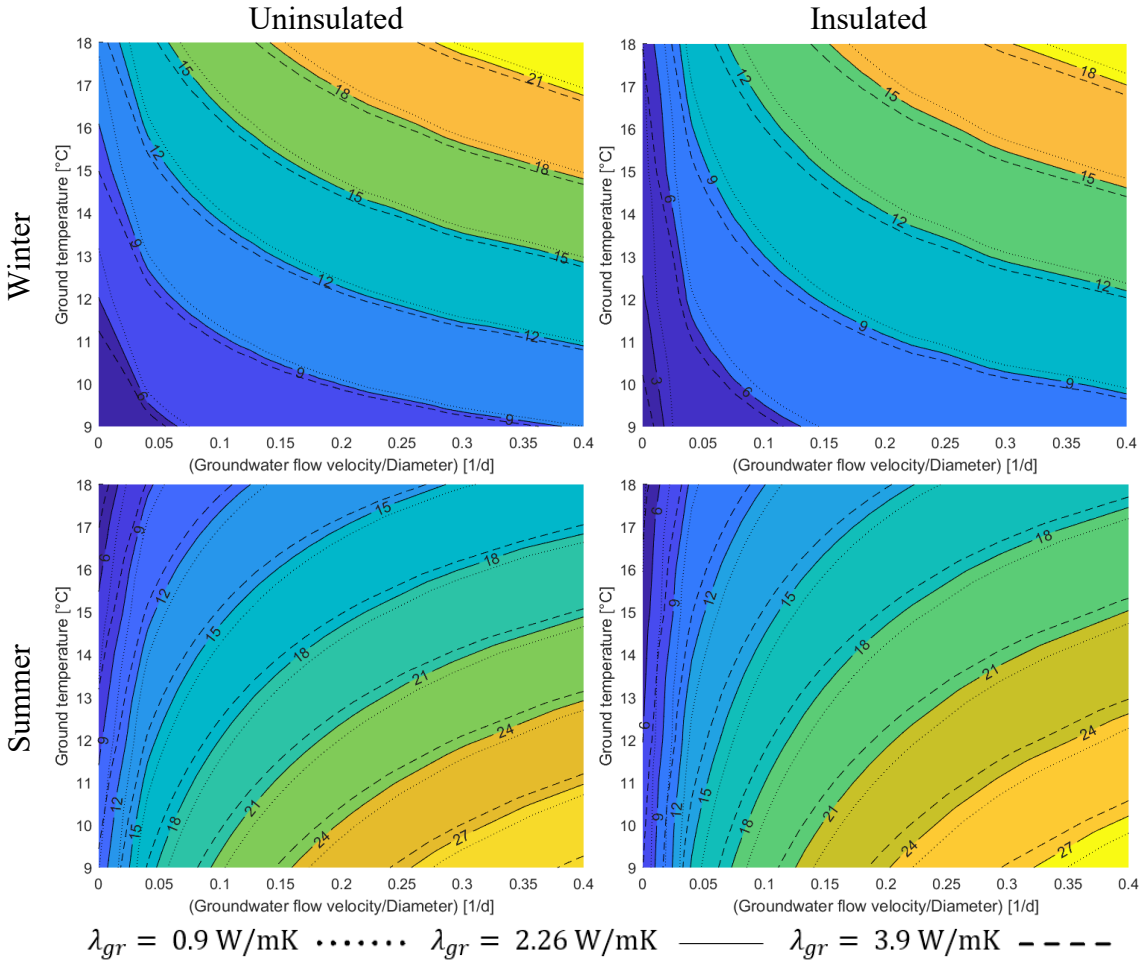

Figure 6-5. Refined design charts for the geothermal output (in W/m) of energy tunnels with perpendicular groundwater flow for various v_{gw}/D_{in} and ground temperatures

6.3 Design charts for parallel groundwater flow

Once again, it was noticeable in all graphs of Figure 5-11 and Figure 5-12 that an increase in the parallel groundwater flow velocity and a decrease in tunnel inner diameter improved the geothermal output of the energy tunnels. Therefore, the geothermal output of each graph is replotted versus the ratio between groundwater flow velocity and the tunnel's inner diameter (v_{gw}/D_{in}) in Figure 6-6 and Figure 6-7 in summer and winter mode, respectively. In

this groundwater orientation, v_{gw}/D_{in} does not make the uninsulated graphs as smooth as the perpendicular groundwater flow cases, but it is still possible to use this characteristic parameter as an indicator of thermal recharge of energy tunnels.

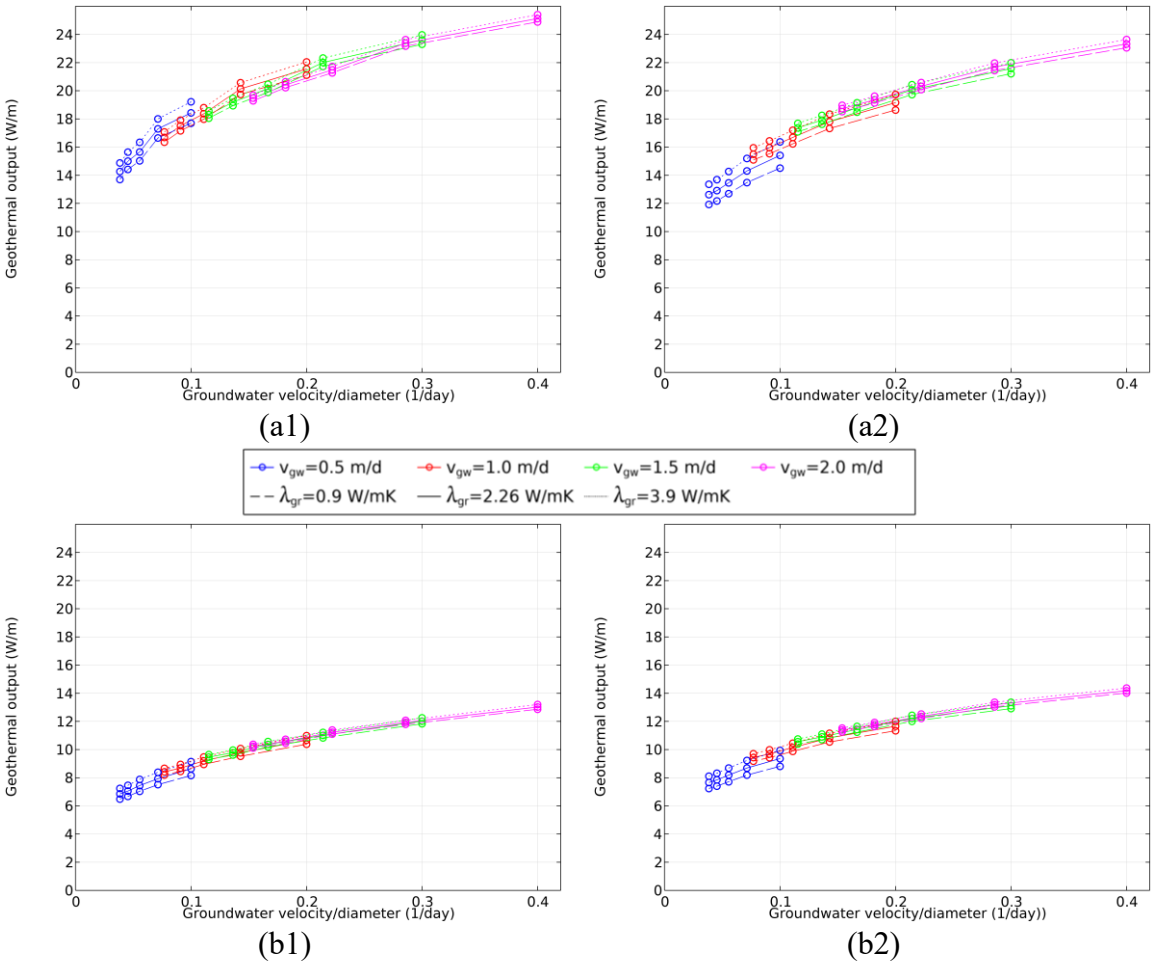

Figure 6-6. Geothermal output versus the ratio between groundwater flow velocity and the tunnel's inner diameter in summer mode with parallel groundwater flow: (a1) uninsulated intrados, T_{ground} = 9 °C and T_{tunnel} = 20.7 °C (a2) insulated intrados, T_{ground} = 9 ° C and T_{tunnel} = 20.7 °C (b1) uninsulated intrados, T_{ground} = 18 °C and T_{tunnel} = 29.7 °C (b2) insulated intrados, T_{ground} = 18 °C and T_{tunnel} = 29.7 °C

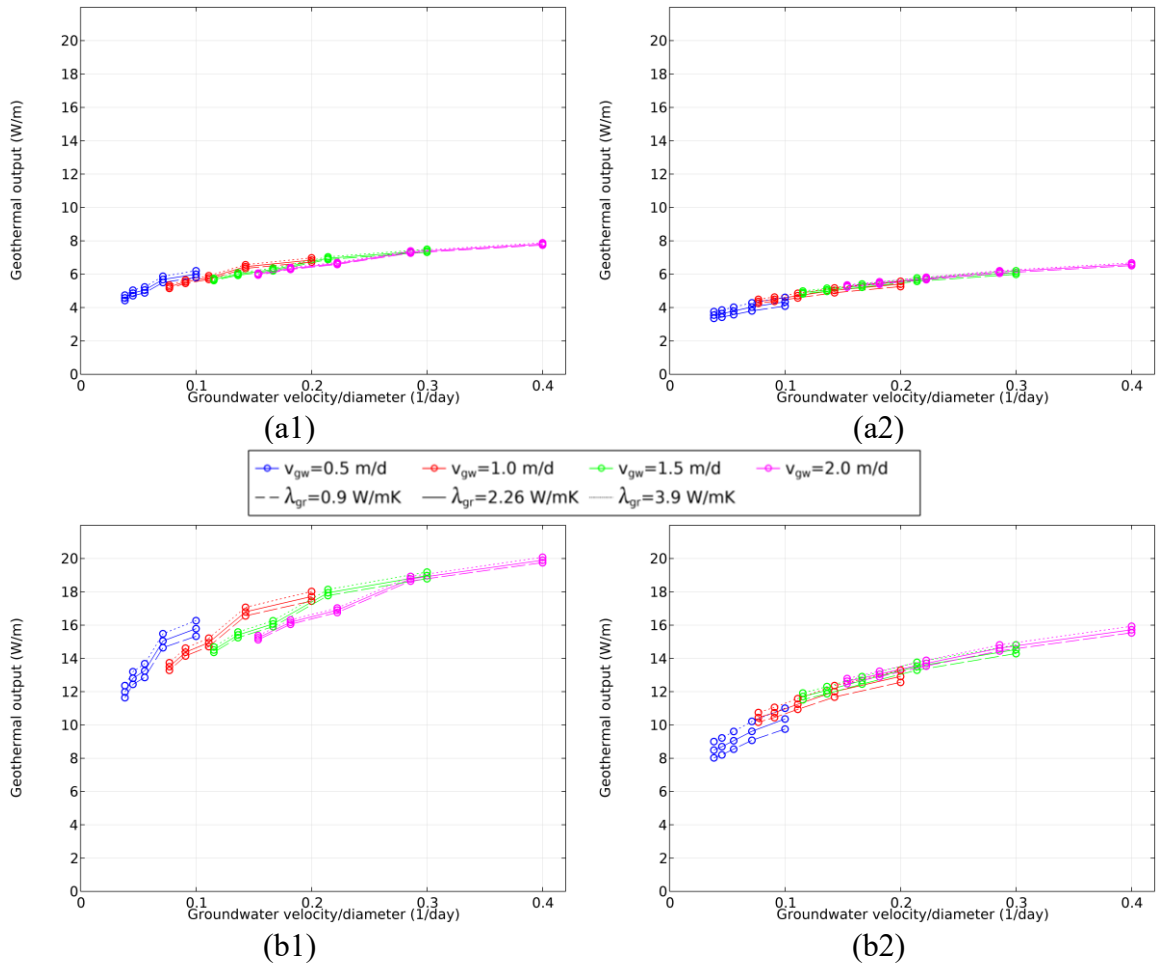

Figure 6-7. Geothermal output versus the ratio between groundwater flow velocity and the tunnel's inner diameter in winter mode with parallel groundwater flow: (a1) uninsulated intrados, T_{ground} = 9 °C and T_{tunnel} = 7.1 °C (a2) insulated intrados, T_{ground} = 9 ° C and T_{tunnel} = 7.1 °C (b1) uninsulated intrados, T_{ground} = 18 °C and T_{tunnel} = 16.1 °C (b2) insulated intrados, T_{ground} = 18 °C and T_{tunnel} = 16.1 °C

Once again it is possible to assume that v_{gw}/D_{in} can be used as a key parameter in determining the geothermal performance of energy tunnels. Therefore, it will be used as the horizontal axis of the design charts for geothermal output of energy tunnels (W/m) when the vertical axis is the ground temperature in Figure 6-8. The lack of smoothness in these charts is dealt with by a fourth order polynomial interpolation for the contour lines which generated the refined design charts of Figure 6-9 for insulated and uninsulated intrados.

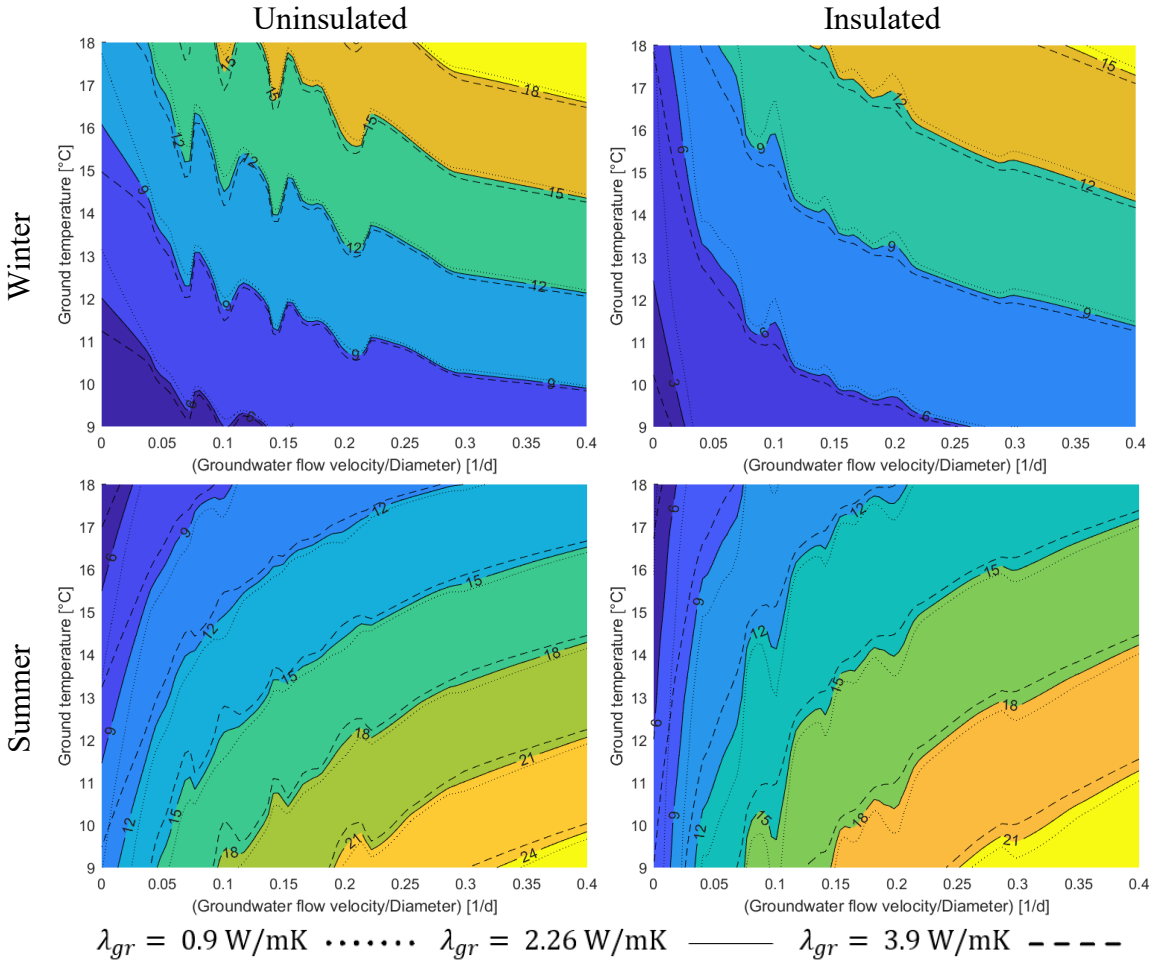

Figure 6-8. Design charts for the geothermal output (in W/m) of energy tunnels with parallel groundwater flow for various v_{gw}/D_{in} and ground temperatures

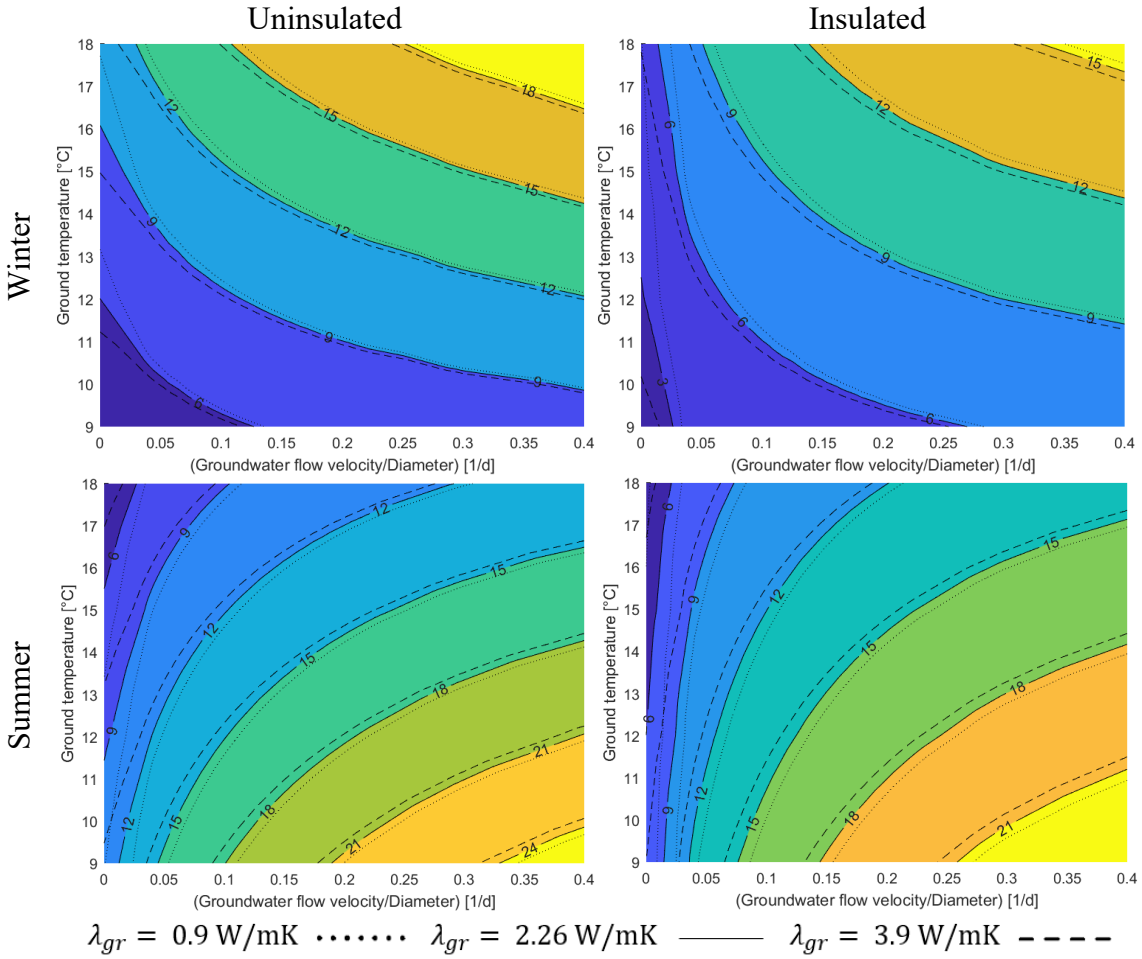

Figure 6-9. Refined design charts for the geothermal output (in W/m) of energy tunnels with parallel groundwater flow for various v_{gw}/D_{in} and ground temperatures

6.4 Procedure for utilizing the design charts

Based on the numerical simulations setup that were chosen to obtain the design charts for energy tunnels of different diameters, there are some conditions that need to be met to obtain the closest field results compared to these charts:

- The absorber pipes diameter and thickness to be equal to 20 and 2 mm, respectively.
- The longitudinal pipe spacing (out of plane direction) should be more than 275 mm.
- The circulating fluid flow velocity should be high enough to be a turbulent flow.

Note 1: An important practical consideration for designing geothermal systems (which was neglected in the present study's numerical models) that ensures proper performance of heat pump is that was not imposed is to assume an inlet-outlet temperature difference (ΔT) of equal or more than 4 °C. Therefore, the minimum value for continuous pipe circuit length (L_{min}) that satisfies a $\Delta T \geq 4$ °C is:

$$L_{min} = \frac{\pi}{4} \rho_f v_f D_{pipe}^2 c_{p,f} \Delta T / \text{Geothermal output}(W/m)$$

Where ρ_f, v_f, D_{pipe}, and $c_{p,f}$ are circulating fluid's density and velocity, pipe diameter, and circulating fluid's thermal capacity.

Note 2: The ring length of all simulated tunnels of the present study was equal to 1.4 m, but it might be needed to design an energy tunnel with the same diameter but a higher ring length. Consequently, the continuous pipe length inside a single ring will be more than the values reported in Table 5-1 that were used in the numerical models of the design charts. Therefore, it is expected to have a reduction in the geothermal performance of the energy tunnel under design compared to the charts' readings in terms of Watts per meter pipe length because the circulating fluid's temperature gets closer to the ground temperature by every meter elongation of the pipe circuit. However, the amount of this reduction is unknown and needs further study.

Having these recommendations in mind, the way to use the charts as a preliminary energy output predictor is described in two ways:

First approach: seeking the energy output (in Watts) of a known tunnel:

- Read the geothermal output (in W/m) from the charts by having D_{in}, v_{gw}, λ_{gr}, and T_{ground}
- The designer finds how much pipe length can be put in a ring's geometry then multiply it by the total number of rings to get the total pipe length for the tunnel
- Multiply the total pipe length by the chart's reading (in W/m) to obtain the energy output of the whole tunnel length (in W)

- Note: Fulfilling the L_{min} criterion might not be possible by the amount of pipe length that can be placed inside a single tunnel ring and therefore, two or more rings need to be connected in series.

Second approach: seeking the number of tunnel rings that satisfy a certain amount of energy demand

- Read the geothermal output (in W/m) from the charts by having D_{in}, v_{gw}, λ_{gr}, and T_{ground}
- Calculate the pipe length needed for the energy demand $= \frac{needed\ Watts}{reading\ of\ charts\ (in\ \frac{W}{m})}$
- The designer finds how much pipe length can be put in a ring's geometry
- The number of needed rings $= \frac{needed\ pipe\ length}{pipe\ length\ capacity\ of\ a\ single\ ring}$
- Note: Fulfilling the L_{min} criterion might not be possible by the amount of pipe length that can be placed inside a single tunnel ring and therefore, two or more rings need to be connected in series.

6.5 Verification of the design charts

To test whether the design charts introduced in this chapter can serve as a fast, preliminary tool for estimating an energy tunnel's geothermal output before construction or even performing numerical simulations, their predictions are benchmarked against performance data drawn from earlier numerical or real case studies in Table 6-1. Energy tunnels' energy assessment is generally done by reporting the geothermal performance in terms of W/m^2. Since the charts of the present study predict the geothermal output of the tunnels in terms of Watts per meter length of the pipes, it is necessary to calculate the ratio of each case's lining outer surface over the absorber pipes length. Multiplication of this ratio to the reported thermal performance in terms of W/m^2 leads to having the equivalent energy output of the energy tunnel per pipe length (i.e. W/m). At this point, the performance of each

case can be simultaneously compared with the design charts of the present study and the charts of Figure 2-24 which were generated by Insana & Barla (2020). It should be notified that in the case of the Turin ML2, the present study's chart readings assumed a perpendicular groundwater flow in the numerical simulation while it had an angle of 30-60° with respect to the tunnel axis.

The accuracy of the predictions by all the design charts are shown in Figure 6-10 and Figure 6-11 for winter and summer, respectively, using the following equation:

$$Accuracy = 1 - \frac{|Study\ result\ -\ Chart\ reading|}{Study\ result} \quad (19)$$

In summer, the average accuracy of the readings of present study's design charts for the uninsulated intrados is 93%, compared to 86% using the previous ones. In winter, the accuracy of all charts dropped significantly due to inability to predict the numerical performance of the Grand Paris Express and Stuttgart energy tunnels. In the Paris case, the tunnel air temperature and heat transfer coefficient were assumed to be constant and equal to 18.96 °C and 15.13 W/m2K, respectively. These values cause the absorber pipes to have a significant heat transfer with the tunnel internal air and reach an unrealistic geothermal performance of 59 W/m2 in the absence of groundwater flow. In the Stuttgart case, the circulating fluid velocity is 0.5 m/s within 20 mm pipes while, in all the charts, the fluid velocity is assumed to be 0.9 m/s within the same pipes. This can cause Reynolds number of the flow to be nearly half the models that were used for generating the design charts and have an overestimation of the thermal performance for the energy tunnel. Eventually, the average accuracy of predictions by the present study's design charts for the uninsulated intrados is 73% compared to 55% using the previous ones. It is noticeable that adding the effect of tunnel diameter to the design charts has significantly improved the reliability of using them as a fast, front-end tool at the thermal design stage of the energy tunnels.

Table 6-1. Comparing the present study's design charts prediction with geothermal performance of previous case studies

Case Study (Numerical or Real)	Inner Diameter [m]	Outer lining surface to pipe length ratio [m]	v_{gw} [m/d] (direction)	v_{gw}/D_{in} [1/d]	T_g [°C]	λ_{gr} [W/mK]	Geothermal performance					
							Study result [W/m² (W/m)]		Previous charts [W/m²] (Insana & Barla, 2020)		New charts uninsulated / insulated [W/m]	
							Winter	Summer	Winter	Summer	Winter	Summer
Grand Paris Express (N) (Cousin et al., 2019)	8.7	0.254	0	0	13	2.1-2.3	59 (15)	-	34	-	7 / 3	-
Hamburg (N) (GEOSOLVING S.r.l., n.d.)	6.95	0.291	0.035 (90°)	0.005	11.2	≈1.7	16.24 (4.66)	37.96 (11.06)	21	37	5 / 2	10 / 7
Jenbach (R) (Franzius & Pralle, 2011; Frodl et al., 2010; Moormann et al., 2016)	12	0.467	1 (0°)	0.083	10	3.3	18-40 (8.4-18.7)	-	28	-	7 / 5	-
Stuttgart (N) (GEOSOLVING S.r.l., n.d.)	9.12	0.286	0	0	11.8-sum 11.5-win	1.8	12.65 (3.62)	27.45 (7.85)	19	22	5 / 2.5	8 / 6.5
Turin ML1 (R) (Insana & Barla, 2020)	6.88	0.279	1.5 (90°)	0.218	17.3	2.26	46-53 (12.8-14.8)	60-66 (16.7-18.4)	85	48	19 / 16	15 / 16
Turin ML2 (N) (GEOSOLVING S.r.l., n.d.)	8.8	0.344	1.08 (30°-60°	0.123	16.5	3.24	38.65 (13.3)	37.81 (13.01)	73	43	16 / 13	14 / 14

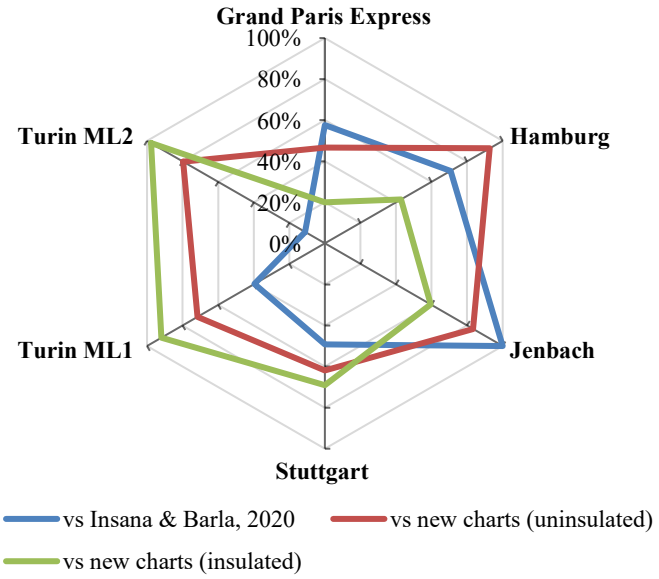

Figure 6-10. Accuracy of the design charts for predicting the thermal performance of the energy tunnel case studies in winter

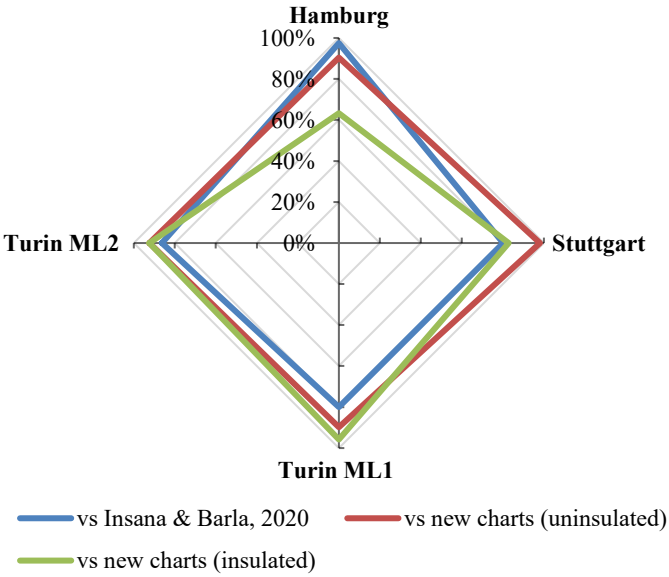

Figure 6-11. Accuracy of the design charts for predicting the thermal performance of the energy tunnel case studies in summer

6.6 Summary

Analyzing the effect of tunnel diameter on the thermal performance of energy tunnels in the previous chapter paves the way for implementing it into preliminary design charts for these energy geostructures. For this purpose, the ratio of groundwater flow velocity over the tunnel inner diameter is introduced as a representative of the thermal recharge of the geothermal system. However, this ratio for the cases with no groundwater flow becomes zero and the effect of diameter changes are neglected. Therefore, design charts are obtained for these cases first, where the effects of ground temperature and thermal conductivity, and tunnel diameter makes the prediction of energy output per absorber pipe length possible with or without tunnel intrados thermal insulation. Later, the ratio of groundwater flow over inner tunnel diameter allows for the same energy output prediction for the cases with parallel and perpendicular groundwater flow directions. In these cases, the points where v_{gw}/D_{in} is zero represents an average geothermal potential for all the tunnels diameters in the absence of groundwater flow. Next, two procedures for using these charts for thermal design of an

energy tunnel are introduced which allow prediction of the thermal output of a tunnel with known characteristics or the necessary number of tunnel rings to achieve a certain thermal energy demand. Finally, some numerical and real cases of energy tunnel studies were chosen to compare their performance with the readings from the newly generated design charts, along with the readings from earlier design charts in the literature in which the role of tunnel diameter was not implemented. It was shown that the accuracy of the newly generated design charts with uninsulated intrados is significantly higher than the rest, attesting to an improvement in this method of geothermal performance prediction for energy tunnels.

7 Conclusions

This thesis tries to demonstrate and quantify the effect of tunnel size on the geothermal performance of energy tunnels. To do so, variations in the diameter of energy tunnels with segmental lining are used to study the size effect. A flexible and fast way to perform this analysis is to use numerical methods to simulate the behavior of energy tunnels inside the ground. Therefore, COMSOL Multiphysics is used to run finite element analysis to simulate the thermo-hydraulic behavior of the energy tunnels.

The first step in using any numerical software for problem-solving is to ensure the validity of its results. Therefore, the software was successfully used to reproduce thermo-hydraulic performance of a previous field test. Next, a parametric study was performed on the validated model to study the effect of inner diameter, groundwater flow and direction, ground temperature and thermal conductivity, seasonality, and intrados insulation on the geothermal output of energy tunnels. This extensive study necessitated 2400 analyses to be finished. In these analyses the continuous pipe circuit length was varied based on the tunnel diameter, therefore the geothermal outputs of the tunnels were represented in terms of Watts per absorber pipe length instead of Watts per m^2 of extrados surface. The reason was that if the pipe spacing inside a specific tunnel would be too high, the amount of geothermal performance in terms of W/m^2 would be significantly low, while the same thing is not expected when representing the geothermal performance in terms of Watts per pipe length.

However, this representation of results (in W/m) needs the pipe rows to be sufficiently spaced for all tunnel diameters to avoid underperformance of a meter of the pipe circuit. This condition was assumed to hold true in this study.

During the analyses it was shown that regardless of other parameters, smaller energy tunnels have higher specific thermal performance (in Watts per meter of pipe length) with the surrounding ground. In the absence of groundwater flow this was due to a higher curvature of a certain tunnel wall perimeter. While, in the presence of groundwater flow the thermal recharge of the ground around the tunnel could be faster.

As it is generally accepted that smaller tunnels have a lining with less thickness, it was found that if the tunnel intrados is not insulated, a smaller tunnel can experience a higher amount of specific thermal performance only by thermal exchange with the tunnel air. However, in summer with the tunnel air temperature of 29.7 °C, that is close to the inlet temperature of 32 °C, the tunnel air reduced the specific performance with respect to the insulated cases.

To make these findings useful for the thermal design stage of energy tunnels, a series of design charts for the absence of groundwater flow or its presence with a perpendicular and parallel direction with respect to the tunnel axis were presented. In cases with non-zero groundwater flow, the ratio of groundwater flow velocity over the tunnel inner diameter is shown to be a key parameter that for a certain ground temperature and thermal conductivity imposes a certain amount of geothermal output for an energy tunnel. The accuracy of these design charts was shown against the recorded geothermal performances of some energy tunnel case studies in the literature. It was found that these new charts have improved the predictions up to 18 % with respect to previously available design charts that did not consider the effect of tunnel diameter. At the same time, the cases that mostly challenged the predictions of these charts showed that the tunnel internal air temperature (not bound to a specific ground temperature) and circulating fluid velocity are important factors that need to find their way into future studies of creating preliminary design charts for energy tunnels. Also, it is the author's opinion that the effect of inlet temperature on the performance of

energy tunnels is significant and needs to be accounted for in any future design chart generation studies.

Reference list

Abesser, C. (2010). Open-loop ground source heat pumps and the groundwater systems: a literature review of current applications, regulations and problems. *British Geological Survey Nottingham*.

Abuel-Naga, H., Raouf, M. I. N., Raouf, A. M. I., & Nasser, A. G. (2015). Energy piles: Current state of knowledge and design challenges. *Environmental Geotechnics*, *2*(4), 195–210. https://doi.org/10.1680/ENVGEO.13.00019

Adam, D., Brunner, A., Markiewicz, R., & Pistrol, J. (2023). Long-term experience of the thermo-active ground source system at the metro station Taborstrasse in Vienna. *Acta Polytechnica CTU Proceedings*, *45*, 1–13. https://doi.org/10.14311/APP.2023.45.0001

Adam, D., & Markiewicz, R. (2009). Energy from earth-coupled structures, foundations, tunnels and sewers. *Geotechnique*, *59*(3), 229–236. https://doi.org/10.1680/GEOT.2009.59.3.229/ASSET/IMAGES/SMALL/GEOT59-229-F15.GIF

Aresti, L., Alvi, M. R., Cecinato, F., Fan, T., Halaj, E., Li, Z., Okhay, O., Poulsen, S. E., Quiroga, S., Suarez, C., Tang, A. M., Valancius, R., & Christodoulides, P. (2024). Energy geo-structures: A review of their integration with other sources and its limitations. *Renewable Energy*, *230*, 120835. https://doi.org/10.1016/J.RENENE.2024.120835

Aydin, M., Şişman, A., Gültekin, A., & Dehghan, B. (2015). An experimental performance comparison between different shallow ground heat exchangers. *Proceedings World Geothermal Congress*, 19–25.

Baralis, M., & Barla, M. (2021). Development and testing of a novel geothermal wall system. *International Journal of Energy and Environmental Engineering*, *12*(4), 689–704. https://doi.org/10.1007/S40095-021-00407-Y/FIGURES/12

Barla, M., & Di Donna, A. (2016). Special Issue on Energy geostructures. *ENVIRONMENTAL GEOTECHNICS*, *3*(4), 188–189. https://iris.polito.it/handle/11583/2654880

Barla, M., & Di Donna, A. (2018). Energy tunnels: concept and design aspects. *Underground Space*, *3*(4), 268–276. https://doi.org/10.1016/J.UNDSP.2018.03.003

Barla, M., Di Donna, A., & Insana, A. (2019). A novel real-scale experimental prototype of energy tunnel. *Tunnelling and Underground Space Technology*, *87*, 1–14. https://doi.org/10.1016/J.TUST.2019.01.024

Barla, M., Di Donna, A., & Perino, A. (2016). Application of energy tunnels to an urban environment. *Geothermics*, *61*, 104–113. https://doi.org/10.1016/J.GEOTHERMICS.2016.01.014

Barla, M., & Insana, A. (2023). Energy tunnels as an opportunity for sustainable development of urban areas. *Tunnelling and Underground Space Technology*, *132*, 104902. https://doi.org/10.1016/J.TUST.2022.104902

Brandl, H. (2006). Energy foundations and other thermo-active ground structures. *Géotechnique*, *56*(2), 81–122.

Brandl, H. (2016). Geothermal Geotechnics for Urban Undergrounds. *Procedia Engineering*, *165*, 747–764. https://doi.org/10.1016/J.PROENG.2016.11.773

Bucci, A., Lasagna, M., De Luca, D. A., Acquaotta, F., Barbero, D., & Fratianni, S. (2020). Time series analysis of underground temperature and evaluation of thermal properties in a test site of the Po plain (NW Italy). *Environmental Earth Sciences*, *79*, 1–15.

COMSOL AB. (2022). *COMSOL Multiphysics Reference Manual v6.2*. COMSOL AB. https://www.comsol.com

Cousin, B., Rotta Loria, A. F., Bourget, A., Rognon, F., & Laloui, L. (2019). Energy performance and economic feasibility of energy segmental linings for subway tunnels. *Tunnelling and Underground Space Technology*, *91*, 102997. https://doi.org/10.1016/J.TUST.2019.102997

Dai, X., Bidarmaghz, A., & Narsilio, G. A. (2023). Energy tunnels: A review of the state of the art and knowledge gaps to harness renewable energy from underground infrastructure. *Tunnelling and Underground Space Technology*, *142*, 105431. https://doi.org/10.1016/J.TUST.2023.105431

Di Donna, A., & Barla, M. (2016). The role of ground conditions on energy tunnels' heat exchange. *Environmental Geotechnics*, *3*(4), 214–224. https://doi.org/10.1680/JENGE.15.00030/ASSET/IMAGES/SMALL/JENGE3-0214-F9.GIF

European Union. (2018). *Directive (EU) 2018/2001 of the European Parliament and of the Council on the Promotion of the Use of Energy from Renewable Sources.*

Franzius, J. N., & Pralle, N. (2011). Turning segmental tunnels into sources of renewable energy. *Proceedings of the Institution of Civil Engineers: Civil Engineering*, *164*(1), 35–40. https://doi.org/10.1680/CIEN.2011.164.1.35/ASSET/IMAGES/SMALL/CIEN-164-1-035-F11.GIF

Frodl, S., Franzius, J. N., & Bar, T. (2010). Design and construction of the tunnel geothermal system in Jenbach /Planung und Bau der Tunnel-Geothermieanlage in Jenbach. *Geomechanics and Tunnelling*, *3*(5), 658–668. https://doi.org/10.1002/GEOT.201000037

GEOSOLVING S.r.l. (n.d.). *Unpublished reports* .

Gopher Heating and Air Conditioning. (n.d.). *Geothermal Heating and Cooling in Savage, Minnesota*. Retrieved December 18, 2024, from https://www.gopherheating.com/products/geothermal/

Insana, A. (2020). *Thermal and Structural Performance of Energy Tunnels*. Politecnico di Torino.

Insana, A., & Barla, M. (2020). Experimental and numerical investigations on the energy performance of a thermo-active tunnel. *Renewable Energy*, *152*, 781–792. https://doi.org/10.1016/J.RENENE.2020.01.086

Kovačević, M. S., Bačić, M., & Arapov, I. (2013). Possibilities of underground engineering for the use of shallow geothermal energy. *Gradevinar*, *64–12*.

Laloui, L., & Di Donna, A. (2013). *Energy Geostructures: Innovation in Underground Engineering*. Wiley-ISTE.

Laloui, L., & Rotta Loria, A. F. (2019). Analysis and Design of Energy Geostructures: Theoretical Essentials and Practical Application. *Analysis and Design of Energy Geostructures: Theoretical Essentials and Practical Application*, 1–1062. https://doi.org/10.1016/B978-0-12-816223-1.00017-5

Lee, C., Park, S., Won, J., Jeoung, J., Sohn, B., & Choi, H. (2012). Evaluation of thermal performance of energy textile installed in Tunnel. *Renewable Energy*, *42*, 11–22. https://doi.org/10.1016/J.RENENE.2011.09.031

Loveridge, F., McCartney, J. S., Narsilio, G. A., & Sanchez, M. (2020). Energy geostructures: A review of analysis approaches, in situ testing and model scale experiments. *Geomechanics for Energy and the Environment*, *22*, 100173. https://doi.org/10.1016/J.GETE.2019.100173

Magdy, A., Ogunleye, O., Mroueh, H., Di Donna, A., & Singh, R. M. (2025). A review of exploiting shallow geothermal energy through tunnels: Current status and future prospects. *Renewable Energy*, *238*, 121958. https://doi.org/10.1016/J.RENENE.2024.121958

Mimouni, T., Dupray, F., & Laloui, L. (2014). Estimating the geothermal potential of heat-exchanger anchors on a cut-and-cover tunnel. *Geothermics*, *51*, 380–387. https://doi.org/10.1016/J.GEOTHERMICS.2014.02.007

Moormann, C., Buhmann, P., Friedemann, W., Homuth, S., & Pralle, N. (2016). Tunnel geothermics – International experience with renewable energy concepts in tunnelling / Tunnelgeothermie – Internationale Erfahrungen zu regenerativen Energiekonzepten im Tunnelbau. *Geomechanics and Tunnelling*, *9*(5), 467–480. https://doi.org/10.1002/GEOT.201600048

Narsilio, G. A., Johnston, I. W., Bidarmaghz, A., Colls, S., Mikhaylovaa, O., Kivi, A., & Aditya, R. (2014). Geothermal energy: introducing an emerging technology.

Proceedings of the International Conference on Advances in Civil Engineering for Sustainable Development. Singapore:[Sn].

Nicholson, D. P., Chen, Q., Pillai, A., & Chendorain, M. (2013). Developments in thermal pile and thermal tunnel linings for city scale GSHP systems. *Thirty-Eighth Workshop on Geothermal Reservoir Engineering*, 8.

Rosso, E., Insana, A., Vesipa, R., Barla, M., & others. (2022). Optimization of the hydraulic circuit for energy tunnels. *International Conference on Computational Methods and Information Models in Tunneling (EURO: TUN)-Book of Abstracts*.

Rotta Loria, A. F. (2020). Energy geostructures: Theory and application. *E3S Web of Conferences*, *205*, 01004. https://doi.org/10.1051/E3SCONF/202020501004

Sadeghi, H., & Singh, R. M. (2023). Driven precast concrete geothermal energy piles: Current state of knowledge. *Building and Environment*, *228*, 109790. https://doi.org/10.1016/J.BUILDENV.2022.109790

Singh, R. M., Sani, A. K., & Amis, T. (2019). An overview of ground-source heat pump technology. In T. M. Letcher (Ed.), *Managing Global Warming* (pp. 455–485). Academic Press. https://doi.org/https://doi.org/10.1016/B978-0-12-814104-5.00015-6

Zhong, Y., Bidarmaghz, A., Narsilio, G. A., & Makasis, N. (2023). Thermo-hydraulic analysis in geothermal energy walls. *Tunnelling and Underground Space Technology*, *132*, 104862. https://doi.org/10.1016/J.TUST.2022.104862